Université de Paris

École doctorale Bio Sorbonne Paris Cité (BioSPC) ED562

Laboratoire "Contrôle de la croissance cellulaire par les nutriments"

Institut Necker Enfants Malades (INEM)

INSERM UMR_S1151 CNRS UMR8253

Tuberous Sclerosis Complex: molecular target of mTORC1 and the role of S6Ks

Par Martina Bonucci

Thèse de doctorat de BIOLOGIE CELLULAIRE ET MOLECULAIRE

Dirigée par Mario Pende

Présentée et soutenue publiquement le 08 Octobre 2019

Devant un jury composé de :

Nathalie Spassky, Directeur de Recherche, École Normale Supérieure, Rapporteur
Marina Mapelli, Professeur Associé, Università degli Studi di Milano, Rapporteur
Guillaume Canaud, Professeur Associé, Université Paris Descartes, Examinateur
Pierre Leopold, Directeur de Recherche, Institut Curie, Examinateur

Except where otherwise noted, this is work licensed under
https://creativecommons.org/licenses/by-nc-nd/3.0/fr/

Titre: “Tuberous Sclerosis Complex: molecular target of mTORC1 and the role of S6Ks”

Résumé : La Sclérose tubéreuse de Bourneville (STB) est une maladie génétique responsable de la formation de tumeurs bénignes dans de nombreux organes. Les kystes rénaux sont des facteurs de morbidité et de mortalité importants chez les patients STB.*TSC1* et *TSC2* sont les gènes mutés chez ces patients dont les protéines codées forment un complexe qui inhibe la voie de signalisation du mTORC1 (mechanistic target of rapamycin complexe 1), qui contrôle la croissance et la division cellulaires. Par conséquent, la perte d'activité du complexe TSC1/2 est associée à une activation incontrôlée de mTORC1.

En cas de TSC, la S6 Kinase 1 (S6K1) joue un rôle prédominant sur les autres kinases de sa famille. S6K1 est une Ser/Thr kinase directement activée par mTORC1.Des études d'épistasie génétique chez Drosophila ont montré que la suppression de *S6k* rétablissait le phénotype de prolifération des mutants *Tsc2* à un niveau normal. Pourtant, l'effet de S6K1 dans la pathogenèse de la TSC n'a pas encore été découvert. Pendant mon doctorat, je me suis demandé comment l’axe mTORC1/S6K1 induisait la kystogenèse rénale.

Nous avons caractérisé un modèle murin qui inactive *Tsc1* dans les tubules rénaux et entraîne une hypertrophie rénale et une kystogenèse. Nous avons ensuite combiné l'inactivation de S6k1 et observé une diminution importante du poids des reins et de la surface kystique et une amélioration de la fonction rénale. De façon intéressante, nous n'avons pas observé aucune différence en termes de prolifération entre les mutants *Tsc1* en présence ou en absence de la S6K1.La division cellulaire orientée (OCD) est un processus qui régule la morphogenèse du tubule du néphron. Au cours de la croissance tubulaire normale, la division se produit alignée avec l'axe du tubule, ce qui permet l'élongation. Une perturbation de l’OCD a été associée au développement de kystes. Nous avons mesuré l’orientation de la division cellulaire dans les tubules rénaux dans nos modèles et nous avons constaté que l’inactivation de *Tsc1* déclenchait une désorientation de la mitose dépendante de S6K1, vu que les angles mitotiques du double mutant *Tsc1/S6K1* étaient corrigés. Le fuseau mitotique est organisé et orienté par les centrosomes, organelles qui, dans les cellules rénales, se trouvent à la surface apicale pendant l'interphase et qui migrent aux deux pôles latéraux pendant la mitose. Nous avons pu observer que l’hyper-activation de la S6K1 provoquait un mauvais positionnement des centrosomes en mitose et en interphase. Des cultures 3D de cellules rénales mutées en *Tsc1* ou *Tsc1/S6k1* ont confirmé que l’inactivation de S6K1 suffit pour rétablir une orientation correcte de la division cellulaire et un positionnement apical du centrosome. Nous nous sommes demandé quel substrat de S6K1 pourrait être responsable de ce phénotype. Nous avons donc réalisé un criblage phosphoprotéomique à l'aide des lignées cellulaires mutées, afin de trouver des protéines phosphorylées par S6K1 dans le contexte de la perte de *Tsc1*.Dans la liste des protéines différemment phosphorylées en l'absence de S6K1, nous avons observé un enrichissement en protéines du cytosquelette et des jonctions intercellulaires. Parmi ces protéines, nous nous sommes concentrés sur Afadin, une protéine qui relie le cortex d'actine aux jonctions adhérentes. Afadin est connue pour se lier à la machinerie du fuseau pendant la mitose et sa présence est importante pour assurer une orientation correcte de la division cellulaire dans les tubules rénaux. Nous avons validé Afadin en tant que substrat de S6K1.Enfin, nous avons invalidé Afadin dans la lignée cellulaire mutante *Tsc1* et avons pu observer une correction du positionnement du centrosome uniquement lorsqu'une forme non phosphorylable d'Afadin était ré-exprimée dans ces cellules. En conclusion, notre travail démontre qu’une dérégulation de l’orientation du fuseau mitotique est importante pour un déclanchement de la kystogenèse rénale et que cela est sous le contrôle de la voie mTORC1/S6K1.

Mots clefs: Sclérose tubéreuse de Bourneville - Polykystose - S6 Kinase - Division cellulaire orientée - Afadin

Title: "Tuberous Sclerosis Complex: molecular target of mTORC1 and the role of S6Ks"

Abstract: Tuberous sclerosis complex (TSC) is a genetic disorder that causes benign tumor formation in many different organs, such as in the brain, kidney, skin, lung, heart, and eyes. Renal cysts are important morbidity and mortality factors in TSC patients. Renal cysts are progressive enlargements of the renal tubules that eventually compromise the filtration capacity of the organ.
TSC1 and *TSC2* are the genes mutated in the patients and code for a protein complex that functions as an inhibitor of the mechanistic target of rapamycin complex 1 (mTORC1) signaling, a master regulator of cell growth.
In case of TSC, S6 Kinase 1 (S6K1) has a predominant role on the other kinases of its family, the AGC kinases, known to be involved in many pathologies. S6K1 is a serine/threonine kinase directly activated by mTORC1. Genetic epistasis studies in Drosophila showed that deletion of *S6k* reverts the overgrowth phenotype of *Tsc2* mutants to normal levels. However, the effect of S6K1 in TSC pathogenesis has not been uncovered yet. During my Ph.D., I asked how mTORC1/S6K1 drives cystogenesis in the kidney.
We characterized a murine model that inactivates *Tsc1* in the renal tubules. The inactivation of Tsc1 led to kidney hypertrophy and cystogenesis. We then combined the inactivation of *S6k1*, and we observed an extensive decrease of the kidney weight and cystic surface and an improvement of renal function. We first quantified the proliferation rate and, interestingly, we could not observe any difference between the *Tsc1* mutants in presence or absence of S6K1 activity.
Oriented cell division (OCD) is a process that regulates the nephron tubule morphogenesis during kidney development. During normal tubular growth, the division usually occurs aligned with the tubule axis, which allows the elongation of the tubule during the proliferative phase, to maintain the correct diameter. Very often a perturbation of OCD has been connected to cyst development. We measured the orientation of cell division in the renal tubules in our models and we found that inactivation of *Tsc1* triggered an S6K1-dependent misorientation of the mitosis and that the mitotic angles in *Tsc1/S6K1* double mutant were corrected as in the controls. The mitotic spindle is organized and oriented by the centrosomes, organelles that, in renal cells, are at the apical surface during interphase and that migrate at the two lateral poles during mitosis to nucleate the spindle microtubules. We could observe that hyperactive S6K1 caused a mispositioning of the centrosomes both in mitosis and in interphase. 3D cultures of renal cells that we mutated for *Tsc1* or *Tsc1/S6k1* confirmed that is sufficient to inactivate S6K1 to restore a correct orientation of cell division and an apical positioning of the centrosome.
We asked which substrate of S6K1 could be responsible for this phenotype. We therefore carried out a phosphoproteomic screening using the cell lines we generated, to find proteins phosphorylated by S6K1 in context of TSC1 loss. In the list of proteins differentially phosphorylated in *Tsc1* and *Tsc1/S6k1* mutant conditions, we found a significant enrichment in proteins of the cytoskeleton and of the cell-to-cell junctions. Among these proteins, we focused on Afadin, protein that connects the actin cortex to the Nectin-based adherens junctions. Afadin is known to bind the spindle machinery during mitosis and its presence has been shown to be important to assure a correct orientation of cell division in renal tubules. We validated Afadin as an S6K1 substrate both in vivo and in culture and using an in vivo kinase assay. Finally, we invalidated Afadin in the *Tsc1*-mutant cell line and we could observe a correction of the centrosome positioning only when an unphosphorylateble form of Afadin was re-expressed in these cells.
To conclude, our work shows that a misorientation of the mitotic division occurs for the development of cysts associated with TSC and is under the control of the mTORC1/S6K1 axis.

Keywords: Tuberous Sclerosis Complex - Polycystosis - S6 Kinase - Oriented cell division - Afadin

Acknowledgments

I sincerely thank the members of the jury: Dr Nathalie Spassky and Pr Marina Mapelli, who kindly accepted to be reviewers and took their time to read my manuscript and give their feedbacks; Pr Guillaume Canaud and Dr Pierre Leopold, who cordially agreed to be examiners.

I want to thank Dr Mario Pende, for the opportunity he gave me to perform my PhD in his laboratory. The last four years have been a very important and forming experience, in which I could learn to work with many different models and techniques, meet researchers and expand my scientific and personal knowledge. All this was thanks to Mario's contribution, who guided me during this, sometimes tough, experience. Grazie, Mario!

A big thank to all the members of the Pende/SGAMA team, past and present. During the best and the worst times, when experiment wouldn't work or only to share some happy moments together, I could always count on you. Merci Vonda et Delphine, pour tous les repas et les beaux moments que on a partagé, pour toutes les fois où vous m'avez aidé et pour toutes les commandes passées au dernier moment ! Thanks to Anton, Chantal, Nate and Chunyu for the laughs and the discussions about typical food (yes, I now accept the existence of pasta mixed with whatever!). Thanks to Stefano, Ganna, Ivan and Cathrine for all the help and the constructive discussions. Thanks to Nic, who shared with me many parts of the project and taught me a lot technical-wise (I mean, I somehow sub-cloned a plasmid thanks to you!), scientific-wise and USA Vs. Europe-wise! Thanks to all the others, the new, the ones that came for a while and the ones that left: it was a pleasure to get to know you and work with you! Merci aux étudiantes qui ont travaillé avec moi, Imane, Amelie, Malorie et Serena, j'ai appris énormément de vous et c'était toujours une grande satisfaction de voir votre progresses et votre super note finale !

Merci à Greg, Laura, David, Merce, Gabriele, Antoine, Talha, Lida et Annachiara, pour toutes les journées passées ensemble, les Saboteurs, l'accrobranche et, plus important, votre amitié !

Grazie a Manuela e Cecilia, due amiche, due bellissime persone che mi sono state affianco e mi hanno aiutata e con cui ho condiviso tantissimi bei momenti e un sacco di cene e pranzi (preparate da Cecilia, ovviamente!).

Un grazie ENORME alla mia coinquilina, migliore amica, psicologa, consulente di stile e di scienza: Bojance, non so davvero come avrei fatto senza di te in questi quattro anni, sei diventata come una sorella! Con la tua razionalità, la tua sensibilità e la tua sincerità mi hai insegnato tanto e hai reso, anche i momenti peggiori, più sopportabili e belli. Fala mnogu Bo! E ovviamente grazie alla tua famiglia, che è diventata un po' la mia famiglia macedone. Vi voglio bene!

Grazie a Manuel, che dietro la sua spensieratezza friulana e la sua fedeltà al San Daniele nasconde un cuore grande e sa essere un grande amico. Grazie per l'aiuto, per le risate, per i concerti e per tutte le birre bevute assieme (ahimè, il mio fegato è meno d'accordo).

Grazie a Giacomo e Federica! Sarebbe stato meraviglioso potervi avere sempre qui, ma, nonostante tutto, la vostra presenza e il vostro affetto non sono mai mancati e siamo sempre riusciti a condividere bellissimi momenti insieme.

Merci, thanks e grazie to all the other friends, to Claudio, Giorgio, Ibrahim, Margaux, Manon, Cisca, Teo, Pippo, Tommi, Marzia, Mary, Vale and all the people working in INEM!

Un grazie speciale alla mia famiglia, che non avrebbe potuto essere più presente di così. Un grazie di cuore ai miei genitori: tutte le chiamate la sera, tutte le volte che vi siete preoccupati quando ero triste e tutte le gioie che abbiamo condiviso; grazie per tutto quello che mi avete trasmesso, tutti i valori, tutto l'affetto e il supporto senza riserve. Siete i migliori!

Grazie alla Chiara, la mia pestifera sorella, con cui risate e grida sono all'ordine del giorno, ma su cui ho sempre potuto contare, no matter what. Sono orgogliosa di te, rimani sempre come sei!

E ora GRAZIE alla vivace e caciarona sfilza di zii, cugini e parenti acquisiti, con cui sono cresciuta e che mi manca sempre, perché senza di loro la vita è noiosa: zia Ziolli, zia Ceci, zia Bojojona, zio Peter, zio Luca, zia Silvia, zio Marino, Giuseppe, Stefano, Elena, Maria e poi Mattia, Federico, Clizia, Alice, Edoardo, Cecilia, Marta, Diego, Ester e Stefano! Non ho parole per dirvi quanto sono grata di fare parte di questa famiglia e quanto non veda l'ora del prossimo pranzo insieme!

Grazie ai miei fantastici nonni, Carmelo e Gianfranco. Grazie alle mie meravigliose nonne, Delfina e Olimpia, che mi piacerebbe tanto poter avere ancora con me in questo importante momento della mia vita. La vostra presenza durante la mia crescita e tuttora ha un'enorme importanza per me. Siete le colonne portanti di questa nostra pazza famiglia, ci avete reso quello che siamo e vi amiamo per questo. Un grazie di cuore!

And, to conclude, thanks to all the people I forgot to mention but that I had the chance to share a part of my life with!

Table of content

INTRODUCTION 1

1. TUBEROUS SCLEROSIS COMPLEX DISEASE 2

1.1. EPIDEMIOLOGY AND PROGNOSIS OF TSC 3
1.2. GENETICS OF TSC 4
1.3. KIDNEY PHYSIOLOGY AND TSC RELATED PATHOLOGY 7
1.4. ANIMAL MODELS OF TSC 14
1.5. TREATMENT OF TSC RENAL DISEASE 18

2. THE TSC COMPLEX 19

2.1. TSC FUNCTION: LESSONS FROM *DROSOPHILA MELANOGASTER* 19
2.2. MTOR SIGNALING AND THE CONTROL OF CELL GROWTH 24
2.3. MTOR-INDEPENDENT TSC 38

3. S6 KINASES 42

3.1. S6KS: AGC KINASES 42
3.2. PHENOTYPES ASSOCIATED WITH LOSS OF S6K1 45
3.3. KNOWN SUBSTRATES OF S6K1 48

RESULTS 55

ANNEXES 113

DISCUSSION 116

REFERENCES 127

TABLE OF FIGURES 146

INTRODUCTION

The mTOR pathway is found upregulated in many forms of renal disease, renal cancer and also in different PKDs. mTOR activation is, therefore, a common feature of PKD, independently on the causative mutation. Nevertheless, the molecular outputs caused by its activation are still not completely understood. We know that mTOR hyperactivation does not contribute only to sustain proliferation, since many other changes occur in the tissue: hypertrophy, increase in cell size, loss of differentiation, changes in shape and in cellular metabolism. All these features are characteristic of the cystic epithelium of TSC patients, but until now how this is achieved and what is the contribution of the substrates activated downstream of mTORC1, is still under study.

Renal TSC manifestation are now either surgically operated, in some cases of renal cell carcinoma and in hemorrhagic angiomyolipomas, or treated with rapalogues, like everolimus or sirolimus. Both angiomyolipomas and renal cysts have shown to respond well to pharmacological inhibition of mTORC1, with a gradual decrease of the lesion burden between 20-70%. However, the lesions never disappear completely and the treatments must be lifelong to avoid relapses. Chronic treatments with rapalogues, though, have many side effects, as development of insulin resistance, due to the inhibition of the mTORC2 induced by prolonged exposure to rapamycin analogues. For these reasons, development of new therapies that target more specifically pathways downstream of mTORC1 are ongoing.

We decided to focus on the mTORC1/S6K1 axis for different reasons: S6K1 is one of the most sensitive substrate to mTORC1 activation status; it is responsible for the control of cell size downstream nutrient and growth factor stimulation; it is the most upregulated kinase in case of TSC, where it becomes responsible also for the phosphorylation of substrates usually of other kinases; and finally, the inactivation of only S6K1 was sufficient to restore at normal levels the overgrowth phenotype related to TSC loss in Drosophila.

Therefore, during my Ph.D. project I investigated the role of S6K1 in the development of PKD caused by TSC, to better understand the pathophysiology of the disease, the molecular mechanisms that link mTORC1 activation to PKD and to evaluate S6K1 as a possible target for the development of future therapies.

1. Tuberous Sclerosis Complex Disease

On May 7 1879, the French physician Désiré-Magloire Bourneville (1840–1909) performed an autopsy on a 15-year-old woman, whose name was L. Marie. His findings, published one year later, represent the first detailed descriptions of clinical and neuropathological features of the disease that still bears his name: the Sclérose Toubérose de Bourneville, in english Tuberous Sclerosis Complex (TSC) (Bourneville, 1880). L. Marie presented the typical signs of the disease as nowadays is described: facial angiofibromas, focal seizures (that the French physician associated with the presence of tubers in the brain cortex) and some "nodules" in the kidney; the latter have been officially associated with the pathology only later, in 1908, by the German Heinrich Vogt (Vogt, 1908).

After a century the two genes responsible for the disease have been identified: TSC1 encoding the protein Hamartin (or TSC1) and TSC2 encoding the protein Tuberin (or TSC2) (van Slegtenhorst et al., 1997; The European Chromosome 16 Tuberous Sclerosis Consortium, 1993). These two proteins together form a complex called TSC, that inhibits the mechanistic Target of Rapamycin (mTOR) complex 1 (mTORC1), the major sensor of nutrients and energy availability and a central controller of cell and tissue growth.

TSC is inherited in an autosomal dominant manner, but in most of the cases a second hit mutation (with consequential loss of heterozygosity) has to occur to trigger the lesions, leading to a genetic mosaicism throughout the organism. For this reason, the clinical features vary widely between individuals, even within the same family.

TSC affects multiple organ systems and it is characterized by the formation of tumors, usually benign, that can become a great burden for the patient's life and that, in some cases, can become malignant (Henske et al., 2016). The clinical features of the disease are distinctive and include malformations of the cerebral cortex (tubers), cardiac rhabdomyomas that can arise during fetal life and usually regress during early childhood, renal cysts and renal angiomyolipomas (AMLs) that contain aneurysmal tumor-derived vascular structures, facial angiofibromas (benign blood vessel-filled tumors on the face), hypomelanotic macules (white patches on the skin) and pulmonary lymphangioleiomyomatosis (LAM), which is a destructive lung disease that almost exclusively affects women (Figure A). Infantile spasms, epileptic seizures, intellectual disability and autism spectrum disorder also occur frequently in patients

with TSC. In this first chapter, I will introduce the epidemiology and prognosis, the genetic and the renal manifestations associated to TSC, focusing on the renal cysts.

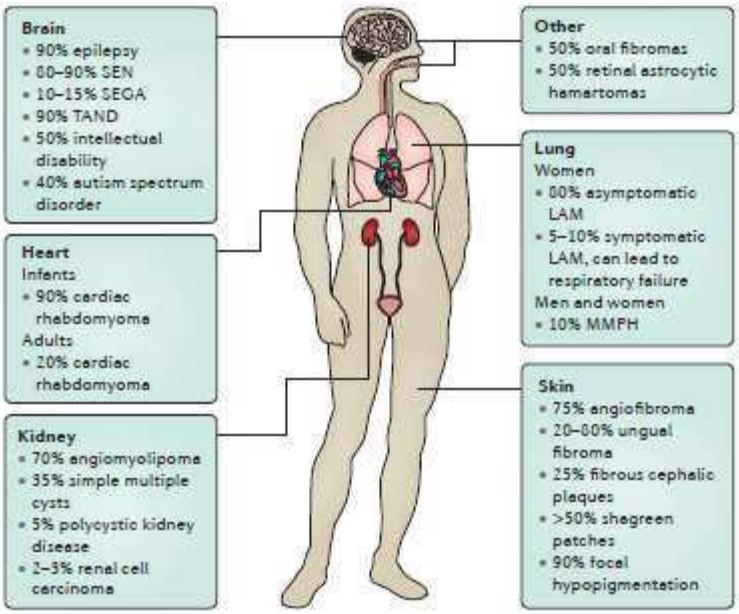

Adapted from Henske et al., 2016

Figure A. Most common affected systems in TSC patients and associated lesions

The most common affected systems and their associated lesions and the percentage of the approximate incidence in TSC patients. SEN: subependymal nodule; SEGA: subependymal giant-cell astrocytoma; TAND: TSC-associated neuropsychiatric disorder; LAM: lymphoangioleiomyomatosis; MMPH: multifocal micronodular pneumocyte hyperplasia.

1.1. Epidemiology and prognosis of TSC

TSC can occur in all races and ethnic groups without preferences for the sex (except for LAM, which affects almost exclusively women). Current estimates place tuberous sclerosis complex affected births at one in 6,000. Nearly 2 million people worldwide are estimated to have TSC, with approximately 8’000 in France. Many cases may remain undiagnosed for years or decades due to the relative obscurity of the disease and the mild form symptoms that may take in some people.

A diagnostic evaluation is often tailored to the individual situation but may include imaging of the brain, heart, lungs and kidneys, cognitive and developmental evaluation, seizure monitoring and an examination by a dermatologist. The identification of a pathogenetic

mutation in TSC1 or TSC2 genes in normal tissue is now considered sufficient to make a definitive diagnosis, although mutations are not detected in all individuals with clinical TSC.

The prognosis for individuals with TSC depends on the severity of their symptoms. Individuals with mild forms of TSC generally have a normal life expectancy. Overall, the most common cause of death in patients with TSC are renal complications and status epilepticus (that is, one prolonged or several epileptic fits in quick succession) or bronchopneumonia. Other leading causes of death documented included brain tumor, LAM and cardiac failure in neonates due to rhabdomyomas. The causes of death in the current era of mTOR inhibition therapy it is yet to be precisely assessed.

1.2. Genetics of TSC

1.2.1. *TSC1* and *TSC2*

Up to now, a total of 2690 unique DNA variants have been identified for *TSC2* (http://chromium.lovd.nl/LOVD2/TSC/home.php?select_db=TSC2), which is found mutated in about 70% of patients with a clinical diagnosis of TSC, and 928 for *TSC1* (http://chromium.lovd.nl/LOVD2/TSC/home.php?select_db=TSC1), mutated in 20% of the cases. Recently, using techniques such as next-generation sequencing and RNA-based approaches, some of the remaining 10% in whom no mutation was initially identified have been shown to have low level somatic mosaicism or intronic splicing variants affecting *TSC1* or *TSC2* (Nellist et al., 2015; Tyburczy et al., 2015). Therefore, the existence of other TSC-causative genes seems now unlikely. Indeed, no mutation in *TBC1D7*, a third subunit of the TSC1-TSC2 complex, or *RHEB*, the mTORC1-activating GTPase substrate of TSC2, have been associated with TSC disease.

Estimates are that one-third of TSC cases are familial whereas two-thirds are sporadic (Choi et al., 2006). All mutation types, including nonsense, missense, insertions, and deletions, have been described in TSC (Curatolo et al., 2015).

The *TSC1* gene is located on 9q34 and it is composed by 23 exons, but the coding sequence is confined to 21 exons between the initial codon (ATG) on exon 3 to the exon 23. Mutations in

TSC1 are often small insertion or deletions (indels) which result in premature termination of the protein. No missense mutation has been found for this gene.

TSC2 gene is located on 16p13 and it is composed by 42 exons. The GTPase-activating protein (GAP) domain is encoded by exons 34 to 38, in which there is a slightly higher rate of mutations (warm-spot). All kind of mutation have been found in *TSC2* gene, insertion, deletion, but also nonsense and missense. Large deletions or rearrangements occur with higher frequency in *TSC2* gene that in *TSC1*, for which this kind of mutations are rare. The *TSC2* gene is only 60bp from the polycystic kidney disease 1 (*PKD1*), gene responsible for polycystic kidney disease; in a small percentage of patients, a large chromosomal deletion of both *TSC2* and *PKD1* can cause a very severe renal polycystosis with TSC features and a very early onset. According to many long-term studies, mutations in *TSC2*, rather than in *TSC1*, are linked with a more severe phenotype, such as early onset of epileptic seizures, lower IQ and higher incidence of dermal, renal and hepatic involvement (Kothare et al., 2014; Rakowski et al., 2006). Nevertheless, both genes show a very high pleiotropy and accordingly individuals with the same mutation can display very different disease manifestations, making the genotype-phenotype correlation and the severity prediction very complex (Caban et al., 2017).

The variable clinical expression of TSC is also due to the fact that in order to have the disease, both alleles have to be mutated in two different moments of the development, following the "two-hit" model of Knudson (Knudson, 1971). In fact, the "first-hit" mutation can be either inherited (in familial cases of TSC) or acquired early during embryogenesis on one allele of either *TSC1* or *TSC2* gene, in this last case leading to genetic mosaicism (in the same organism only some cells will be heterozygotes for the mutation) (Figure B). Only when the second allele is hit by a second mutation ("second-hit"), the lesions will develop, as a result of a loss of heterozygosity (LOH).

In conclusion, the variety of the mutational landscape in both *TSC1* and *TSC2* genes, the "two-hit" mechanism and the mosaicism in sporadic cases, concur to determine a highly broad spectrum of disease manifestations and severity.

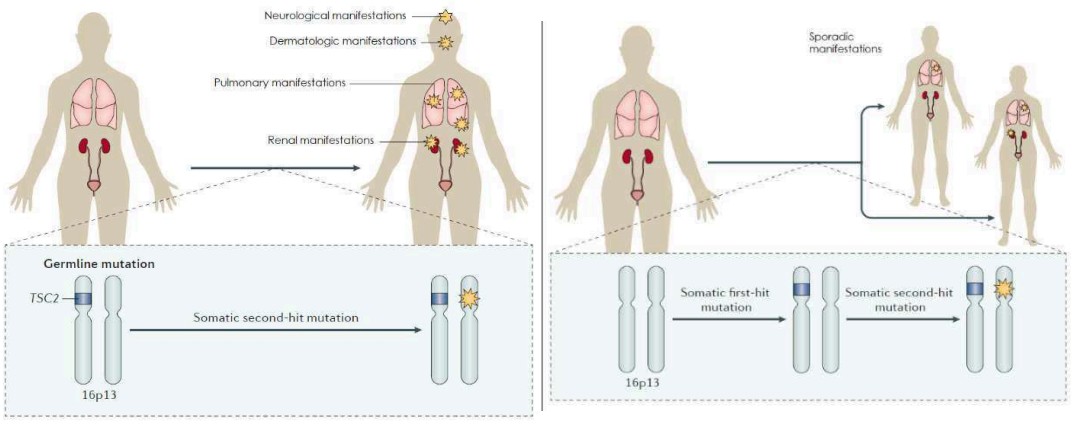

Adapted from Henske et al., 2016

Figure B. "Two-hit" model in inherited and somatic TSC.

In inherited TSC, a mutated allele is inherited from one of the parents and, during embryogenesis another mutation occurs on the second allele, driving the development of lesions generally in multiple organs. In this case all the cells of the organism will be heterozygote for the first mutation except for the cells in the lesions that underwent a LOH. In somatic TSC, the first allele contracts the mutation during the first stages of embryogenesis, while the second is mutated later in a smaller subset of cells. The patients will be mosaic heterozygote and, on average, with a lower severity.

1.2.2. Murine *Tsc1* and *Tsc2*

In *Mus musculus*, the *Tsc1* gene is on Chromosome 2 and it is composed by 23 exons orthologous to human's *TSC1* (including the un-translated exons 1 and 2) and 11 transcripts, of which only 4 are translated into protein. The human and mouse coding regions are 86% identical and the intron size is also very similar (https://www.ensembl.org/Mus_musculus/Gene/Summary?g=ENSMUSG00000026812;r=2:28641228-28691167; Cheadle et al., 2000).

The *Tsc2* gene is, instead, on Chromosome 17. It is composed, as its human orthologue, by 42 exons and 22 transcripts are known, of which 8 code for protein. It shares an 88% of identity with the human gene (http://www.ensembl.org/Mus_musculus/Gene/Summary?db=core;g=ENSMUSG00000002496;r=17:24595816-24632630).

1.3. Kidney physiology and TSC related pathology

1.3.1. Kidney physiology

The kidney is the principal organ that controls and regulates the osmolarity and the volume of the corporal fluids, the electrolytic balance and that filtrates the blood to eliminate the waste products of metabolism. Murine and human kidney have a high resemblance both in structure and in functionality, therefore, in the following paragraphs, I will refer to both organisms in general.

In a sagittal section of the kidney (Figure C1), we can observe a clear external part, called cortex, and a darker internal part, called medulla. The medulla is organized in conical-shaped regions, called renal pyramids, whose bases lay on the cortex and whose apexes point toward the renal calyxes which continue into the renal pelvis. The renal pelvis is connected to the ureter and the ureter to the bladder. Urine follows this path in its way to the excretion.

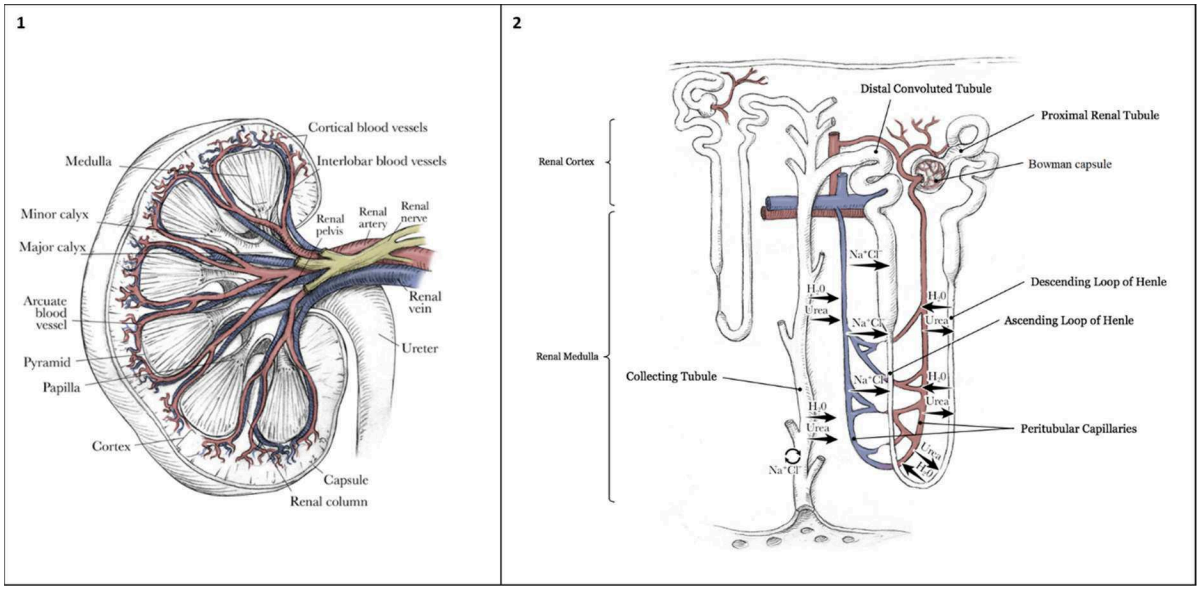

Adapted from www.ebmconsult.com

Figure C. The kidney.

Cross section of a human kidney with the principal macroscopic structure and the blood vessels (a). Scheme of a cortical nephron with the permeability for H_2O, Urea and NaCl in the different tracts.

The functional unit of the kidney is the nephron (Figure C2). Each human kidney contains around 1.2 million nephrons.

The nephron is a monolayer tubular structure subdivided in the following subunits:

- The glomerulus: a nod of capillaries surrounded by an epithelial calyx called Bowman capsule. The blood coming from the periphery passes through the capillary nod where it is ultrafiltrated thanks to the pores in the endothelial membranes. The liquid is conveyed into the tubular system through the Bowman capsule. The pores in the glomerular capillaries retain all the blood elements (cells and macromolecules) that are bigger than about 70 kDa. All the rest, meaning small proteins, solutes (i.e. glucose and amino acids) water and waste, are sent into the tubular system.

  The proximal convoluted tubule: the longest portion of the nephron. This tract is permeable to ions like Na^+ al Cl^-, to glucose, to amino acids, to other macromolecules and to water, thanks to a selected expression of active transporters and aquaporins in the apical membrane of the tubular cells.
- The Henle's loop: composed by a descendent and an ascendant tract. The descendent tract is permeable only to water, while the ascendant tract is permeable to ions and urea but not to water. It therefore forms a crescent gradient in the surrounding parenchyma that allows the passive reabsorption of around 10% of the water and the concentration of urine.
- The distal convoluted tubule and the collecting duct: the last tract of the nephron, it allows the further absorption of salts and water if needed. This tract is able to respond to the needs of the organism regarding the concentration of the urines. Blood volume, pressure and osmolarity are sensed by the hypothalamus that releases vasopressin, a neuroendocrine antidiuretic hormone, in response, for example, to increase in blood osmolarity or decrease in blood volume. When vasopressin is released, it induces an accumulation of aquaporin2 (AQP2) on the apical surface of the collecting duct cells. This triggers further water absorption and concentrates urine. Vice versa water absorption is inhibited in this tract by low levels of vasopressin.

Given the complexity of this important system, it is fundamental that the renal epithelium maintains its integrity, its diameter and its zonal differentiation, in order to pursue its function and to respond to the organismal needs.

1.3.2. TSC-related renal disease

Renal disease is the most common cause of death in TSC patients. Death results from chronic kidney disease (CKD), often associated with surgical removal of tumors and cysts or with acute hemorrhage. The renal manifestation of TSC include angiomyolipomas (Figure D2), epithelial cysts (Figure D1) and renal cell carcinomas -RCC- (Figure D3) (Lam et al., 2018).

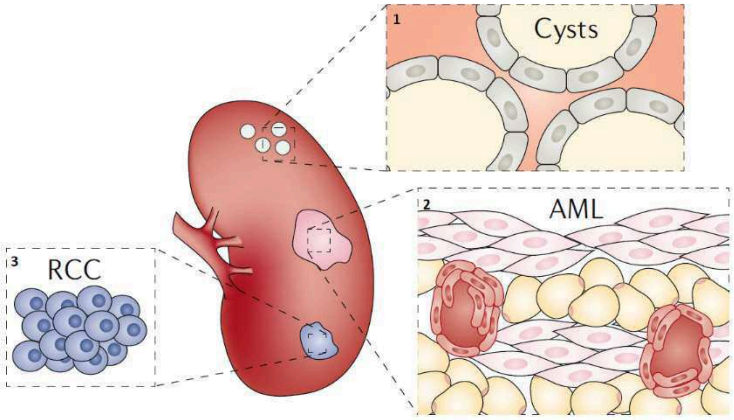

Adapted from Lam et al., 2018

Figure D. The renal lesions in TSC patients

The most common renal lesions in TSC patients: (1) renal cysts; (2) AML, angiomyolipoma; (3) RCC, renal cell carcinoma.

Angiomyolipomas are benign tumors composed, as the name suggests, by different cell types, including adipocytes, smooth muscle cells, cells that express melanocytic markers and abnormal vasculature. All these different cell types derive from the same progenitor, because genetic analysis of many angiomyolipomas established that they all bear the same second-hit genetic mutation. The gold standard in angiomyolipoma diagnosis is the positivity to the immunohistology with anti-HMB45 antibody (premelanosome protein -PMEL). This protein, together with others expressed in these tumors, are typical markers of melanocytes, the melanin-producing cells. Melanocytes derive from the neural crest, group of cells generated during development by the ectoderm in the area of the neural tube invagination. The neural crest cells typically undergo an epithelial-to-mesenchymal transition (EMT) to migrate in different part of the body and differentiate in many kinds of cells, i.e. melanocytes, smooth

muscle cells and glial cells. All these cell types are typically found in TSC-associated tumors and this led to hypothesize that neural crest-derived cells are the cells of origin of these tumors. This will be further discussed in another sub-chapter (1.4).

Epithelial cysts are described as fluid-filled enlargements of the nephron epithelium. Approximately 35-50% of the TSC patients develop multiple renal cysts. TSC-associated cysts are peculiarly composed by enlarged and unshaped epithelial cells (named columnar epithelium) (Figure E, white arrow), element that allows them to be distinguished from the cysts associated with autosomal dominant polycystic kidney disease (ADPKD), cysts typically surrounded by thin and spread epithelial cells.

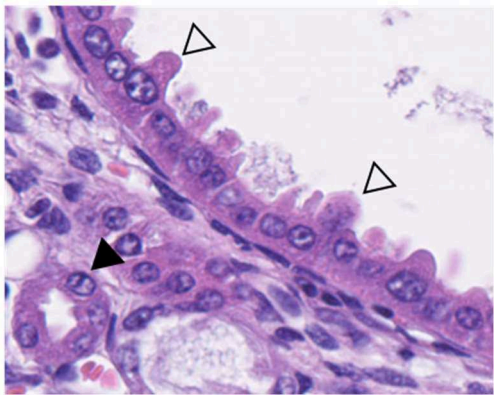

Figure E. Epithelium in TSC-associated cyst

Hematoxylin-Eosin of a 3-month-old Tsc1-mutant murine kidney (Ksp-Cre; Tsc1fl/fl). Black arrow: normal tubule, cubical epithelium; empty arrows: columnar epithelium lying cyst. Note the bigger size of Tsc1-mutant cells and the drop-like shape of their apical part.

Epithelial cells are not always symptomatic in TSC patients and very often have an adult onset. In the 2% of the patients, though, a large chromosomal deletion of the contiguous *TSC2* and polycystic kidney 1 (*PKD1*) genes triggers a very severe early onset polycystic kidney disease difficult to treat.

A small percentage of patients (2-4%) develop malignant RCC. The incidence of this type of tumors in TSC patients is higher than the one of the general population, indicating that the loss of TSC1 or TSC2 is the cause of RCC in these patients.

The RCCs found in TSC patients are very similar among them, but they partially differ from the conventional RCCs. Hallmark features of TSC-associated RCCs are prominent papillary architecture (Figure F). This suggested a peculiar tumorigenic pattern associated with TSC.

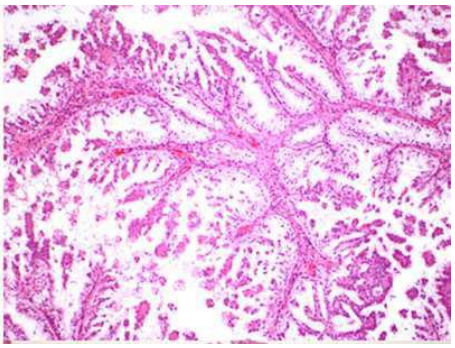

Adapted from Tyburkzy et al., 2014

Figure F. Human RCC

Hematoxylin-Eosin of a papillary RCC from a TSC patient.

Intriguingly, no additional driver mutations have been identified with whole-exome sequencing of TSC-associated RCCs, suggesting that TSC1 or TSC2 loss are the only causative genetic mutations in these cases (Tyburczy et al., 2015). Epigenetic alterations or extra-mTORC1 activity of TSC1 or TSC2 mutations in these tumors could shed light on this subject.

1.3.3. TSC and polycystic kidney disease

Polycystic kidney disease (PKD) is defined as the presence of multiple epithelial cysts in the nephron tubules. Cysts are usually present in all the tract of the nephron, but they likely originate from the distal region or from the collecting ducts.

The most common form of PKD is autosomal dominant polycystic kidney disease (ADPKD). In ADPKD, cysts develop in utero and slowly grow, generally being symptomatic only in adulthood. ADPKD is due to mutations in either *PKD1* or *PKD2* genes, which encode for polycystin 1 (PC1) and polycystin 2 (PC2) respectively. PC1 and PC2 are transmembrane proteins which form a heterodimeric complex. They are particularly enriched at the primary cilium, a microtubule-based digitiform organelle with function of antenna. ADPKD follows, similarly to TSC, the “two-hits” model.

PC1 is a big membrane protein with 11 transmembrane domains. The role and the function of PC1 is mostly still unclear, but it is known that it interacts, through its cytosolic N-terminal, with PC2. PC2 is a 6 transmembrane domain protein. Four copies of PC2 associate at the membrane to form the cation channel of the transient receptor potential (TRP) family. The PC1-PC2 interaction seems to regulate the Ca^{2+} influx in the cell, although it is not clear whether this is direct or indirect (Bergmann et al., 2018).

Although not much is known about the exact function of the PC1/PC2 complex, some more is known about the signaling activated by the loss of this complex's function. The putative mechanisms of cyst formation is briefly described below and they are common to many polycystic kidney diseases (Bergmann et al., 2018).

- *Increase in proliferation*. The decrease in Ca^{2+} influx activates the mitogen activated pathway kinases (MAPKs) and the PI3K/AKT pathway, which results into proliferative, pro-survival and anti-apoptotic stimuli. The decrease in Ca^{2+} levels also releases the inhibition of the adenylate cyclase 6 (AC6), enzyme that converts ATP in cAMP. The increase in cAMP activates the protein kinase A (PKA), which concurs to activate the MAPKs pathway. Other pro-growth pathways that are activated in PKD are the janus kinase (JAK)/signal transducer and activator of transcription (STAT), the epithelial growth factor receptor (EGFR) and the mTOR pathways. This also allows metabolic changes as a decrease in fatty acid oxidation, increase glucose consumption and a consequential increase in aerobic glycolysis and reactive oxygen species (ROS).
- *Fluid secretion*. Increase in cAMP and decrease in ATP lead to the accumulation of AMP that inhibits the AMP-activated protein kinase (AMPK). This modifies the activity of membrane channels as the cystic-fibrosis transmembrane conductance regulator (CFTR, Cl^- permeable channel mutated in patients with cystic fibrosis), that triggers the secretion of fluids into the growing cysts. Intratubular fluid accumulation generates a mechanical stress on the neighbor epithelial tubular cells and perturbates the flow of the urine (Ghata et Cowley, 2017). In normal conditions, this flow is sensed through the primary cilium (PC). In fact, only in presence of fluid flow, the PC bends and activates the tumor suppressor liver kinase B1 (LKB1) that, through AMPK, inhibits mTORC1 and prevents abnormal cell growth (Bohelke et al, 2010). The decrease in flow

does not allow the PC bending and therefore promotes the mTORC1-dependent overgrowth and proliferation.

- *Inflammation and fibrosis*. Cyst formation in PKD is accompanied by a massive inflammatory infiltrate and fibrosis. Modification of extra-cellular matrix (through indirect effect of PC1 on integrins), production of cytokines and apoptosis of neighbor epithelial cells determine an increase in inflammation in particular driven by macrophages and interstitial fibroblasts. The activated macrophages raise the levels of cytokines and therefore the inflammation in the tissue, promoting fibrosis. The fibrotic tissue confers a chronic inflammation status that strongly impacts the renal function.
- *Misorientation of cell division*. In order to lengthen the tubule, renal cells must organize and orient their mitotic division parallel to the longitudinal axis of the tubule itself. Only in this way the diameter of the tubule can be maintained during the postnatal proliferative phases of the organ. In PKD, however, the tubular cells cannot orient their mitotic spindle with the tubule (Fischer et al., 2006), due to defects in planar cell polarity (PCP) and apico-basal polarity establishment. PCP is the coordinated alignment of cell polarity across the tissue plane, defined through the asymmetric localization of cortical PCP components, cell-to-cell communication and the following intracellular signal transduction. It is still not known whether these defects in cell polarity and orientation are a cause or an effect of the cyst formation, but they are found in almost all cystic disease with a study which reports a defect in cell division orientation also in case of TSC-related cysts (Bonnet et al., 2009).
- *Modification of the primary cilia*. Mutations in genes encoding for proteins that reside or have a function in the primary cilium, the hairlike antenna of the cells described above, give rise to multiorgan disorders that almost always include cystic disease or chronic kidney disease among their features (Hildebrandt et al., 2011). Besides ADPKD, mutations in other ciliary proteins cause ciliopathies. For example, the von-Hippel Lindau (VHL), caused by loss of function mutations in the *VHL* gene, characterized by tumors in the kidney and in the brain and renal cysts. Autosomal recessive polycystic kidney disease (ARPKD), another ciliopathy correlated with cysts and fibrosis in kidney and liver; it is caused by homozygous loss of function of polycystic kidney and hepatic disease 1 (*PKHD1*), gene coding for the ciliary protein fibrocystin, but of which the pathophysiology is still unclear. Moreover, nephronophthisis, Joubert's Syndrome,

Meckel's Syndrome and Bardet–Biedl syndromes are other examples of ciliopathies that feature renal cysts. Although we know that the primary cilia control many important signaling pathways, such as Wnt and PCP pathways, it is still not known how defects in primary cilia drive cystogenesis and many laboratories are still trying to figure it out.

1.4. Animal models of TSC

The beginning of the study of TSC disease is marked by the fortuitous discovery of a spontaneous rat model called the Eker rat, by the name of Eker R., the first to describe it in 1954 (Eker, 1954). This mutant was the first (and, for decades, the only) autosomal dominant hereditary animal model of predisposition to cancer, specifically of renal adenoma and carcinoma. After the discovery, the scientific community did not pay much attention to the Eker rat, until Alfred Knudson, one of the first cancer biologists, recognized its importance for cancer biology and decided to bring this rat to the United States and to start a series of pathologic and genetic studies that culminated in the discovery of the gene which mutated causes the "Eker predisposition": the *Tsc2* gene (Yeung et al., 1994; Kobayashi et al., 1995).

The pathological lesions developed by the Eker rat are cystadenomas (Figure G1) that can vary from tubular hyperplasia (Figure G2) to pure cysts, to cysts with papillary projections or adenomas (Figure G3), to, although in a small proportion, malignant carcinomas (Figure G4) (Kwiatkowski, 2010).

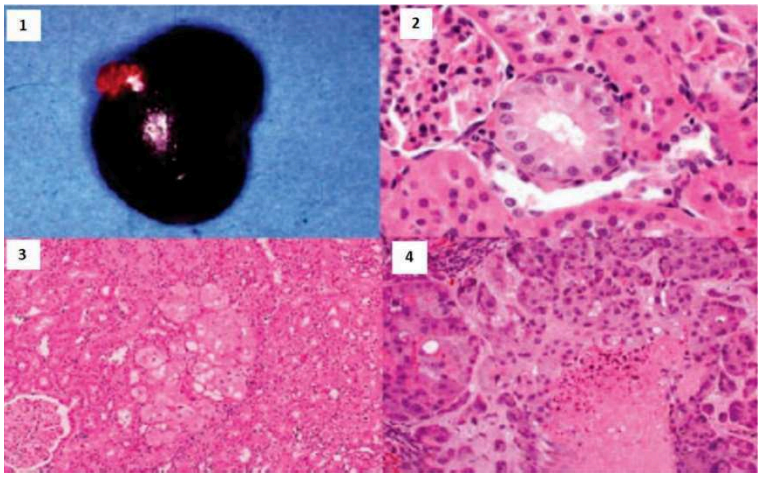

Adapted from Kwiatkowski, in "Tuberous Sclerosis Complex: Genes, Clinical Features, and Therapeutics", 2010

Figure G. Eker rat kidney tumors

Gross view of an Eker rat kidney with an exophytic cystadenoma (1). Hematoxylin-Eosin staining of (2) hyperplasic tubule, early stage; (3) renal adenoma; (4) renal carcinoma.

Next, histological studies and 3D reconstructions have defined that the cysts and the cystadenomas start to develop in the proximal tubules or in the collecting duct and that, subsequently, they grow along the nephron to expand throughout the whole kidney.

Although these tumors have no pathological relationship with the typical angiomyolipomas found in TSC patients, the study of the Eker rat led to seminal achievements not only in the TSC field, but more generally in cancer biology. In fact, it provided the evidence to the mathematical model of Alfred Knudson, who hypothesized in the early 70s the recessive nature of tumor-initiating gene mutations and the concept of tumor suppressor genes and loss-of-heterozygosity (LOH) relevant to carcinogenesis, what is called the "Two-hit" hypothesis. Indeed, it was the recognition of *Tsc2* as the gene mutated in the Eker rat that allowed the demonstration, almost three decades later, of this hypothesis (Kobayashi et al. 1997): Hino and coworkers introduced a transgenic copy of the *Tsc2* gene in the Eker rat and could perfectly compensate the loss of endogenous *Tsc2*, in a dose dependent manner.

Apart from the Eker rat, other murine models have been developed by different labs in more recent years. Heterozygote and homozygote mutants for both *Tsc1* and *Tsc2* were generated and characterized by the laboratories of David Kwiatkowski and Okio Hino in the early 2000s, using the Cre/Lox system. They could both show that the complete loss of either *Tsc1* or *Tsc2* was embryonic lethal (embryos die around gestation day E9-12) and that the phenotypes of

the heterozygote mice were similar for both genes (Kobayashi et al., 1999; Onda et al., 1999; Kobayashi et al., 2001; Kwiaktowski et al., 2002). Mice showed liver hemangiomas and renal cystadenomas as predominant lesions at the age of 6-12 months and LOH was seen fairly consistently.

The generation of transgenic mice with floxed *Tsc1* or *Tsc2*, allowed the development of tissue specific models of inactivation of these two genes. Brain and kidney have been, and are still, the most targeted and studied organs connected with TSC disease and the majority of the mouse models created attempted to recapitulate the symptoms in these organs.

Regarding the kidney, many laboratories have been trying to generate a model for angiomyolipomas, mesenchymal benign tumors. Two models that showed angiomyolipoma-like lesions were the *Pax8-rtTA; TRE- LC1; Tsc1*$^{fl/+}$ mice (Gonçalves et al., 2017) and the *CAGGGCre–ER; Tsc1*$^{fl/fl}$ model, developed by our laboratory (Liang et al., 2014). The first is a doxycycline- induced knockout of *Tsc1* at 8–10 weeks of age in the precursor of epithelial cells of the nephron. The second is a tamoxifen-inducible whole-body knockout of *Tsc1* at E15.5. In both models, mice develop similar small renal lesions that express the markers of angiomyolipomas (Figure H).

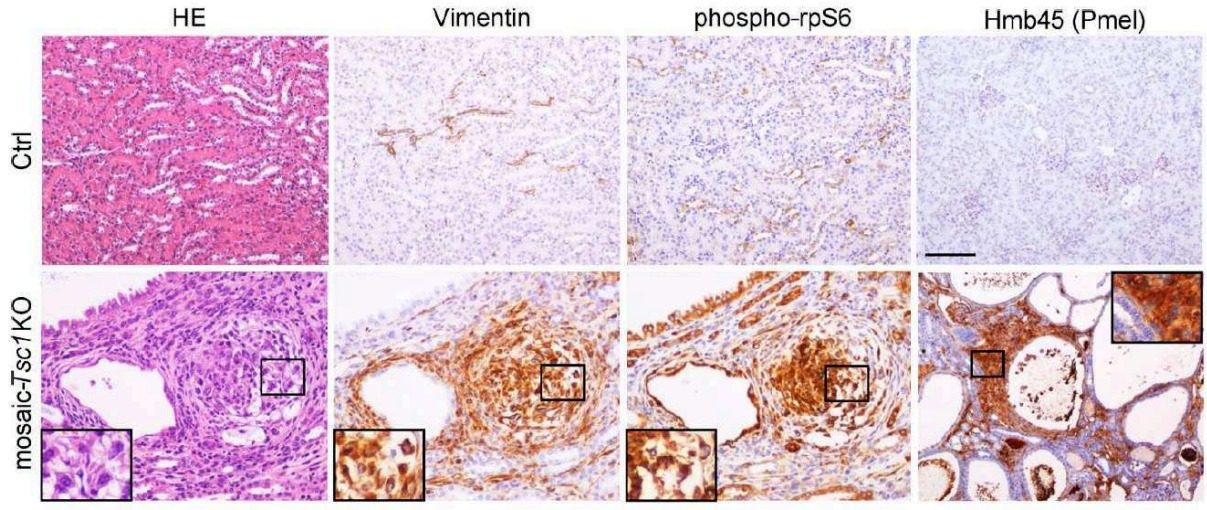

Adapted from Liang et al., 2014

Figure H. Immunohistological analysis of renal tumors of *CAGGGCre–ER; Tsc1*$^{fl/fl}$ animals

Immunohistological analysis of renal tumors of CAGGGCre–ER; Tsc1$^{fl/fl}$ *animals with the principal markers of angiomyolipomas (Vimentin and Hmb45) and of mTOR activation (phospho-rpS6). Only the tumors present in* Tsc1-*mutant mice are positive for these markers.*

Nevertheless, the cells of origin of angiomyolipomas are still uncertain. Previous work suggested that these lesions may arise from neural crest-derived cells, as for example podocytes or, more in general, perivascular epithelioid cells (PEC), which surround blood vessels and express both mesenchymal and epithelia/melanocytic markers. These cells reside in the kidney and possess the ability to trans-differentiate. In the *Pax8-rtTA; TRE- LC1; Tsc1*$^{fl/+}$, though, the cells that lack *Tsc1* are epithelial cells, therefore proposing that the angiomyolipomas might originate from epithelial precursors.

Moreover, several other groups knocked out *Tsc1* or *Tsc2* in renal epithelial cells or mesenchymal cells, approaches that all result in polycystic kidney disease (Gonçalves et al., 2017; Lam et al., 2017; Pema et al., 2016; Ren et al., 2016). Taken together, these studies suggest that, in TSC patients, epithelial cysts can derive from both epithelial and mesenchymal cells, with no evident differences between *Tsc1* and *Tsc2* loss.

We could assert that the murine models for TSC disease, which show a preponderant polycystic kidney disease, do not show perfect match with the human patients that preferentially present mesenchymal lesions in the kidney (angiomyolipomas) and cortical tubers in the brain (a phenotype not recapitulated in any mouse model). This could rely on intrinsic differences between mice and humans, both at the developmental level or, most probably, at the level of the cellular environment.

However, these animal models have provided insights in the molecular role of TSC1 and TSC2. These discoveries allowed the possibility of targeting the patients with mTORC1 inhibitors as rapamycin analogues or, nowadays, to propose therapies that target other downstream pathways. In this field, research is still actively understanding the roles, the effects and the mechanisms of regulation of the mTORC1 signaling in pathophysiology.

Importantly, the tumors in the animal models also follow the “two-hit” mechanism of tumor development as seen in patients, thus demonstrating the great importance of the use of animal models in the TSC field.

1.5. Treatment of TSC renal disease

Angiomyolipomas are abnormally highly vascularized tumors that, when bigger than 3 cm in diameters, risk spontaneous ruptures and hemorrhages. Therefore, embolization (surgical occlusion of blood vessels) or removal of the tumor can be an option in TSC patient management. Nevertheless, the tumors usually recur after surgery (Lam et al., 2018). Cysts are difficult to surgically operate, but, if the renal function is very compromised, they may require transplant.

The discovery of mTOR inhibitors has changed the therapeutic approach toward TSC patients. Everolimus and sirolimus, the two soluble analogues of rapamycin (allosteric inhibitor of mTORC1), underwent clinical trials for the management of angiomyolipomas (EXIST-1 and EXIST-2; Kingswood et al., 2016). The trials showed that angiomyolipoma response rate was 53.3% for everolimus compared with 0% for placebo. Angiomyolipoma volume reductions with everolimus were sustained over 48 weeks of treatment. Long-term data show continued shrinkage of angiomyolipoma with everolimus therapy and no bleeding was observed. In one study of 15 patients with cystic disease, everolimus treatment reduced cyst number, diameter and volume. In all 15 patients, cyst burden was reduced by 71% (Siroky et al., 2017).

Despite the high efficacy, these treatments need to be lifelong, because interruptions cause sudden relapse. Due to the long treatments, rapalogues have different side effects as stomatitis,mucositis and mouth ulceration (∼50%), hypercholesterolemia (20-40%), hypertriglyceridemia (12-50%), infections (40-70%), hypophosphatemia (11%), hematologic abnormalities (leukopenia, neutropenia, 10-40%), and proteinuria (4-30%) (Kingswood et al., 2016). The side effects are due to the immunosuppressant action of rapalogues and on the inhibition, in long term treatments, of the mTORC2, that can cause insulin resistance and diabetes. Nevertheless, the mTOR-inhibitors are the first-line therapeutic approach in the management of TSC patients. Other types of mTOR inhibitors, like the ATP-competitive Torin1 (Thoreen et al., 2009) are very efficient inhibitors of both mTORC1 and mTORC2, but are not approved for patients. To avoid relapses, researchers are currently focused on developing cytocidal treatment strategies, to eliminate rather than merely suppress TSC- related angiomyolipomas, cysts and RCCs.

2. The TSC complex

As I mentioned above, *TSC1* and *TSC2*, were identified during the nineties. However, their function was not understood until later.In fact, these two genes encode for two large proteins, respectively Hamartin (or TSC1, 150 kD) and Tuberin (or TSC2, 200 kD), that share almost no homology with each other, but that are conserved throughout eukaryotes including yeast (Huang et Manning, 2008). A big step into the discovery of the function of TSC1 and TSC2 has been finding that they interact with each other (Plank et al., 1998; van Slegtenhorst et al., 1998). The two proteins interact with a stoichiometry of 1:1 and with a very strong binding that resists multiple steps of purification.

Thanks to different studies, it has been understood that it is the complex that is important for the function: in fact, missense mutations that affect the stability of the complex, preventing the interaction between TSC1 and TSC2, are commonly found in patients (Hodges et al., 2001); moreover, mouse models of TSC have been generated by deletion of either *Tsc1* or *Tsc2* genes, leading to similar phenotypes (Onda et al., 1999; Kobayashi et al., 1999); and finally, TSC1 binding is important to prevent TSC2 ubiquitin-dependent proteasomal degradation (Benvenuto et al., 2000; Chong-Kopera et al., 2006).

The TSC1-TSC2 complex was believed to function as a heterodimer since the discovery, in more recent years, of a third subunit: TBC1D7 (Dibble et al., 2012). This subunit, although it has been shown to be important for the proper function of the complex, does not appear to be important for the development of the TSC disease, at least so far.

2.1. TSC function: lessons from *Drosophila melanogaster*

It is at the beginning of the new millennium that the powerful genetic model of *Drosophila* came to help the TSC research. Experiments of mutagenesis identified Tsc1 and Tsc2, both singularly and together, as responsible for a cell autonomous eye-overgrowth phenotype, which is only partially due to an increase in cell number and, more prominently, to an increase

in cell size (Gao et al., 2001; Potter et al., 2001; Tapon et al., 2001; Ito et Rubin, 1999). Increased expression of both Tsc1 and Tsc2 led to the opposite phenotype that is smaller eyes with fewer ommatidia.

A molecular pathway known to control cell and organismal growth was the PI3K-Akt-TOR-S6K pathway, shown to be a central mechanism of growth regulation through Insulin/Insulin-like growth factor 1 (IGF-1) signaling (Stocker and Hafen, 2000). In fact, flies lacking the Insulin receptors or their ligands are smaller as a result of decrease in both cell number and cell size. Moreover, depletion of the lipid kinase Phosphoinositide-3-kinase (PI3K) -activated by the Insulin signaling- or overexpression of the antagonist lipid phosphatase phosphatase and tensin homolog (PTEN) result in a decrease in cell number and size comparable to the one derived from Insulin receptor loss. PI3K and PTEN balanced activities determine the levels of the second messenger PIP3 and, indeed, an increase in PIP3 levels is responsible for the overgrowth phenotype in both PI3K overexpression and PTEN loss-of-function.

Activated downstream of PI3K pathway, the Serine/Threonine kinase Akt was also shown to positively regulate cell size and proliferation. Similarly, another Serine/Threonine kinase was shown to be regulated by the Insulin/PI3K signaling and to be an important regulator of cell size exclusively (not cell number): S6 Kinase (S6K). This protein was known to phosphorylate ribosomal protein S6 (RPS6) leading to an increase in the translation of 5' TOP (terminal oligopyrimidine tract) mRNAs that largely encode components of the translational apparatus.

Last but not least, studies in yeast highlighted the central role of the Serine/Threonine kinase target of rapamycin (TOR, mechanistic TOR -mTOR- in mammals) in sensing nutrient availability to stimulate cell growth and specifically protein translation in case of presence of nutrients. In 1998 Sabatini's lab demonstrated that mTOR activates the initiation of translation through direct activation of S6K (phosphorylated on $Threonine^{389}$) and inactivation of eukaryote initiation factor 4E (eIF4E) binding protein (4E-BP1) (phosphorylated on $Threonine^{35-45}$) to prevent its binding to eIF4E and therefore release the inhibition of translation initiation (Burnett et al., 1998).

Thanks to seminal studies in the early 2000s (Gao et al., 2001; Potter et al., 2001; Tapon et al., 2001; Potter et al., 2002; Gao et al., 2002), the epistatic link between the PI3K-Akt-TOR-S6K pathway have been described. To briefly summarize the discoveries, it was demonstrated that Tsc1 or Tsc2 deletion rescued the growth defect induced by InR or Akt loss but it did not rescue

the one caused by loss of TOR. Similarly, overexpression of Tsc1 or Tsc2 counteracted the overgrowth caused by overexpression of Akt or InR, but not the one caused by overexpression of S6k. Finally, flies deleted of Tsc1 and Tsc2 together with deletion of PTEN showed an addictive phenotype that is a more severe overgrowth, strongly suggesting that TSC1/2 function in a pathway, parallel to PTEN, that converges in the insulin pathway and that is downstream to Akt.

The genetic epistasis studies and their finding and a model derived from these findings are summarized in the Table A and Figure I respectively.

Reference	TSC modification	Relative phenotype	Insulin pathway related gene modification	Relative phenotype	Phenotype of the double modification
Gao et al., 2001	*Tsc1 -/-*	eye-overgrowth	*InR -/-*	smaller eye	eye-overgrowth
			Akt -/-	smaller eye	eye-overgrowth
			Pten -/-	eye-overgrowth	more severe eye-overgrowth
Potter et al., 2001	*Tsc1* and *Tsc2* overexpression	smaller eye	*InR* overexpression	eye-overgrowth	normal eye
			S6k ovrexpression	eye-overgrowth	eye-overgrowth
	Tsc1 -/-	eye-overgrowth	*InR -/-*	smaller eye	eye-overgrowth
			Akt -/-	smaller eye	eye-overgrowth
			Pten overexpression	smaller eye	eye-overgrowth
	Tsc2 -/-	eye-overgrowth	*S6k -/-*	smaller eye	normal eye
Tapon et al., 2001	*Tsc1* and *Tsc2* overexpression	smaller eye	*Pten* overexpression	smaller eye	more severe defects in eye growth
			S6k ovrexpression	eye-overgrowth	eye-overgrowth
Gao et al., 2002	*Tsc1 -/-*	eye-overgrowth	*Tor +/-*	not reported	50% size reduction
			Tor -/-	smaller eye	smaller eye
			S6k -/-	smaller eye	normal eye

Table A. Genetic epistasis studies in Drosphila

Genetic epistasis studies in Drosphila and the genotypes of the different mutants used in the studies, single or in combination with either Tsc1/2 loss or overexpression.

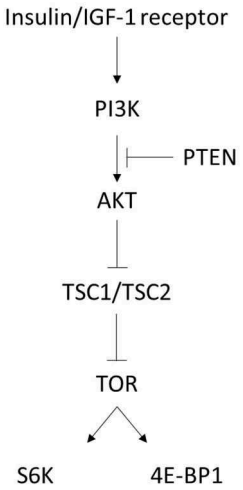

Figure I. Tsc1 and Tsc2 function in *Drosophila*

Genetic model for the function of Tsc1 and Tsc2 in Drosophila, thanks to the genetic epistasis studies of the early 2000s.

As a further confirmation of these genetic studies, two other works in *Drosophila* (Inoki et al., 2002; Potter et al., 2002) and one in mammals (Manning et al., 2002) demonstrated the molecular link between the PI3K/Akt with TSC2 and, therefore, to TOR and S6K. These studies showed that Akt directly phosphorylates TSC2 on two residues, Serine^{924} and Threonine^{1518} in *Drosophila* (respectively Serine^{939} and Threonine^{1462} in human's TSC2) to inhibit the activity of the TSC1/2 complex in presence of growth factors and nutrients, downstream of the Insulin/PI3K pathway. The inhibition of TSC was linked with an activation of TOR/mTOR and phosphorylation of its substrates S6K and 4E-BP1. Mutant TSC2, in which the two Akt sites were mutated in Alanine -to prevent their phosphorylation-, blocked the activation of TOR/S6K in response to nutrients and growth factors.

2.1.1. TSC and Rheb: mind the GAP

Among the many questions around TSC and TOR, a very big one was still left unanswered: how does TSC1/TSC2 complex inhibit mTOR?

As mentioned above, the definition of TSC1 and TSC2 structure and domains did not help much at the beginning, given that the two proteins share very little homology with each other and

with other proteins. Nevertheless, the putative GTPase-activating protein (GAP) domain in TSC2 attracted some interests.

GAPs downregulate the activity of small GTP-binding proteins (G proteins). These proteins are intrinsically able to hydrolyze GTP to GDP but are active only when bound to GTP, thus inhibiting and self-regulating their own state (Li et al., 2004). In their GTP-bound state, the G proteins are able to interact with many proteins and, through these interactions, activate or inactivate signaling pathways. The cycling between active-GTP-bound and inactive-GDP-bound states, is accelerated or slowed-down by GAPs and guanin nucleotide exchange factors (GEFs) respectively (Figure J). GEFs promote the exchange between GDP and GTP linked to the G-protein, thus activating it, while the inhibiting GAPs increase the efficiency of GTP-hydrolysis of G-proteins.

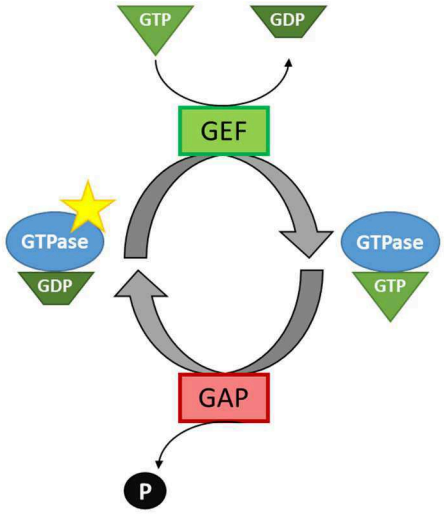

Figure J. Regulation of GTPases

Schematic model for the mechanism of action of GEF and GAP in the control of GTPases.

TSC2 was shown to weakly increase the GTPase activity of Rab5 and Rap1 *in vitro* (Wienecke et al., 1995; Xiao et al, 1997), demonstrating the functionality of this domain. However, it was not known whether this activity was actually present *in vivo*.

Meanwhile, genetic studies in *Drosophila* placed a new small G-protein in the TSC-TOR pathway: Ras homologue enriched in the brain (Rheb). Rheb is an atypical member of the Ras superfamily, given the very low GTPase activity compared to the others small G-proteins of

the family. It is ubiquitously expressed, despite being enriched in brain (as the name says). It was first discovered in a screening of seizure-induced mRNA and it was found to be accumulated in the cortex and in the hippocampus after long term potentiation (LTP).

In 2003, three different studies placed Rheb in the insulin signaling, downstream of TSC1/TSC2 and upstream of mTOR/S6K pathway (Patel et al., 2003; Saucedo et al., 2003; Stocker et al., 2003). As a matter of fact, Rheb was shown to regulate cell growth through mTOR/S6K and to be inactivated by the TSC complex. Furthermore, biochemical studies demonstrated the actual GAP activity of TSC2 on Rheb and its importance in the mTOR pathway. TSC1/TSC2 complex overexpressed and immunoprecipitated showed GAP activity toward Rheb both *in vitro* (Inoki et al., 2003; Castro et al., 2003; Tee et al., 2003; Garami et al., 2003) and *in vivo* (Zhang et al., -Pan-2003) and overexpression of TSC1 and TSC2 markedly increased the GDP-bound form of Rheb. Overexpression of Rheb increased mTOR phosphorylation and the downstream S6K and 4E-BP1 that still remained rapamycin-sensitive, therefore confirming that Rheb acts upstream of mTOR (Inoki et al., 2003; Garami et al., 2003; Tee et al., 2003). Moreover, point mutations in the GAP domain of TSC2 prevented the inhibition of Rheb and the activation of mTOR/S6K but not the binding to TSC1 (Tee et al., 2003). Finally, Rheb was farnesylated at the C-terminus and this was shown to be important for Rheb to optimally associate with membranes, especially lysosomal membrane, where also mTOR is found, and to function as an activator of mTOR signaling (Tee et al., 2003; Castro et al., 2003) by directly binding it (Long et al., 2005).

Thanks to these studies at that time the epistatic relationship between the different components of the insulin/PI3K/mTOR pathway was defined. On the other hand, the molecular mechanisms that lead to the activation of mTOR by nutrients and growth factors remained elusive for other years and some are still unclear.

2.2. mTOR signaling and the control of cell growth

In the late 1960s, Lee Hartwell isolated and studied mutants of yeast with defects in macromolecule synthesis, cell morphology and cell division. He then decided to focus on the mutants with impaired cell division, the *cdc* (cell division cycle) mutants, discovering the genetic of the cell-cycle in yeast that led him to the Nobel Prize in 2001. Very importantly, he

also made a distinction between cell proliferation and cell growth. In fact, although these two concepts are often used interchangeably, the former defines cell division that ultimately leads to increase in cell number, while the latter is the macromolecules synthesis that leads to an increase in cell mass or size (Schmelzle and Hall, 2000). Of course, proliferation and growth must be tightly regulated and linked to each other, in order to assure a correct development both in unicellular (as budding yeast) and multicellular organisms, but the two concepts are two distinct and separable mechanisms. The mechanisms of cell division have been studied thanks to Hartwell since the 60s, but the study of cell growth started only later, thanks to a very fortunate discovery in a far pacific island.

2.2.1. Rapamycin and the discovery of TOR

During an expedition in the island of Rapa Nui (Easter Island) in 1964, a sample of soil was collected, to screen for new antimicrobial molecules. Some years later, a compound was isolated from this soil, which displayed antifungal properties but also immunosuppressant and anti-cancer capacities (Vézina et al., 1975; Martel et al., 1977; Eng et al., 1984). This molecule was named rapamycin, from the name of the island in which the bacterium that produces it (*Streptomyces hygroscopius*) was isolated.

Rapamycin was found to have similarity in the chemical structure with another immunosuppressant, FK506 (Figure K) and it was shown that they both bind with high affinity and inhibit the FK506-binding protein 12 (FKBP12), a peptidyl-prolyl isomerase that, only when in complex with FKBP12 or rapamycin, could suppress T-cells activation (Schreiber, 1991).

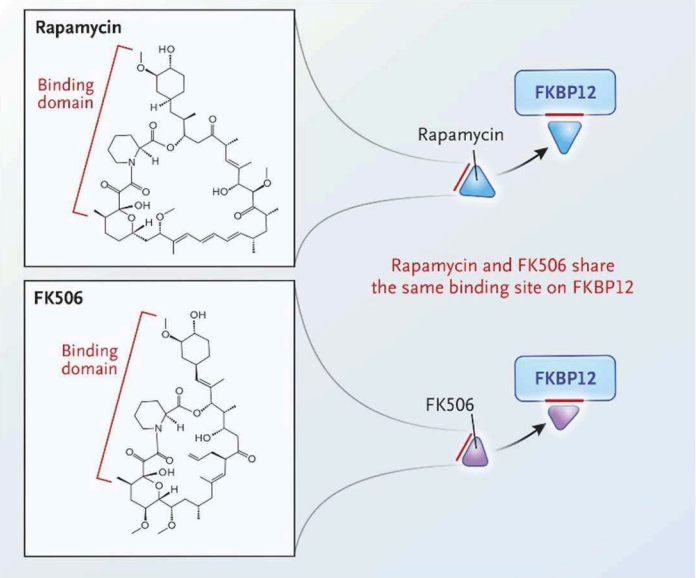

Adapted from Manning, 2017

Figure K. Rapamycin and FK506 structure

Chemical structure of rapamycin and FK506. Their structure similarity allows both of them to bind to FKBP12.

Again, *S. cerevisiae* came to hand. In 1991, Michael Hall and his colleagues undertook a genetic screening in the budding yeast of mutants resistant to rapamycin: as expected they found mutant in the FKBP12 yeast homologue (FRP1) but also in two other genes called target of rapamycin 1 and 2 -TOR1 and TOR2- (Heitman et al., 1991). The mutants FRP1 conferred resistance to rapamycin but FRP1 loss did not affect growth by itself. The concomitant loss of TOR1 and TOR2, however, triggered an arrest of cell proliferation similar to the one caused by rapamycin (Kunz et al., 1993) and suppression of only TOR2 caused a complete impairment of cell growth, supporting the role of the proteins encoded by these genes as biological targets of the rapamycin-FKBP12 and important regulators of cell growth and proliferation. The discovery of the TOR proteins in yeast and of their counterpart in mammals (Brown et al., 1994; Sabatini et al., 1994; Sabers et al., 1995), opened the way to the study of the TOR signaling and of the regulation of cell growth.

For the sake of simplicity, in the next chapters I will describe only the mammalian mTOR signaling pathway. The reference for the following paragraphs is a very comprehensive review by Saxton and Sabatini (Saxton et Sabatini, 2017), unless otherwise stated.

2.2.2. mTOR and the complexes

mTOR (mechanistic target of rapamycin) is a 290 kDa protein member of the PI (phosphoinositide) kinase-related protein kinase (PIKK) family of atypical serine/threonine kinases. Despite the similarity of their catalytic domain with the catalytic domain of the lipid kinases (PI3Ks and PI4Ks), none of the PIKK has lipid kinase activity.

mTOR exists in the cell as part of two different protein complexes, mTOR complex 1 (mTORC1) and mTOR complex 2 (mTORC2). mTORC1 consists of 5 proteins (FigureL, left): mTOR, regulatory protein associated with mTOR (Raptor), mammalian lethal with Sec13 protein 8 (mLST8) and the 2 inhibitory subunits proline-rich Akt substrate of 40kDa (PRAS40) and DEP domain containing mTOR interacting protein (DEPTOR).

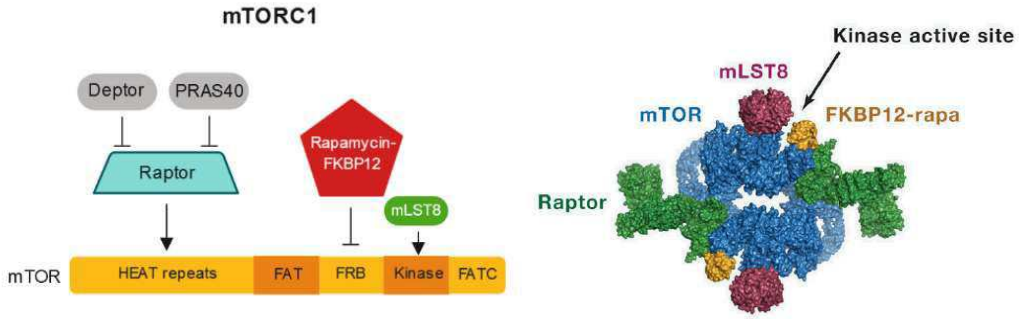

Adapted from Saxton et Sabatini, 2017

Figure L. mTORC1

mTORC1 subunit and respective binding sites on mTOR (left). Cryo-EM structure of mTORC1 in complex with the FKBP12-rapamycin complex (right).

Raptor functions as a scaffold protein to help the binding of mTOR with its substrates and it also determines the cellular localization of mTORC1; without Raptor, mTORC1 does not function. mLST8 interacts with the catalytic domain of mTOR and seems to stabilize the kinase activation loop. This pentameric complex needs to dimerize to be in its active form, forming a mega complex with a lozenge shape, through interactions between the HEAT domains of mTOR and Raptor (Figure L, right).

The Cryo-EM studies that showed the mTORC1 structure, also revealed that, to inhibit mTORC1 function, the FKBP12-rapamycin complex binds to the FKBP12-rapamycin binding

domain (FRB) domain next to the catalytic domain and renders the active site inaccessible for the substrates.

On the other hand, mTORC2 is characterized by its insensitivity to (acute) rapamycin, due to the different partners of mTOR in this complex (Figure M). A part from mTOR and mLST8 that are conserved, Raptor is replaced by rapamycin insensitive companion of mTOR (Rictor), which likely serves similar scaffold functions. Given its different size and structure, the binding of Rictor to mTOR covers the FRB domain, conferring to mTORC2 the insensitivity to rapamycin. Long term exposure to the drug, though, abrogate the activity of mTORC2, probably because of the inability of rapamycin-bound mTOR to incorporate into new mTORC2. Finally, stress-activated map kinase-interacting protein 1 (mSin1 or MAPKAP1) and proline-rich protein 5 and 5-like (Protor1 and 2), together with DEPTOR, participate to the mTORC2 as inhibitory subunits.

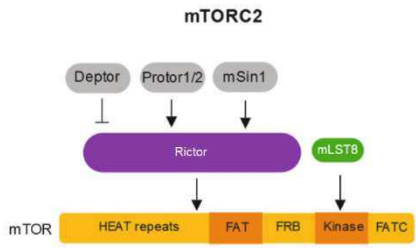

Adapted from Saxton et Sabatini, 2017

Figure M. mTORC2 subunits and respective binding sites on mTOR.

2.2.3. Upstream of mTORC1

mTORC1 is considered the major sensor of the energy status and nutrient availability of the cells and the master regulator of anabolism and cell growth. Thus, in physiological conditions, its activation only occurs when the cells have enough energy to boost anabolism. mTORC1 can be activated by different stimuli, the principals being: growth factors, amino acids and energy and oxygen status.

Growth factor signal transduction has been already discussed in the previous paragraphs and it converges on the TSC complex. In fact, multiple growth factor pathways signal to mTORC1 through inhibiting or activating the TSC complex, including the insulin/insulin-like growth factor 1 (IGF-1) pathway, that, through class I PI3Ks, activates Akt, which, in turn,

phosphorylates and inhibits TSC2 to activate mTORC1. It has been recently shown that insulin stimulates acute dissociation of the TSC complex from the lysosomal surface, where subpopulations of Rheb and mTORC1 reside. The TSC complex associates with the lysosome in a Rheb-dependent manner, and its dissociation in response to insulin requires Akt-mediated TSC2 phosphorylation (Menon et al., 2014).

Other tyrosine kinase-dependent receptors are known to inhibit TSC complex through the Ras signaling and the mitogen activated protein kinases (MAPK) pathway that activates ERK and RSK to phosphorylate and inhibit TSC2. Activation of Ras also signals through activation of the PI3K/Akt branch. Apart from the tyrosine kinase receptors, also the developmental Wnt pathway and the inflammatory TNFα pathway can activate mTORC1 through inhibition of TSC1.

Nevertheless, TSC does not senses only the growth factors. An important trigger of cell metabolism is glucose; glucose availability is sensed by many pathways. For example, glucose deprivation decreases the ratio of ATP on ADP-AMP and AMP is a direct ligand of AMP-activated protein kinase, an enzyme that triggers glucose uptake and catabolism. AMP binding primes AMPK to be subsequently activated by LKB1 and, once activated, AMPK can inhibit mTORC1 by phosphorylating and activating TSC2 (Huang et Manning, 2008) and by phosphorylating Raptor.

The oxygen availability is another regulator of mTORC1 activation, in part through AMPK activation caused by a decrease in ATP production due to loss of mitochondrial respiration, but also through the hypoxia-induced factor α (HIFα) and its transcriptional target REDD1.

Important sources of energy, both directly and through anaplerosis, and building blocks for many metabolic pathways, protein-derived amino acids constitute a significant part of eukaryotes' diet and their levels drastically increase after feeding. Amino acids (AAs) have been known to be important for mTORC1 activation since many years, but only recently great breakthroughs have helped to clarify how their sensing actually works, although many questions are still unanswered.

It was the discovery of the Rag-GTPases that started the digging into the AA's sensing and that brought to the definition of the model depicted in Figure N. Briefly, Rags are found at the lysosomal membrane where they form heterodimeric aggregates composed by RagA or RagB with RagC or RagD. The Rags are tethered to the lysosomal membrane thanks to the big

Ragulator complex (composed by MP1, p14, p18, HBXIP and C7ORF59), a GEF for the Rags, and are located in proximity of Rheb. When AAs are present in the cells, Ragulator promotes the GTP-bound state of RagA/B and the complex is, in this way, able to recruit mTORC1 to the lysosomes where it is activated by Rheb. Knowing that Rheb is active at the lysosomes only when the TSC complex is inhibited by the presence of growth factors and that active Rheb is necessary for mTORC1 activation by AAs/Rags, it means that both AAs and growth factors are needed to fully activate mTORC1.

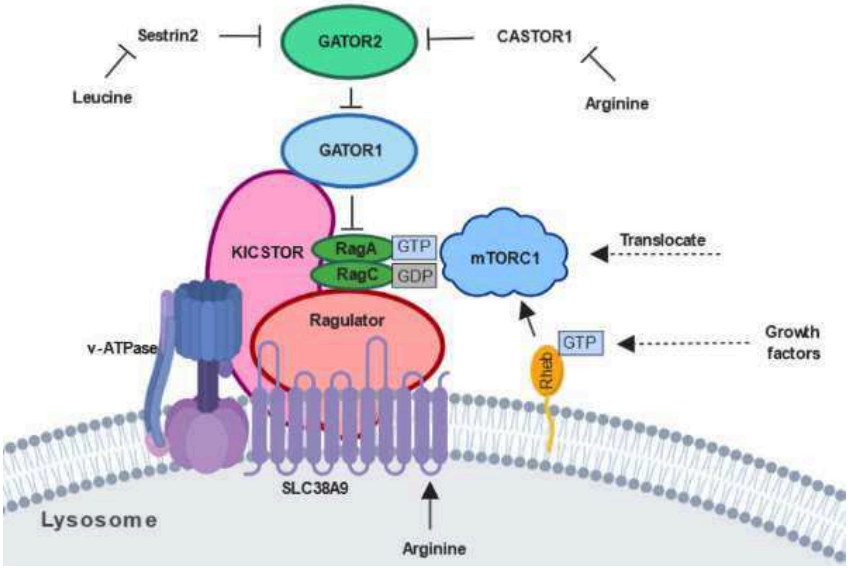

Adapted from Saxton et Sabatini, 2017

Figure N. Scheme of the complex of regulation of mTORC1 at the lysosome.

The presence of AAs is sensed both at the lysosome and in the cytosol. AAs are present in the lysosome due to autophagy or after dietary-proteins are degraded. On the lysosomal membrane, in contact with the Ragulator/Rags complex, there is a v-ATPase that interacts with the AAs' transporter SLC38A9. When AAs are present inside the lysosome, the SLC38A9 promotes their transport and activates the v-ATPase, which in turn triggers the Ragulator/Rag and, therefore, the mTORC1 activation.

The cytosolic AAs are sensed by the complex GATOR1 (composed by DEPDC5, Nprl2 and Nprl3), tethered to the lysosomal membrane, possibly in proximity of Ragulator, through KICSTOR complex (composed by Kaptin, ITFG2, C12orf66 and SZT2). GATOR1 functions as a GAP for Rags proteins, thus inhibiting mTORC1 activation. GATOR2 (consisting in Mios,

WDR24, WDR59, Seh1L and Sec13), inhibitor of GATOR1, is bound and inhibited by Sestrin2 only when the latter it is not bound to leucine. Whereas, in case of AAs presence, Sestrin2 binds leucine and detaches from GATOR2 releasing its inhibition. GATOR2 is now free to bind and stop GATOR1, finally allowing the activation of mTORC1. Sestrin2 seems to work not only as a direct and acute sensor of leucine, but its transcription is also induced upon stress caused by prolonged AAs starvation, through the transcription factor activating transcription factor 4 (ATF4).

As Sestrin2 for leucine, the cellular arginine sensor for mTORC1 (CASTOR1) is able to bind arginine and inhibit GATOR2 in a mechanism that resembles the one of Sestrin2.

Apart from these central pathways that converge on GATOR2/1, other mechanisms of AAs' sensing have been reported which do not necessarily involve inhibition of GATOR2. Nevertheless, this is still a very hot topic and many laboratories are still actively looking for understanding it, given the several questions still open.

2.2.4. Downstream of mTORC1

The understanding of nutrient availability, through the sensing of growth factors, AAs and glucose, and of cellular energy and oxygen presence, allows mTORC1 to activate the metabolism according to the circumstances. In fact, as seen in the previous paragraph, once the conditions are favorable, mTORC1 gets activated and stimulates anabolism, i.e. macromolecule biosynthesis, glycolysis and oxidative respiration, while disfavoring catabolic reactions such as autophagy (Figure O). In order to do so, it acts through several direct and indirect mechanisms, by phosphorylating different substrates.

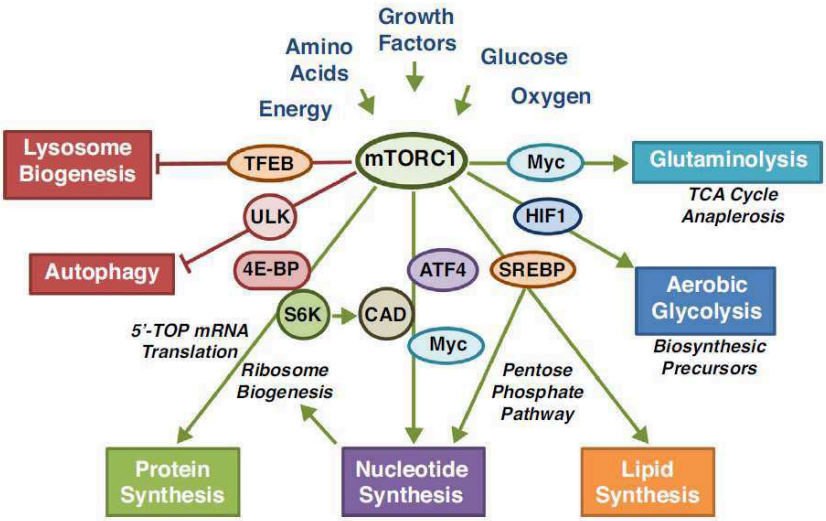

Adapted from Ben Sahra et Manning, 2017

Figure O. mTORC1: input and output signals

Schematic view of the inputs and outputs of mTORC1 and of its principal substrates in the network.

Protein translation. mTORC1 regulates protein translation mainly through two substrates: eukaryotic initiation of translation factor 4E binding protein 1 (4E-BP1) and ribosomal protein S6 kinase (S6K).

Protein translation is a process that requires a very high amount of energy; therefore, it is very tightly regulated, especially at the initiation step (Ma et Blenis, 2009). The initiation of translation starts with the binding of eukaryotic initiation of translation factor 4E (eIF4E) to the 5'-cap structure of the mRNA (Figure P). This recruits the rest of the eIF4F complex, composed by eIF4E, eIF4G and eIF4A (and eIF4B), which in turn engages the pre-initiation complex formed by other eIF factors (i.e. eiF3 and the Ternary complex) and the 40S subunit (the small) of the ribosome. Once these complexes are formed, the scanning of the mRNA to find the AUG and the following translation can occur.

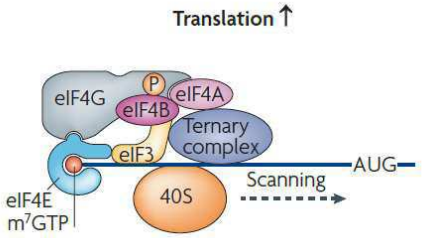

Adapted from Ma et Blenis, 2009

Figure P. Translation initiation complex

The binding of eIF4E to the 5'-cap results in the recruitment of rest of the eIF4F complex that allows translation initiation to proceed.

4E-BP1 is an inhibitor of translation initiation (Figure Q, left). In its hypophosphorylated form, it binds to eIF4E preventing its interaction with the rest of the eIF4F complex. When mTORC1 gets activated, it phosphorylates 4E-BP1, surely on $Thr^{37/46}$, and this primes 4E-BP1 to be phosphorylated (either from other unknown kinases or from mTORC1 itself) on $Ser^{65/83/101/112}$ and on Thr^{70}. Hyperphosphorylated 4E-BP1 detaches from eIF4E and allows the recruitment of the eIF4F complex and of the pre-initiation complex to the 5'-UTR and the starting of translation.

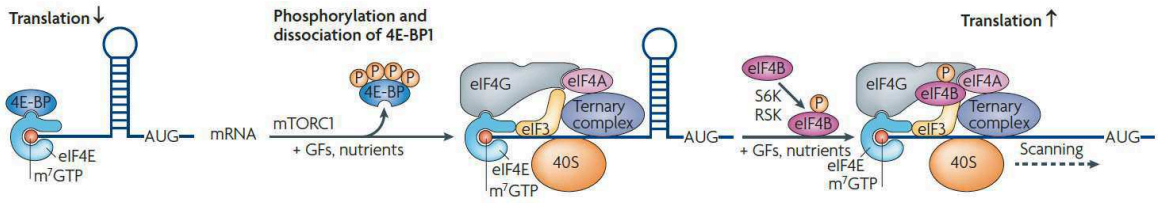

Adapted from Ma et Blenis, 2009

Figure Q. mTORC1-dependent regulation of translation initiation

mTORC1-dependent phosphorylation of 4E-BP1 provokes the detachment of 4E-BP1 from the 5'-cap and the recruitment of eIF4E and of the rest of the eIF4F complex to start the scanning of the AUG. The 5'-UTR of the majority of the mRNAs forms secondary structure that prevent the scanning. S6K-dependent phosphorylation of eIF4B activates the helicase activity of the eIF4B/eIF4A complex to allow translation.

The mRNA bases of the 5'-UTR (untranslated region) tend to self-pair forming secondary structures that prevent the correct binding of the translation machinery on the mRNA and the

consequent scanning. For this reason, the eIF4A subunit of the eIF4F complex possesses RNA-helicase activity to linearize the 5'-UTR, although with a low efficiency (Figure Q, right). A cofactor for eIF4A is eIF4B, whose function is to stimulate the RNA-helicase activity of eIF4A. eIF4B is post-translationally modified by S6K through phosphorylation on the Ser^{422}, modification that has been proven to increase the efficiency of eIF4A activity (Holz et al., 2005).

S6K exerts a role on protein translation also through phosphorylation-mediated degradation of programmed cell death 4 (PDCD4), an inhibitor of eIF4B (Dorello et al, 2008), and through binding of S6K1 Aly/REF-like target (SKAR), a component of the exon-junction complex that increases the yield of translation of pre-spliced mRNA (Ma et al., 2008).

Lipid and nucleotide synthesis. In order to sustain cell growth, the cell must increase its membrane and increase the mass and the number of organelles like the mitochondria, the Golgi and the endoplasmic reticulum. In order to do so, mTORC1 activates important controller of lipid biosynthesis as sterol responsive element binding protein (SREBP). SREBP is activated indirectly by S6K1 (Duvel et al., 2010) or through mTORC1-dependent inhibitory phosphorylation of Lipin1, a phosphatidic acid phosphatase that also acts in the nucleus to inhibit SREBP target gene expression (Peterson et al., 2011). This metabolic shift promoted by mTORC1 is also correlated with a shift from oxidative phosphorylation to glycolysis, to create intermediate metabolites for biomass production. This is done primarily through the increase in translation of hypoxia inducing factor 1 α (HIF1α), which drives the expression of several glycolytic enzymes.

Another process that is important to sustain cell growth and, especially, during cell proliferation, is the synthesis of nucleotides. Ribosomes contain ribosomal RNA (rRNA) that comprise around the 50% of the cellular nucleotides; therefore, the increase in nucleotide synthesis not only is important during DNA replication or for mRNA transcription, but also for ribosome biogenesis and protein synthesis (Ben-Sahra et Manning 2017). Nucleotide precursors are either uptaken from the external environment or synthetized *de novo*. mTORC1 has been shown to upregulate the *de novo* pyrimidine and purine synthesis in different ways. Activation of SREBP drives an upregulation of the pentose phosphate pathway (PPP), which allows the formation of NADPH for energy and of Ribose-5-phosphate, precursor of both

purine and pyrimidine (Ben-Sahra et al., 2016). Moreover, induction of Myc promotes the expression of many enzymes in the purine/pyrimidine pathways (Liu et al., 2008). mTORC1 also increases the translation of activating transcription factor 4 (ATF4), a transcription factor important for endoplasmic reticulum stress response, that also stimulates the transcription of enzymes of the mitochondrial tetrahydrofolate (m-THF) pathway. This pathway leads to the transformation of Serine in Formate, intermediate in the purine synthesis (Ben-Sahra et al., 2016). Finally, mTORC1 is able to fine tune the nucleotide *de novo* synthesis in response to nutrient availability. In fact, nutrients promote the mTORC1-dependent activation of S6K1 that phosphorylates and boosts the activity of the enzyme carbomoyl-phosphate synthetase 2/aspartate transcarbamylase/dihydro-orotase (CAD), enzyme responsible for the first three steps of the pyrimidine synthesis (Ben-Sahra et al., 2013; Robitaille et al., 2013).

Catabolism inhibition. To induce cell growth, the activation of an anabolic state must be correlated with an inhibition of catabolism. In normal conditions, autophagy and ubiquitin-proteasome system (UPS) are the major pathway controlling protein turnover and are also important to produce energy and building blocks in case of nutrient deprivation. mTORC1 inhibits autophagy directly through the phosphorylation of unc5-like kinase 1 (ULK1), Ser/Thr kinase which complexes with other proteins triggering autophagy initiation. Under nutrient deprivation, AMPK promotes autophagy by directly activating ULK1 through phosphorylation of Ser^{317} and Ser^{777}. When mTORC1 is active, though, it prevents ULK1 activation by phosphorylating it on Ser^{757} and disrupting its interaction with AMPK (Kim et al., 2011).

mTORC1 has also been shown to regulate autophagy at later stages through the phosphorylation of UV radiation resistance-associated gene product (UVRAG), to inhibit autophagosome maturation (Kim et al., 2015). It also decreases, further in the autophagic flux, the fusion between the autophagosome and the lysosome by blocking lysosome biogenesis. One of the major factors responsible for transcription of genes involved in lysosome biogenesis is transcription factor EB (TFEB). mTORC1 sequesters TFEB into the cytosol by phosphorylation on Ser^{142}, preventing its nuclear entrance and avoiding the generation of new lysosomes (Settembre et al., 2012).

The UPS is responsible for the majority of protein degradation in the cell. Recently, two groups have shown contrasting evidence of the action of mTORC1 on the proteasome. In fact,

mTORC1 inhibition has been connected with an increase of proteasomal degradation through inhibition of extracellular signal-regulated kinase 5 (ERK5) (Rousseau et Bertolotti, 2016). On the other hand, sustained mTORC1 activation increases nuclear factor erythroid-derived 2-related factor 1 (NRF1), that induces transcription of proteasomal component and therefore boosts protein turnover (Zhang et al., 2014). The contrasting results may reflect a different demand of the cell in the two contexts: when mTORC1 is inhibited, the cell needs to compensate the lack of amino-acids pool with a rapid degradation of proteins through both autophagy and UPS, therefore activating the proteasome; conditions of mTORC1 hyperactivation, however, highly increase the anabolism of the cells, thus the need to activate the proteasome to generate energy for sustainment. Further data are needed to understand the important relationship between the UPS and mTORC1.

We can conclude that by increasing anabolism and decreasing the catabolism of cellular components, mTORC1 induces the use of diet-derived molecules and energy to build new macromolecules to sustain growth.

2.2.5. mTORC2

The second complex formed by mTOR is much less known compared to mTORC1. According to the knowledge so far, mTORC2 seems to be activated only through the insulin/PI3K signaling (Figure R). mTORC2 regulatory subunit mSin1 contains a phosphoinositide-binding domain (PH domain), which allows its detachment from mTORC2 and the recruitment to the membrane in case of activation of the insulin signaling pathway (Liu et al., 2015).

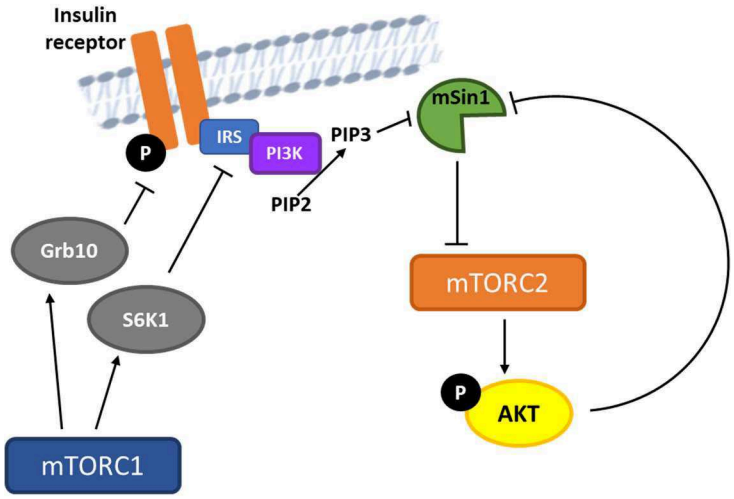

Adapted from Saxton et Sabatini, 2017

Figure R. mTORC2 activation

mTORC2 activation through the Insulin/PI3K pathway and the retrograde negative control of mTORC1 on mTORC2.

Once mSin1 is at the membrane, mTORC2 can be fully activated. It is still not clear how mTORC2 is activated, although it might be activated at the level of the ribosomes downstream PI3K activation (Zinzalla et al., 2011). After its activation, mTORC2 can phosphorylate and activate Akt, which in turn seems to likely actuate a positive feedback loop on mTORC2 by phosphorylating and inhibiting mSin1 (Yang et al., 2015).

Interestingly, the activation of mTORC1 results in a concomitant and direct negative feedback on mTORC2 signaling. In fact, Grb10 and S6K1, direct substrates of mTORC1, have been shown to inhibit the PI3K activation by, respectively, inhibiting the insulin/IGF-1 receptor and phosphorylation-dependent degradation of insulin receptor substrate 1 (IRS-1) (Hsu et al., 2011; Yu et al., 2011; Shah et al., 2004; Harrington et al., 2004). This feedback inhibition has a great importance in understanding why rapalogues (analogues of rapamycin used in clinics) do not work as anti-cancer treatment as expected. In fact, the activation of mTORC2 that occurs after treatment with mTORC1 specific inhibitors, confers a pro-survival and proliferative stimulus to the cells.

Principal substrates of mTORC2 are Akt, SGK, PKC and PKA, all member of the AGC kinase family (from the name of the first kinases of this family identified, PKA, PKG and PKC), known to play key roles in relevant intracellular signaling pathways. The majority of these kinases

need a double phosphorylation event: one on the regulatory T-loop domain, through autophosphorylation or by another AGC kinase, the phosphoinositide-dependent kinase 1 (PDK1); and a second, not always necessary, by other kinases on the C-tail docking site.

The most known substrate of mTORC2 is Akt. Akt (aka PKB) is activated by membrane translocation and by two different phosphorylation events (Su et Jacinto, 2012): upon growth factor stimulation, the PIP3 produced by PI3K provokes the recruitment of Akt at the membrane where it is phosphorylated on Thr^{308} by PDK1; this phosphorylation is necessary and sufficient to activate the catalytic activity of Akt towards substrates as TSC2 and glycogen synthase kinase 3 (GSK3). However, a second phosphorylation on Ser^{473} by mTORC2 is needed to sensitize Akt to other substrates such as forkhead box O1/3 (FOXO1/3) and this phosphorylation is particularly elevated in cancer. Through its substrates, Akt induces cell proliferation, survival, motility and growth, conferring a great growth advantage to cancer cells.

The first mTORC2 substrate to be identified was protein kinase (PK) Cα (PKCα), a regulator of the actin cytoskeleton (Jacinto et al., 2004; Sarbassov et al., 2004). In more recent years, many other members of the PKC family, all involved in cytoskeletal regulation, have been reported to be mTORC2 targets (Gan et al., 2012; Li et Gao, 2014), suggesting a central role of mTORC2 in regulating cell shape and migration. Another AGC kinase regulated by mTORC2 is serum and glucocorticoid-induced kinase 1 (SGK1), protein that regulate ion transports through the control of the activation of ion channels (Garcìa-Martinez et Alessi, 2008).

In conclusion, mTORC2 stimulates proliferation, cytoskeletal remodeling, migration, survival and ion transport and its activity is tightly regulated by mTORC1 through negative feedback loops.

2.3. mTOR-independent TSC

The central and wide role of mTORC1 and the strong phenotype mTORC1-related in Tsc1 or Tsc2 loss of function mutants, made complicated to study the mTORC1-independent effects of TSC1 and TSC2. Nevertheless, in the literature there are some examples of non-canonical functions of TSC1 and TSC2. The strength of these studies is very debated, due to the difficulty

in proving the mTORC1-independence. For example, the use of rapamycin to discriminate if an effect is dependent or independent of mTORC1 can be misleading, because not all the mTORC1 branches are equally inhibited by rapamycin (Kang et al., 2013).

Regarding actions of TSC1 or TSC2 non-mediated by mTORC1, it has been shown that TSC1 colocalizes with the centrosome in dividing and non-dividing cells (Astranidis et al., 2006). Centrosomes are the main microtubule organizing centers, fundamental to form the mitotic spindle during mitosis and to be the basal body of primary cilia in interphase. Mouse embryonic fibroblasts (MEFs) lacking Tsc1 or Tsc2 showed longer cilia, more centrosomes and more ciliated cells (Hartman et al., 2009). Interestingly, rapamycin treatment could restore the primary cilium length in MEFs but failed to reduce the frequency of ciliation. A link between TSC and primary cilia length has been shown by other groups in mice and zebrafish (Bonnet et al., 2009; Armour et al., 2012; DiBella et al., 2009). In zebrafish the primary cilium lengthening was reverted upon treatment with rapamycin or deletion of S6k1, but no increase in the number of ciliated cells was observed (Yuan et al., 2012-Table S1). The hypothesis of a mTORC1-independent control of ciliogenesis is, thus, yet to be confirmed.

Another putative exclusive role of TSC proteins is in endocytosis control. Tsc2 deficient cells have been shown to have enhanced micropinocytosis independent of autophagy and insensitive to rapamycin (but sensitive to Torin1, an active site inhibitor of mTOR kinase) (Filippakis et al., 2018). This role in micropinocytosis seems to be mediated by class 3 PI3K, a class of PI3K involved in regulation of autophagy and endocytosis, that is, therefore, hypothesized to be activated downstream of TSC2 independently of mTORC1. The increased uptake in Tsc2 KO cells, that have low levels of autophagy, suggests that these cells have the ability to sustain their increased anabolism by taking energy and molecules from the medium through micropinocytosis.

An intriguing link is the one between the TSC complex and mTORC2. mTORC2 activity is severely blunted in TSC-deficient cells. This is, only partially, explained by the existence of the negative feedback loop exerted on mTORC2 by mTORC1, because prolonged treatment with rapamycin and downregulation of Raptor or Rheb failed to restore fully the phosphorylation of Akt on Ser^{473} (Huang et al., 2008; Huang et al., 2009). Moreover, the TSC1/TSC2 complex was found to physically associate with mTORC2 and not with mTORC1. This link between

mTORC2 and the TSC complex is yet to be further studied, because it could provide an evidence of the control of the actin cytoskeleton by the TSC complex through mTORC2.

Finally, TSC1 and TSC2 have been proven to act independently on the formation of the TSC complex. For example, TSC2 can act as a transcription repressor for epiregulin (*EREG*), gene that encodes for a member of the epidermal growth factor family found upregulated in TSC lesions (Pradhan et al., 2014). Furthermore, the overexpression of TSC1 in Eker rat cells lacking Tsc2 could suppress cell proliferation by concomitant downregulation of cyclin E (Miloloza et al., 2002). Finally, the most conserved domain, between yeast (*S. pombe*) and humans, in TSC1 is not the TSC2 binding domain (T2-ID), but rather an N-terminal putative transmembrane region (TM) and a C-terminal coiled-coil (CC) are very well evolutionary conserved (Figure S). This could imply that other functions of TSC1, associated with the two previously mentioned domains, might be important and independent on the formation of the complex with TSC2.

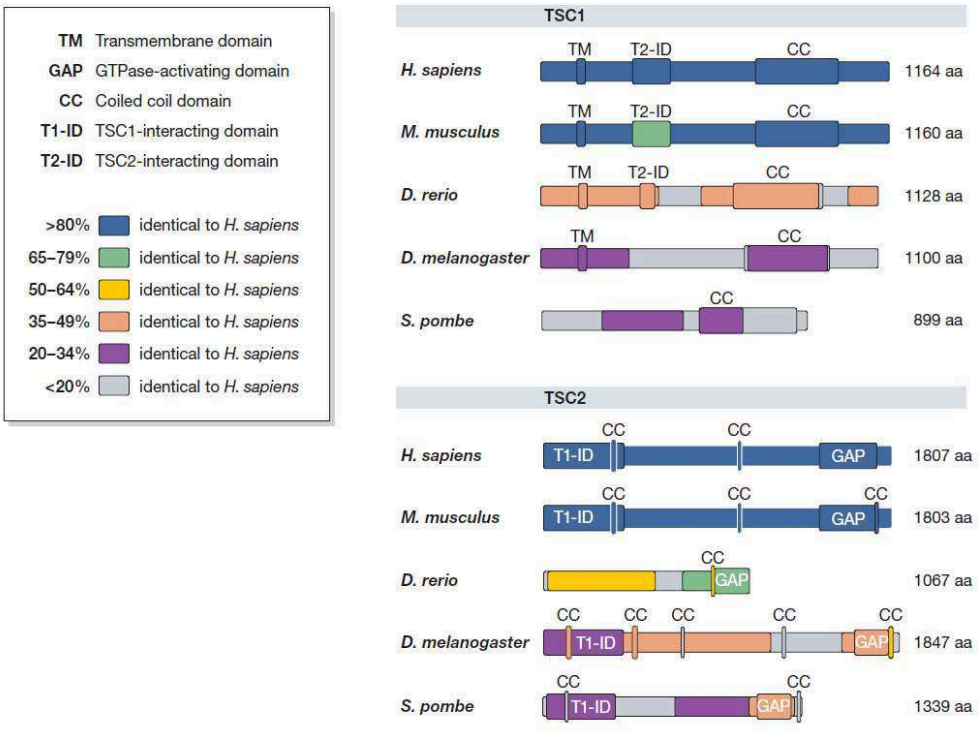

Adapted from Neuman et Henske 2011

Figure S. Evolutionary conservation of TSC1 and TSC2 structure

Regions and levels of homology, relative to human TSC1 and TSC2 proteins in the indicated organisms, shown by color coding, with relative legend.

In conclusion, a comprehensive understanding of the roles of TSC1 and TSC2 will help to provide better treatment for TSC patients and to complete our knowledge of the pathway. Nevertheless, as mentioned at the beginning, the study of the non-canonical functions of TSC is complicated by the difficulties in separating the phenotype associated with mTORC1 hyperactivation and rather the one associated with TSC1 and TSC2 exclusively. Studies with inhibitors of the catalytic site of mTOR (Torin1) and TSC1/TSC2 mutants lacking domains not-involved in the TSC complex formation will help to dichotomize the functions downstream TSC1 or TSC2 inactivation.

3. S6 Kinases

The most widely used histological marker on TSC-related biopsies and, in general, to detect mTORC1 activation, is the phosphorylation of ribosomal protein s6 (RPS6 or S6). RPS6 is a protein that composes the small 40S ribosomal subunit of eukaryotic ribosomes. It was discovered 40 years ago to be the first ribosomal proteins to undergo post translational modification, specifically phosphorylation, induced by growth factors, nutrients or mitogens (Gressner et Wool, 1974; Thomas et al., 1980).

The first RPS6 kinase identified was isolated from *Xenopus l*. oocytes and it was a 90 kDa protein termed p90 ribosomal protein S6 Kinase (RSK). However, two studies few years later (Blenis et al., 1987; Jeno et al., 1988) brought up another protein as the major kinase responsible for S6 phosphorylation in mouse and chicken: a 70 KDa protein with a very high specificity and efficiency of phosphorylating S6, named p70 S6 kinase (p70S6K, now S6K1). P70S6K is coded by a gene named *RPS6KB1* that produces 3 isoforms: the p70S6K; the p85S6K, generated by a second translation start codon, contains 21 AAs more than the isoform at 70kDa at its N-terminus (Grove et al., 1991); the p31S6K, a splicing variant without any catalytic domain (Karni et al., 2007). Some years later a protein homologous to the p70S6K was found and the two proteins were thereafter named S6K1 and S6K2 respectively (Gout et al., 1998; Shima et al., 1998; Lee-Fruman et al., 1999).

3.1. S6Ks: AGC Kinases

S6Ks belong to the family of the AGC kinases. This family of proteins is composed by 60 kinases so far described, that therefore account for almost the 12% of the known kinases (518). The AGC kinases are Ser/Thr kinases very highly conserved throughout evolution and that therefore play very important roles in a wide plethora of intracellular signaling pathways (Su et Jacinto, 2011).

The majority of the AGC kinase have the peculiarity to be activated by two subsequent phosphorylation events and S6Ks follow this pattern. The mechanism of activation of S6K1 has been studied and it is depicted in Figure T.

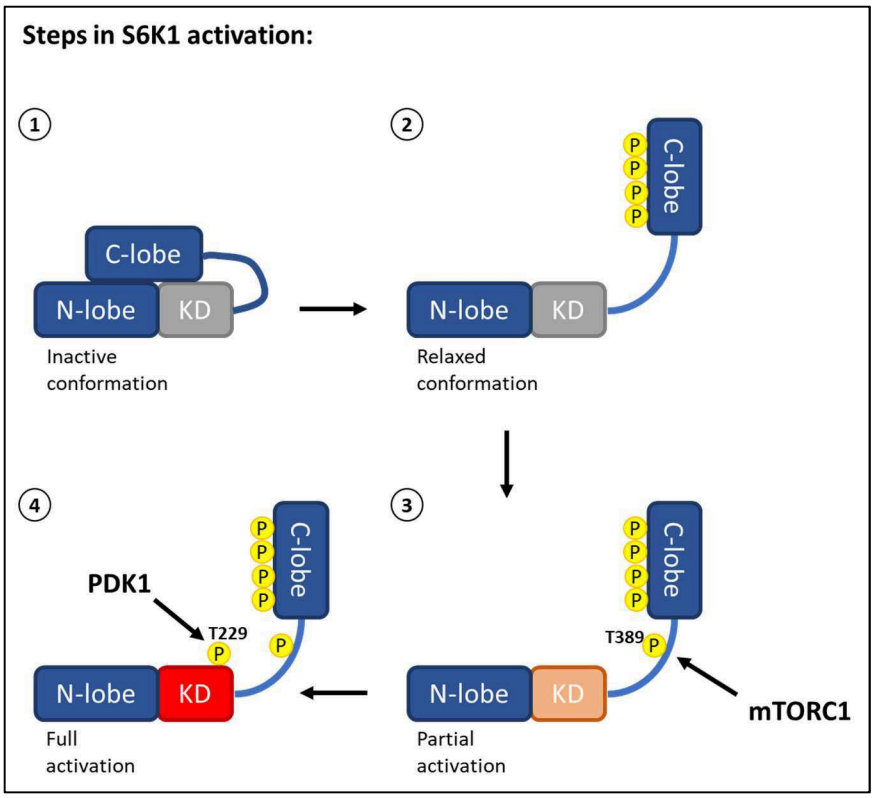

Adapted from Pavan et al., 2016

Figure T. Model of regulation of S6K1 activity by multi-site phosphorylation.

The S6K1 and S6K2 structure is composed by an N-terminal domain also called N-lobe, followed by a kinase domain (KD) linked by a linker region to the C-terminal C-lobe. It has been proposed that in its inactive state S6K1's C-lobe interacts with the N-lobe in a close conformation, which does not allow substrate recognition (Figure T1). Mitogens were shown to induce different consequential phosphorylation, starting from the first ones on the C-terminal region on $Ser^{411/418/421/424}$ (Figure T2). These events relieve the inhibition correlated with the closed state and enable the access to the linker region. The phosphorylation of this four Serine is anyway not critical for the full activation of the kinase. In fact, no kinase has been proven to phosphorylate these sites *in vivo* and mutation of all the four Serine into Alanine (phospho-deficient) or into Glutamic acid (phospho-mimetic) or deletion of the C-terminus only modestly affected the basal activity of S6K1 (Magnuson et al., 2012 and references therein). Once the conformational state becomes open, the N-terminal region, containing a sequence of 5 AAs (FDIDL), is rendered accessible. This sequence is a very

conserved TOR signaling (TOS) motif, important for mTORC1 recognition and interaction with its substrates. The accessibility to the TOS motif and the open conformation lead to the phosphorylation of the Thr^{389}, located in the linker region, by mTORC1 (Figure T3). The phosphorylation of this residue is necessary for S6K1 to be recognized and fully activated by PDK1 through phosphorylation on Thr^{229} (Figure T4). A similar mode of activation has been proposed also for S6K2, with different residues phosphorylated by mTORC1 and PDK1: Thr^{388} and Thr^{229} respectively.

Thus, the phosphorylation event mediated by mTORC1 is what determines the activation of S6Ks in response to nutrients and growth factors.

Intriguingly, a study in 2013 (Kang et a., 2013), established S6K1 as a "low quality" substrate of mTORC1. Some sites phosphorylated by mTORC1 are more sensitive than others to rapamycin and this led to the hypothesis that mTORC1 has a preference for some sites more than others. What Sabatini's lab demonstrated is that the Thr^{389} of S6K1 is very sensitive to rapamycin and to AAs starvation and it is also phosphorylated less efficiently than, for example, the $Thr^{37/46}$ of 4E-BP1, an mTORC1 site very insensitive to rapamycin. They conclude that, in order to switch off the growth program, mTORC1 substrates are hierarchically organized allowing a fine tuning of its substrates. In particular S6K1 is a substrate very sensitive to the lack of "pro-growth" stimuli. This highlights the importance of understanding the role of this protein especially in pathological situations in which it is constitutively activated and not-responding to nutritional state changes.

S6K1 is by far the most studied between the two S6Ks, because it is the one responsible for the strongest phenotypes associated with cell growth, it is often upregulated or mutated in cancer and because it has some exclusive substrates not shared with S6K2. Therefore, for the rest of the chapter, I will focus on S6K1, with only some references to S6K2.

3.2. Phenotypes associated with loss of S6K1

Deletion of S6K1 in animals is associated with some fascinating phenotypes that we are still trying to fully understand. The most visually striking is a reduction in total body size. Both in *Drosophila* (Montagne et al., 1999; Figure U1), in mice (Shima et al., 1998; Pende et al., 2000; Pende et al., 2004; Figure U2) and in *C. elegans* (Selman et al., 2009; Figure U3), the inactivation of *S6k1* (or of its orthologues *dS6k* in *Drosophila* and *rsks-1* in *C. elegans*) causes a decrease in body size.

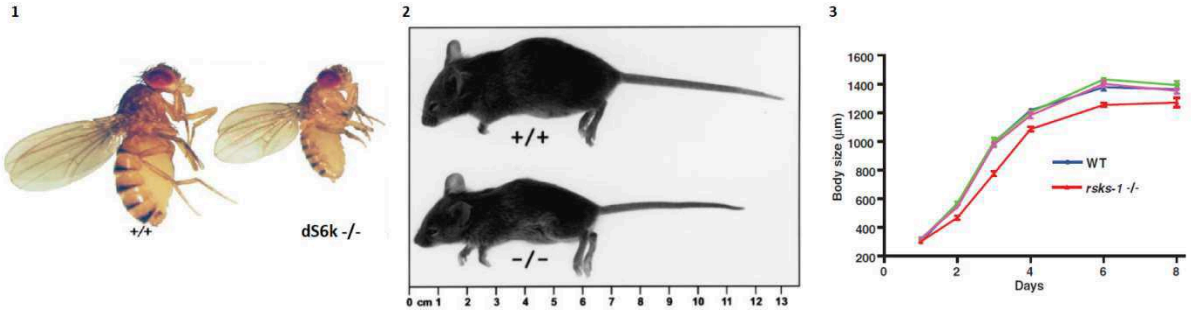

Montagne et al., 1999; Shima et al., 1998; adapted from Selman et al., 2009

Figure U. Reduced body size in S6K1-mutant

Body size is reduced in models of S6K1 loss in Drosophila (1), mouse (2) and C.elegans (3).

Most notably, this decrease in organismal size is not correlated with a proliferative defect or developmental delay, but rather with a reduction in cell size that generates a proportional decrease of the size of all organs. A smaller cell size for these animals was reported for pancreatic β-cells (Pende et al., 2000), for muscle cells (Ohanna et al., 2005) and for adipocytes (Um et al., 2004), with no evidence of an effect of S6K2 (Pende et al., 2004; Ohanna et al., 2005).

This reduction of cell size was correlated with reduction of plasmatic insulin levels (Pende et al., 2000), increased sensitivity to glucose and insulin (Um et al., 2004), preference in burning fat instead of using glucose and a mild AMPK-activating energy stress (Um et al., 2004; Aguilar et al., 2007). Intriguingly, all these metabolic changes in S6K1 mutants are the same that occur in animals treated with rapamycin or under caloric restriction (Harrison et al., 2009; Kenyon 2005), suggesting that is S6K1 the translator of nutrient abundance into a pro-growth status

both at the cellular and organismal level and that its absence is interpreted by the body as a scarcity of resources for growth.

In culture, only proliferation and not size of *S6k1* KO cells is sensitive to rapamycin (Ohanna et al., 2005) whereas only the size and not the proliferation of 4E-BP1/2 double KO (dKO) cells is sensitive to ATP-competitive mTOR inhibitors (Dowling et al., 2010), leading to the hypothesis that mTORC1 controls proliferation mostly through 4E-BP1 and growth through S6K1.

S6K1 mutant mice are also unsusceptible to insulin resistance and obesity induced by high fat diet (HFD). The first is explained by the fact that S6K1 is involved in the negative feedback on the insulin-PI3K signaling through inhibitory phosphorylation of the signaling transducer insulin receptor signaling 1 (IRS-1) (Um et al., 2004; Tremblay et al., 2007; see previous sub-chapter 2.2.5). In this way, *S6k1* KO cells can still remain sensitive to insulin signaling without development of type 2 diabetes.

On the other hand, the scientific community is still trying to understand the exact mechanism by which loss of S6K1 protects against age- and HFD-induced obesity. Some possible explanation are that, in general, lack of S6K1 set the organism as if it was in caloric restriction, so there is decrease insulin production, due to decrease in pancreatic β-cells (Pende et al., 2000), and an increase usage of fatty acid rather than glucose that are not accumulated into adipocytes but instead used for energy (Um et al., 2004; Aguilar et al., 2007). Moreover, decreased adipogenesis has been documented in mice lacking S6K1 (Carnevalli et al., 2010). However, the decreased pancreatic β-cell size and the impaired adipogenesis are probably not enough to explain the striking effect of S6K1 whole body deletion. Actions on the central nervous system (CNS) have been hypothesized, especially in the hypothalamus, where the appetite control is exerted (Cowley et al., 2001). A study by Guan's lab in 2009 showed a rapamycin-sensitive increase in appetite and, consequentially, body weight in animals devoid of Tsc1 in the anorexigenic hypothalamic neurons, due to an increase in release of leptin (Mori et al., 2009). However, the anorexigenic hormone leptin induces increase in hypothalamic mTORC1/S6K1 activity to induce satiety and inhibition of mTORC1 activation after leptin treatment prevent the decrease in food intake (Cota et al., 2006). In the same way, overexpression of constitutively active S6K1 or of a dominant negative S6K1, respectively decrease or increase food intake and body weight, showing that leptin signaling through mTOC1/S6K1 in the hypothalamus modulates energy balance toward a leaner phenotype

(Blouet et al., 2008). It is, therefore, possible a role of mTORC1/S6K1 at the hypothalamic level, with consequential control of the food intake, but more research will be required to unravel the complex regulations behind it.

Finally, another phenotype of the S6K1 KO mice is a retardation of aging and age-related pathologies. Similarly to the decreased body size, also the lifespan increase seen in S6K1 KO animals is equivalently observed in organisms under caloric restriction or treated with rapamycin (Fontana et al., 2010 and references therein). From yeast to primates, organisms that undergo caloric restriction age slower and an inhibition of the mTOR pathway is always observed. The proposed mechanisms by which mTOR/S6K1 axis drives aging are many. mTORC1 inhibition of autophagy can be detrimental, because autophagy would help to clear damaged proteins and organelles such as mitochondria, the accumulation of which are also associated with aging and age-related diseases. However, no convincing evidence of a role of S6K1 on autophagy have ever been reported, excluding this mechanism as possible explanation for longer lifespan in *S6k1* KO animals. S6K1 loss, though, could decrease the protein translation and, in this way, decrease the proteotoxic and oxidative stress related with age-dependent accumulation of misfolded proteins (Selman et al., 2009; Saxton et Sabatini, 2017). Moreover, mTORC1 can promote cellular senescence, an irreversible cell-cycle arrest in G1 that occurs also in aging tissues and that is correlated with age-related disease (Alimonti et al., 2010; Zhang et al., 2013). Our lab recently published the discovery of a new substrate of S6K1, the DnaJ homolog subfamily C member 2/Zuotin Related Factor 1 (DNAJC2/ZRF1) (Barilari et al., 2017). ZRF1 is found hyperphosphorylated in Tsc1 KO MEFs with increased mTORC1 signaling and its phosphorylation decreases upon deletion of S6K1. ZRF1 is a DNA-binding protein shown to antagonize the polycomb repressive complex 1 (PRC1) and retrieve the inhibition on the Ink4a/ARF locus encoding pro-senescence proteins as p16 (Richly et al., 2010). It is therefore possible that a delay in onset of senescence in tissues and in stem cells pool, important to be kept able to regenerate damaged tissues, is one of the mechanisms by which mTORC1 and S6K1 inhibition lengthen the lifespan and improve age phenotypes.

Being obesity one of the greatest risk factor for aging and age-related pathology, especially cardio-vascular and endocrinological, the organismal metabolic alteration caused by inhibition of mTORC1/S6K1 signaling, which mimics a diminished calorie intake, could be at the basis of the retarded age-related decline in physiological and cellular functions.

3.3. Known substrates of S6K1

For decades RPS6 has been thought to be the only substrate of S6K, although, still now, we don't know the effects of the phosphorylation of this ribosomal protein. The activation of S6K1 and the increase in phosphorylation of RPS6 was initially connected with the translation of a subclass of mRNAs called the 5'-terminal oligopyrimidine (TOP), all characterized by the presence of an oligopyrimidine tract at their 5'-terminus. TOP mRNAs consist in about 90 transcripts that encode multiple component of the translation apparatus, as ribosomal proteins and translation factors (Meyuhas et Dreazen, 2009). Rapamycin selectively blocks the mitogen-associated induction of this class of mRNAs and a study showed that rapamycin would act through S6K1-dependent RPS6 phosphorylation to exert this inhibition (Jefferies et al., 1997). In addition, RPS6 is located near the mRNA/tRNA-binding site, at the interface between large (60S) and small (40S) subunit of the ribosome, in a position considered ideal to alter the translation efficiency (Nygard et al., 1982). Nevertheless, multiple studies afterwards confuted the involvement of both S6Ks and RPS6 in the translation of 5'-TOP mRNAs and in general in the basal translation efficiency of cells and mice (Shima et al., 1998; Pende et al., 2004; Barth-Baus et al., 2002; Mieulet et al., 2007).

Although not involved in 5'-TOP mRNA translation, RPS6 remains an important substrate of S6Ks. In fact, MEFs derived from mice with both *rpS6* alleles mutated to prevent the phosphorylation of the 5 mitogen-stimulated residues (*rps6*$^{P-/-}$), display a reduction in cell size that is not worsened by rapamycin treatment (Ruvinsky et al., 2005). RPS6 is therefore considered an important S6K1 substrate in control of the cell size. However, the persistence of phosphorylated RPS6 in *S6k1* KO mice due to the presence of S6K2, the lack of phenotype associated with S6K2 loss and the absence of difference between *S6k1* KO and *S6k1/S6k2* dKO mice (Pende et al., 2004; Ohanna et al., 2005) and, finally, the normal size of *rps6*$^{P-/-}$ mice (Ruvinsky ey al., 2005; data from our lab), suggest that the phosphorylation of RPS6 is not the only event that contribute to the definition of cell size downstream of S6K1.

In more recent years, new substrates of S6K1 have been brought into light, breaking the initial dogma that would place RPS6 as its only substrate. Up to now, 26 substrates have been accepted as direct targets of S6K1 and the processes they are involved in are various. We could summarize them into four classes (Figure V): substrates involved in protein synthesis and

mRNA processing; in metabolic program and anabolism; in cell survival; in negative feedback on the insulin signaling.

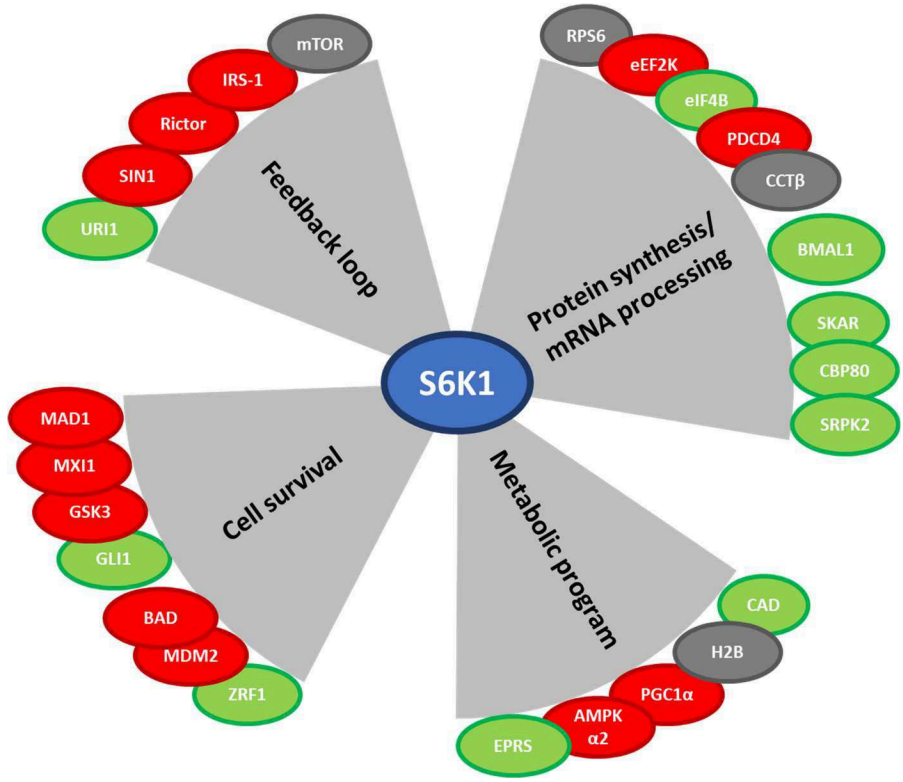

Figure V. Substrates of S6K1

Substrates of S6K1 divided in classes accordingly to the function of their S6K1-dependent phosphorylation.

3.3.1. Protein translation

Numerous S6K1 targets are involved in translation at different levels. In general, S6K1 increases the efficiency of translation at the level of the initiation, through stimulation of eIF4B/A helicase complex both directly (activation of eIF4B) and indirectly (inhibition of PDCD4, inhibitor of eIF4A) (see previous sub-chapter 2.2.4). S6K1 also phosphorylates and inactivates eukaryotic elongation factor 2 (eEF2) kinase (eEF2K), therefore increasing the activity of eEF2, factor that catalyze the codon shifting (the codon-by-codon scanning of the ribosomes on the mRNA) during translation elongation (Wang et al., 2001). Through phosphorylation of chaperonin containing TCP-1 subunit β (CCTβ), S6K1 seems to promote

protein folding of the nascent polypeptide, although it is still unknown the specific effect exerted by this phosphorylation event (Abe et al., 2009).

Moreover, S6K1 plays a role in the regulation of mRNA processing, for example by phosphorylating Serine/Arginine rich protein kinase 2 (SRPK2), protein that, when phosphorylated, induces the splicing and increase the stability of lipogenic transcripts by regulating splicing factors activity (Lee et al., 2017). It has been reported an S6K1-dependent induction of the splicing also through stimulation of the cap-binding complex (CBP), which promotes splicing by co-transcriptionally binding the 5'cap of the nascent mRNA. It was shown a connection between S6K1 phosphorylation of the 5'cap-binding protein 80 (CBP80), protein of the CBP, and induction of mRNA splicing, but the mechanisms are still unknown (Wilson et al., 2000). Newly spliced mRNAs are then translated more efficiently than the non-spliced ones when SKAR, phosphorylated by S6K1, binds the exon junction complex together with S6K1 (Ma et al., 2008).

Finally, a new role of S6K1 in the circadian clock-regulated translation has been uncovered very recently (Lipton et al., 2015). The circadian clock synchronizes cellular function to light/dark cycle by coordinating rhythmic transcription via a transcription-translational feedback loop. In mammals, brain muscle aryl nuclear translocase like-1 (BMAL-1) is a transcription factor that, together with circadian locomotor output cycles kaput (CLOCK), accumulates with a daily rhythmicity allowing the cyclic expression of clock-controlled genes (CCG), genes involved in many aspects of physiology, metabolism and behavior. Sahin's lab discovered that BMAL-1 also control cyclic translation by rhythmically associate with the translation machinery during the peak of its accumulation, only when phosphorylated by S6K1.

3.3.2. Metabolic program

Along with the regulation of protein synthesis efficiency, S6K1 induces an increase in lipid production and storage. In general, S6K1 induces lipid biogenesis by acting on SRPK2, as mentioned earlier, but also by inhibiting AMP-activated protein kinase (AMPK) (Dagon et al., 2012) and PPARγ coactivator 1 α (PGC1α) (Lustig et al., 2011), two potent inductor of fatty acid oxidation, gluconeogenesis and mitochondrial biogenesis. Another substrate involved in

adipogenesis is the newly founded γ glutamylprolyl-tRNA synthetase (EPRS) (Arif et al., 2017). Phosphorylation of EPRS by S6K1 induces its release from the aminoacyl tRNA multisynthetase complex and promotes the noncanonical functions of EPRS beyond protein synthesis. Phospho-deficient EPRS mice displayed a decrease in body weight, in adipose tissue mass and increase in lifespan, similarly to S6K1 deficient mice. In adipocytes, phosphorylated EPRS induces the expression of a fatty acid transporter at the plasma membrane, to increase the lipid uptake, highlighting the importance of this substrate in the metabolic control of the mTORC1/S6K1 axis. S6K1 induces adipogenesis also through phosphorylation of the histone 2B (H2B) and subsequent recruitment of a methylase which induces the de-repression of lipogenic genes (Yi et al., 2016).

Furthermore, also the nucleotide synthesis is partially controlled by S6K1, through the phosphorylation of CAD, which boosts the efficiency of pyrimidine synthesis after nutrient stimulation (see previous sub-chapter 2.2.4).

3.3.3. Feedback loop

Physiologically, it is important to counteract the mitogen-stimulated signaling, to balance it and to regulate its actions. An important node in this respect is S6K1. Through phosphorylation, S6K1 promotes the inhibition and the degradation of IRS-1, the transducer of the insulin receptor activation. In addition, S6K1 shuts-down mTORC2/Akt axis by phosphorylating Rictor (Treins et al., 2010; Dibble et al., 2009) and mSin1 (Liu et al., 2013), two subunits of the mTORC2. Although the effect of these phosphorylation is still debated, a phospho-mimetic mutant form of mSin1 is unable to interact with mTOR and Rictor and, inversely, a phospho-deficient form leads to increased Akt phosphorylation. Similarly, Rictor seems inhibited by S6K1 phosphorylation.

S6K1 is involved, also, in a negative feedback of its own pro-survival signaling. Through phosphorylation, it induces the disassembly of the complex between its substrate, the mitochondrial unconventional prefoldin RPB5 interactor (URI), and the protein phosphatase 1 γ (PP1γ), that, thus, activates a PP1γ-dependent negative feedback program that decreases S6K1 activity, in this way altering the threshold for apoptosis (Djouder et al., 2007).

At last, S6K1 can phosphorylate mTOR itself on two different residues, however the function of this modification is still unknown (Holz et Blenis, 2005).

3.3.4. Cell survival

Although S6K1 has mainly been linked to cell size control, there are reports of a function of this kinase also on cell survival related to cancer. mTORC1 and mTORC2 mediated signaling are very frequently mutated in many cancer types, due to direct mutations or to mutations in several of their upstream regulator. Amplification of the S6K1 gene *RPS6KB1* has been associated with poor prognosis in breast cancer (Barlund et al., 2000). However, the evidence for S6K1 signaling in mTOR-mediated tumorigenesis remain limited (Magnuson et al., 2012).

S6K1 acts on programmed cell death (apoptosis) and on cell-cycle arrest through phosphorylation of murine double minute 2 (MDM2), ZRF1 and Bcl-2/Bcl-X_L-antagonist causing cell death (BAD). MDM2 is the E3 ubiquitin ligase responsible for the degradation of p53, the pro-apoptotic and pro-senescence protein activated in case of DNA damage. In case of DNA damage, S6K1 partially contributes to the activation of p53 response by phosphorylation-dependent retention of MDM2 in the cytosol, therefore explaining, by some extent, the increase in senescence and apoptosis observed when the mTORC1 pathway is abnormally active (Lai et al., 2010). S6K1 also controls the p16-dependent senescence induction through activation of ZRF1 (Barilari et al., 2017), concurring in this way to the arrest of the cell cycle. Anyway, the mTOR/S6K1 axis can also promote survival in conditions favorable to growth. Phosphorylation of BAD triggers its degradation and the consequential stabilization of the anti-apoptotic proteins B-cell lymphoma (BCL) XL and 2 at the mitochondria (Harada et al., 2001).

S6K1 contributes also, with other AGC kinases, to upregulate the activity of the well-known oncogene Myc, which triggers sustained proliferation and transformation. S6K1 has been shown to concur in the inhibition of two Myc antagonists, MAX interactor 1 (Mxi1) and MAX dimerization protein 1 (MAD1), in this way sustaining Myc-dependent gene expression (Huang et al., 2018; Zhu et al., 2008).

In the absence of a functioning TSC complex, the AGC kinases controlled by mTORC2 are downregulated through the retrograde negative control in which S6K1 has a central role. In

this condition, S6K1 is predominant and it can compensate the lack of activity of the other AGC kinases by phosphorylating some of their substrates. This has been shown for example for glycogen synthase kinases 3 (GSK3s), kinases with a very wide plethora of known substrate that regulate, among many others, the Wnt and the insulin pathways. GSK3s have been known for long time to be inactivated downstream insulin/PI3K signaling because phosphorylated by Akt. However, in condition of Tsc1 or Tsc2 loss, it is S6K1 that phosphorylates GSK3s (Zhang et al., 2006). This aberrant phosphorylation leads to decreased GSK3s activity and phosphorylation of downstream substrates and contributes to the growth factor-independent proliferation of TSC-deficient cells. This finding opened the investigation of the cross-talk and substrate-sharing among the AGC kinases, many of which share overlapping features in their substrate specificities and that may contribute to the complex landscape of many diseases, like the Tuberous Sclerosis complex.

Finally, developmental programs may be regulated by S6K1 in specific conditions. Glioma-associated oncogene homolog 1 (GLI1) is a transcription factor downstream of sonic hedgehog (SHH) pathway regulating gene involved in survival and differentiation. It has been shown that, in esophagus cancer, GLI1 can be activated through a mechanism dependent on tumor necrosis factor α (TNFα)/mTORC1/S6K1 (Wang et al., 2012). S6K1-mediated phosphorylation of GLI1, independently on SHH signaling, protects GLI1 from degradation and sustains its oncogenic function.

RESULTS

mTOR controls cell division rate and orientation in Tuberous Sclerosis Complex Polycystic Kidney through distinct effectors

Martina Bonucci [1,2,3,4], Nicolas Kuperwasser [1,2,3,4], Serena Barbe [1,2,3], Vonda Koka [1,2,3], Delphine de Villeneuve [1,2,3], Chi Zhang [1,2,3], Nishit Srivastava [5], Xiaoying Jia [6], Matthew P. Stokes [6], Frank Bienaimé [1,2,3], Marco Pontoglio [1,2,3], Fabiola Terzi [1,2,3], Benedicte Delaval [7], Matthieu Piel [5], Mario Pende [1,2,3,*]

[1] Institut Necker-Enfants Malades, 14 rue Maria Helena Vieira Da Silva, CS 61431, Paris, France

[2] Inserm, U1151, Paris, F-75014, France

[3] Université Paris Descartes, Sorbonne Paris Cité, Paris, France

[4] These authors contributed equally to this work

[5] Institut Curie, PSL Research University, CNRS, UMR 144, F-75005 Paris, France

[6] Cell Signaling Technology INC, 3 Trask Lane, Danvers MA 01923

[7] CRBM, CNRS, Univ. Montpellier, 1919 Route de Mende, 34293, Montpellier, France.

Keywords: TSC, oriented cell division, mTOR, S6 kinase, polycystic kidney

Running title: Misoriented cell division in TSC

* Correspondence: M. Pende
14 Rue Maria Helena Vieira Da Silva, CS61431, 75993 Paris cedex 14
Tel: 0033 1 72 60 63 86, Fax: 0033 1 72 60 64 01. **E-mail: mario.pende@inserm.fr**

Abstract

Polycystic kidney disease is commonly observed in Tuberous Sclerosis Complex (TSC) and other genetic disorders causing mechanistic Target of Rapamycin (mTOR) hyperactivation. However, the mechanistic targets of mTOR responsible for cyst formation remain to be established. Here we show that S6 kinase 1 (S6K1) selectively controls the orientation, but not the rate, of cell division in *Tsc1*-mutant kidney. mTOR/S6K1 hyperactivity alters the axis of cell division, due to centrosome mispositioning in both interphase and mitotic cells. This defect is revealed *in vivo* and in sphere formation assays *in vitro*, where cells rely on cell junctions to correctly define centrosome localization. Mass spectrometry-based phosphoproteomic screenings for novel S6K1 substrates display an enrichment of differential phosphorylation in proteins involved in cell adhesion and the actomyosin cortex. Afadin, an actin binding protein regulating the Nectin and Cadherin adhesion systems, is phosphorylated by S6K1 and accumulates with E-cadherin at the apical surface in *Tsc1*-mutant cells, to the detriment of lateral junctions. Phospho-deficient Afadin rescues sphere formation in *Tsc1* and *Afadin* knockout cells. Our data reveal key alterations in centrosome positioning and cell adhesion contributing to cyst formation in a context of hyperactive mTOR and S6K1.

Introduction

Tuberous Sclerosis Complex (TSC) is a genetic disease resulting from inherited or *de novo* mutations in the *TSC1* and *TSC2* genes (Henske et al., 2016). The *TSC1* and *TSC2* gene products associate in a complex with GTPase-activating protein (GAP) activity toward the Ras homolog enriched in brain (Rheb) protein (Menon et al., 2014). As a consequence of TSC1/TSC2 loss-of-function mutations, the GTP-loaded form of Rheb constitutively activates the mTOR kinase complex 1 (mTORC1) at lysosomal membranes. Since mTORC1 is a master regulator of growth (Saxton and Sabatini, 2017), TSC patients suffer from hamartomas, which are benign tumours in multiple organs, including the brain, the lung, the heart, the skin and the kidney (Henske et al., 2016). In addition, TSC patients display an increased risk of developing polycystic kidney disease, which may represent an important morbidity and mortality factor. Additional types of familial kidney cancers, including Birt-Hogg-Dubé (BHD), Cowden and Peutz-Jeghers diseases share the common features of mTOR activation and cyst formation, before cancer onset (Schmidt and Linehan, 2016). An intense remodelling of the tissue underlies polycystic kidney development (Bergmann et al., 2018). Increased proliferation rates are accompanied by alterations in cell survival, fluid secretion, dedifferentiation, alterations in basement membrane and epithelial cell polarity. Which molecular targets of the mTORC1 pathway promote the various cellular responses in the context of kidney polycystosis, remains largely unknown.

The kidney phenotype of TSC mutants has distinctive features as compared to the mutants associated with most cases of autosomal dominant polycystic kidney disease (ADPKD), the polycystin 1 and 2 gene (*Pkd1* and *Pkd2*) mutants (Armour et al., 2012; Bergmann et al., 2018; Pema et al., 2016). As observed in mouse models, *Pkd1*/*Pkd2* mutants in tubular

epithelia develop an early-onset and severe polycystic disease during late embryogenesis-early postnatal life when proliferation rates are maximal (Ma et al., 2013; Pema et al., 2016). Conversely, the cysts in *TSC* mutants start to form after postnatal day 20 (P20), when the wave of proliferation in wild type tissues is over (Armour et al., 2012; Pema et al., 2016; Yeung et al., 1994; Zhou et al., 2009). The tubular epithelium lining the cysts is flat in *Pkd1*/*Pkd2* mutants, while it has a columnar appearance in *TSC* mutants. Finally, the length of primary cilium, apical hair-like sensor organelle, is normal in *Pkd1*/*Pkd2* mutants, while *TSC* mutant cells display longer cilia. Despite these differences, a crosstalk between the two pathways has been documented (Pema et al., 2016). *TSC*-mutant mouse embryonic fibroblasts (MEFs) have altered expression or trafficking of the *Pkd1* or *Pkd2* gene products (PC1 or PC2), respectively. In addition, the deletion of one allele of *Pkd1* aggravates the cystic phenotype of *TSC1*-deficient kidneys, while transgenic overexpression of *Pkd1* alleviates the disease. Taken together, these data suggest that TSC1/2 and PC1/2 may act in parallel pathways regulating cyst formation, with some extent of possible cross-talk.

One main physiological function of mTORC1 is to integrate diet nutritional cues and promote intracellular macromolecule biosynthesis, i.e. the synthesis of lipids, proteins, glycogen, RNA and DNA (Saxton and Sabatini, 2017). In addition, mTORC1 also suppresses autophagic degradation of intracellular material. Among the known substrates of mTORC1, Eukaryotic Translation Initiation Factor 4E Binding Proteins (4E-BPs) repress cap-dependent translation; Lipin1 is a phosphatidic acid phosphatase involved in transcriptional regulation of lipogenic genes; Unc-51 Like Autophagy Activating Kinase 1 (Ulk1) and Autophagy And Beclin 1 Regulator 1 (Ambra1) are involved in the control of autophagic flux; Transcription Factor EB (TFEB) regulates lysosome biogenesis; Growth Factor Receptor Bound Protein 10 (Grb10) mediates the negative feed-back control of insulin signaling; S6 kinase 1 (S6K1) regulates cell

size. However, in the pathological setting of TSC, the molecular targets of mTORC1 that mediate cyst formation are elusive.

Genetic epistasis experiments in the fruit fly *Drosophila* were the first to assess the contributions of TOR and S6K in the overgrowth of TSC mutants (Gao et al., 2002). Homozygous mutant clones for *Tsc1* or *Tsc2* in *Drosophila* ommatidia are 90% larger as compared to wild type. The genetic deletion of *Tor* causes a dramatic atrophy in both wild type and TSC-mutant backgrounds, shrinking the cells to 25% of wild type. *S6k* deletion has a mild effect on wild type flies, but it is sufficient to blunt TSC-mutant overgrowth, precisely to the level of wild type cells. These data suggest two important considerations: first, TOR deletion affects multiple targets involved in growth control, causing severe cellular atrophy; second, the overgrowth phenotype of TSC mutants may be exquisitely sensitive to S6K inhibition, which may represent a valuable strategy to rescue TSC mutants to a wild type function. While *Drosophila* flies contain a single *S6k* gene, mammalian cells express two homolog proteins, S6K1 and S6K2 (Pende et al., 2004; Shima et al., 1998). They belong to the AGC family of serine/threonine kinases and may share redundant targets with Akt1-3, 90 KDa Ribosomal Protein S6 Kinase 1-4 (Rsk1-4), Serum/Glucocorticoid Regulated Kinase 1-3 (SGK1-3) and protein kinases C (PKC) family members (Pearce et al., 2010). However, mTORC1 specifically activates S6K1 and S6K2 by phosphorylating their hydrophobic motif, whereas the hydrophobic motifs of Akt, SGK and PKC are phosphorylated by mTORC2 (Sarbassov et al., 2005). Since TSC mutations selectively up-regulate mTORC1 (Menon et al., 2014), S6Ks are the only AGC kinases activated in this disease, with the other kinases being unaffected or suppressed as a consequence of the negative feed-back regulation of mTORC1 on mTORC2 (Huang and Manning, 2009). S6Ks are also extremely sensitive to mTORC1 inhibition by the allosteric inhibitor rapamycin, while the phosphorylation of other mTORC1 substrates may be

relatively spared (Kang et al., 2013). Taken together, these evidences prompt the investigation of the role of S6K in TSC pathological lesions and in rapamycin-sensitive responses.

Here we take advantage of a well-characterized model of *Tsc1* deficiency in kidney tubular cells, leading to polycystic kidney in adult mice (*Ksp-Cre; Tsc1*$^{fl/fl}$) (Pema et al., 2016). We show that mTORC1 controls two distinct branches of tubular cell proliferation, an S6K1-independent branch regulating the rate of cell proliferation, and an S6K1-dependent branch regulating the oriented cell division. *S6k1* deletion in the *Tsc1* mutant background re-establishes the correct centrosome position and axis of cell division. We show that the S6K1 phosphoproteome is enriched in proteins involved in the cell adhesion system and actomyosin cortex. We identified a novel S6K1 substrate, Afadin, that contributes to the regulation of cell adhesion and oriented cell division.

Results

To score for the epistatic interaction of TSC1 and S6K1 in polycystic kidney development, we compared *Ksp-Cre; TSC1$^{fl/fl}$* with *Ksp-Cre; TSC1$^{fl/fl}$; S6K1$^{-/-}$* kidneys. *Ksp-Cre* expression drives recombination of the floxed alleles in kidney tubular cells starting from E14.5 (Shao et al., 2002). As previously reported (Armour et al., 2012; Pema et al., 2016; Zhou et al., 2009), *Tsc1* deletion resulted in kidney overgrowth and cyst formation (Fig. 1A). At post-natal day 90 (P90), the kidney to body weight ratio was 14-fold greater than wild type (Fig. 1B), due to both fluid retention and increased cell mass. Strikingly, kidney overgrowth of *Tsc1* mutants was blunted by the deletion of *S6k1*. The cystic index was sharply reduced by S6K1 inactivation (Fig. 1C). This led to a net amelioration of kidney function, as assessed by plasmatic urea levels that returned to wild type levels in the *Ksp-Cre; Tsc1$^{fl/fl}$; S6k1$^{-/-}$* mice (Fig. 1D). Since increased cell proliferation might contribute to cyst formation, cell cycle progression was scored using an anti-Bromodeoxyuridine (BrdU) antibody, after pulsing with BrdU, and an anti-phospho Histone H3 antibody. The former labels S-phase cells and the latter mitotic cells. As shown in Figure 1E-1H, *Tsc1* deletion caused a more than 20-fold increase in tubular cell proliferation as compared to the wild type. Surprisingly, *S6k1* inactivation did not affect the proliferation rate of *Tsc1*-mutant cells. Taken together, our data indicate that it is possible to separate cell proliferation and cyst formation, consistent with previous reports (Sharma et al., 2013). In the absence of S6K1, mTORC1 still up-regulates the rate of cell proliferation, though the tubular cells are protected against tubular enlargement.

These data were confirmed in another mouse line of *Tsc1* deficiency, the *CAGGCre-ER^{TM}; Tsc1$^{fl/fl}$* mouse line. As we previously reported (Liang et al., 2014), this ubiquitously expressed and temporally regulated Cre transgenic allele allows the mosaic deletion of *Tsc1*

in every tissue after tamoxifen (TM) administration at P1, thus recapitulating the multisystemic features of the disease. In kidneys, the overgrowth phenotype of *CAGGCre-ER^{TM}; Tsc1$^{fl/fl}$* mice was milder as compared to *Ksp-Cre; Tsc1$^{fl/fl}$* mice, leading to a 9-fold increase in kidney to body weight ratio at P90 (Supplementary Fig. S1A). Of note, *S6k1* deletion was sufficient to partially blunt the overgrowth, while the combined deletion of *S6k2* did not further reduce kidney weight. Consistent with the *Ksp-Cre; Tsc1$^{fl/fl}$* model, *S6k1* deficiency did not have an impact on tubular cell proliferation, but rather on cyst formation (Supplementary Fig. S1B and S1C). Thus, S6K1 activity, but not S6K2, is a major determinant of cyst formation in mouse models of TSC.

In *Tsc1* mutant kidneys, tubular enlargement was not observed prior to 20 days of postnatal life. However, in a precystic stage at P20, S6K activity was already up-regulated in *Ksp-Cre; Tsc1$^{fl/fl}$* kidneys, as assessed by immunoblot analysis using phospho-specific antibodies against S6K substrates (Fig. 2A). *S6k1* deletion impaired phosphorylation of Carbamoyl-Phosphate Synthetase 2, Aspartate Transcarbamylase, And Dihydroorotase (CAD) and Rapamycin-insensitive companion of mTOR (RICTOR), which were previously reported to be S6K1-specific substrates (Fig. 2B) (Ben-Sahra et al., 2013; Treins et al., 2010). The phosphorylation of ribosomal protein S6 (RPS6) was not completely inhibited in *S6k1*-deficient kidneys, owing to the presence of S6K2 (Pende et al., 2004). Consistent with the TSC1/2 complex selectively controlling mTORC1 (Huang and Manning, 2009), Akt phosphorylation by mTORC2 was not increased in TSC mutants, but there was a tendency to a decrease due to the negative feedback of mTORC1 on mTORC2. These changes in mTORC1/S6K1 signal transduction correlated with changes in cell size, a reliable read-out of S6K1 activity (Ohanna et al., 2005; Pende et al., 2000). The tubular cell surface at P20 was larger in *Tsc1* mutants, an effect that required S6K1 activity (Fig. 2C and 2D)

Next, we asked whether *Tsc1* deletion altered the orientation of cell division in this pre-cystic stage displaying high mTORC1/S6K1 activity. We therefore set up a tissue clearing method to measure in 3D the angle of cell division relative to the tubular lumen at P20. After tissue clearing, mitotic cells were labelled using phospho-histone H3 staining and the tubular lumen was decorated using fluorescent wheat germ agglutinin (WGA) lectin. As expected, in wild type cells, the axis of cell division was parallel to the tubular lumen, as in the great majority of mitotic events the angle of cell division relative to the lumen was less than 20°(Fig. 2E and 2F). However, in TSC mutants the angle of cell division was random, with an even distribution from 0° to 90°. *S6k1* inactivation re-established the correct distribution of cell division angles observed in wild type tubules. Therefore, the S6K1-dependent misorientation of cell division in TSC mutants is an early, possibly causative, event concurring to cyst formation.

To dissect the cellular and molecular alterations underlying misoriented cell division by hyperactive mTORC1/S6K1 signaling, mouse Inner Medullary Collecting Duct-3 (mIMCD3) cells were edited using CRISPR-Cas9 in order to delete the *Tsc1* gene alone or in combination with the *S6k1* (Supplementary Fig. S2A). As expected, the *Tsc1* deletion conferred constitutive activation of the mTORC1 pathway even in serum- and nutrient-free conditions, as shown by the band-shift of the mTORC1 substrate 4E-BP1 and the phosphorylation of the S6K1 substrates Rictor and Eukaryotic Translation Initiation Factor 4B (eIF4B) (Fig. 3A). In addition, mTORC1 activation in the *TSC1*-deficient cell line suppressed mTORC2-dependent Akt phosphorylation, due to the negative feed-back loop of mTORC1/S6K1 on mTORC2. Thus, the different branches of mTOR signaling are properly regulated by the TSC1 and S6K1 transduction elements in these newly-edited kidney cell lines.

mIMCD3 cells can be maintained in culture for many passages due to SV40 transformation and are commonly used to study epithelial polarity, as they form polarized spheres after 5 days in Matrigel-embedded cultures from a single cell. Cell number was equivalent among the three genotypes at the end of the 5 day-sphere assay, with an average of around 16 cells corresponding to 5 doubling times (Fig. 3B). Cell volume and cell mass were measured in single cells by fluorescent dye exclusion (Cadart et al., 2014). *Tsc1*-deficient cells in G1 phase displayed a 20% increase in both cell volume and cell mass that required S6K1 activity (Fig. 3C and 3D). Accordingly, cell density, defined as the ratio of cell mass and cell volume, did not differ among the three genotypes (Supplementary Fig. S2B). The differences in cell volume among the three genotypes were also observed at the beginning of mitosis and during the mitotic round-up (Supplementary Fig. S2C). Heterogeneity in the volume of the two daughter cells was not observed, as the ratio of the larger and smaller daughter cell was equivalent in the three genotypes (Supplementary Fig. S2D). Taken together, while *Tsc1*-deficient mIMCD3 cells do not have a proliferative advantage over wild type in an SV40-transformed background, they display an S6K1-dependent increase of volume and mass throughout different phases of the cell cycle, consistent with the cell size measurements in kidneys (Fig. 2C). As shown in Fig. 3E and 3F, the length of the primary cilia correlated with cell size, and was longer in *Tsc1*-deficient cells as compared to wild type and *Tsc1/S6k1*-deficient cells.

The sphere formation assay in 3D-Matrigel embedded cultures of mIMCD3 cells is a common method to evaluate oriented cell division and cell polarity (Giles et al., 2014). Wild type cells embedded in Matrigel formed a polarized sphere, with interphase cells displaying a γ-Tubulin-positive centrosome at the apical surface and an Arl13b-positive primary cilium pointing towards the lumen (Fig. 4A). More than 50% of wild type spheres had polarized cilia

after 5 days in culture (Fig. 4B). In contrast, *Tsc1*-deficient cells had a dramatic impairment in sphere formation: primary cilia pointed in different directions while lumens were small and irregular. Strikingly, *S6k1* deletion was sufficient to rescue sphere formation.

Mitotic spindle orientation determines the axis of cell division and maintains planar cell polarity in epithelia (di Pietro et al., 2016). The centrosome duplicates at the end of interphase, close to the apical membrane. The two centrosomes then migrate and relocate to the lateral membranes during mitosis, to then return to the apical surface after cytokinesis. To score for mitotic spindle orientation, centrosomes were labelled with γ-Tubulin antibodies and mitotic phases were recognized by DAPI staining of DNA. In anaphase and metaphase, the centrosomes of wild type cells were correctly positioned at the lateral membranes (Fig. 4C). In the majority of anaphase and metaphase wild type cells, the axis of cell division was perpendicular to the center of the sphere (Fig. 4D). In contrast, in *Tsc1* mutant cells, the spindle axis was misoriented, with frequent cases of a centrosome facing the lumen in mitotic cells. Again, this defect was rescued by the deletion of *S6k1*. Finally, centrosome position was also determined *in vivo* in mutant mice at P20, corresponding to the pre-cystic stage. Co-staining of the centrosomal markers FGFR1 Oncogene Partner (FOP) and γ-Tubulin were used to detect the centrosomes in tubular cells (Fig. 4E) and calculate the angle of intersection with an apico-basal line crossing the center of the nucleus (Fig. 4F). While the centrosome in the majority of wild type tubular cells at interphase was positioned at an angle between 0° and 20°, the centrosome in *Tsc1*-deficient cells was frequently found distant from the apico-basal axis, in a position closer to lateral junctions (Fig. 4E and 4G). Consistent with other measurements in cultured cells, centrosome mispositioning in the TSC kidney also required S6K1 activity.

Centrosome positioning is tightly regulated by cell geometry and influenced by the following factors: i) determinants of the apical complex (aPKC and Par3/Par6); ii) the shape and contractility of the actomyosin cortex; iii) the LGN/NuMA complex which exerts pulling forces for astral microtubules at the cell cortex; iv) the interaction with the basal matrix through the integrin system; v) cell-to-cell junctions through the cadherin system (di Pietro et al., 2016). As a first attempt to dissect the contributions of these factors in the TSC phenotype, the γ-Tubulin-positive centrosome and the Arl13b-positive primary cilium were stained relative to the apical domain detected by Par3 and aPKC antibodies (Fig. 5A and Fig. 5B). *Tsc1*-mutant cells were able to properly locate the apical complex at the interface with the lumen, ruling out the possibility that a defect in the establishment of apical polarity concurs to the mispositioning of the cilia and centrosome.

Then we asked whether *Tsc1* mutants had an intrinsic defect in orienting the mitotic spindle. Single cells were grown on a fibronectin-coated L-shape micropattern. In this system, the cell relies on the integrin system to define the basolateral domain. If there are no defects in the integrin system and there are no intrinsic defects in the actomyosin cortex and mitotic spindle, cell division will be oriented with a fixed angle relative to the L-shaped micropattern (Fig. 5C). TSC mutants performed well in this test, similar to wild type (Fig. 5D). The orientation was slightly affected in *Tsc1/S6k1*-deficient cells, possibly as a result of a smaller cell size and a reduced surface in contact with the fibronectin pattern. Taken together, these data would rather point to a non-cell autonomous defect in TSC1 mutants to correctly position the spindle. This defect is therefore revealed when cells are grown in a soft environment and next to each other, as observed *in vivo* and in Matrigel-embedded cultures. In these conditions, cells mainly rely on cell-cell junctions and adhesion systems to correctly position the centrosome and mitotic spindle.

The published literature on S6K substrates does not readily suggest putative targets involved in centrosome positioning and adhesion cues. Thus, we set out to uncover the S6K1 phosphoproteome by phosphopeptide enrichment coupled with liquid chromatography tandem mass spectrometry (LC-MS/MS) comparison of the *Tsc1*- and *Tsc1/S6k1*- deficient mIMCD3 cells (Rush et al., 2005). The two cell lines were compared in serum- and nutrient-free conditions, which accentuated the sensitivity to the *Tsc1* mutation for mTORC1 signaling (Fig. 3A). To have a broad representation of phosphopeptides, two different methods of phosphopeptide enrichment were performed in parallel. The first method took advantage of commercially available antibodies recognizing phosphorylated serine/threonine (S/T) preceded by arginine (R) residues, a motif commonly recognized by AGC kinases including S6K. We decided to combine an antibody recognizing the RXXS/T motif (where X indicates any amino acid), and an antibody recognizing the RXRXXS/T motif, as their pattern of phosphoprotein detection in western blot was not superimposable (Supplementary Fig. S3). The second method used Fe-NTA Immobilized Metal Affinity Chomatography (IMAC) to enrich for phosphopeptides. 15444 unique phosphopeptides were identified after IMAC enrichment and 1355 after AGC-motif enrichment, with a common subset of 839 phosphopeptides, indicating that the two methods are complementary, allowing broader coverage of the phosphoproteome than either enrichment alone (Table S1). Importantly, the great majority of known S6K substrates were identified and quantified in the analysis (Fig. 6A and 6B, Table S2). Out of 27 S6K substrates reported in the literature in different cell types, 12 were significantly down-regulated in *Tsc1/S6k1*-mutant cells as compared to *Tsc1* mutants from the IMAC screen and 9 from the AGC screen. The combination of the two screens covered more than 50% of reported S6K substrates, highlighting the ability to find target phosphorylation sites of interest using this methodology.

Next, we ran a gene ontology (GO) analysis to evaluate whether the differentially phosphorylated peptides were enriched in specific functional classes over the total phosphopeptides detected in each screen. The AGC-motif screen did not show any significant class due to the limited set of detected peptides. However, the IMAC screen revealed that the GO terms of actin binding, cell junctions, cytoskeleton and alternative splicing were significantly overrepresented in the *Tsc1* Vs *Tsc1/S6k1* differentially phosphorylated peptides (Table S3). To select putative direct substrates of S6K1, we focused on phosphopeptides in both screens that were down-regulated in *Tsc1/S6k1*-deficient cells and that contained an AGC-motif (Fig. 6A and 6B, Table S4). Among the proteins with a function in the regulation of oriented cell division were the following: Afadin, an actin binding protein and adaptor protein regulating the nectin- and cadherin-based adhesion systems (Mizutani and Takai, 2016); Slingshot Protein Phosphatase 1 (SSH1), a phosphatase for the actin binding protein cofilin (Huang et al., 2006); Microtubule Actin Crosslinking Factor 1 (Macf1), a spectraplakin binding actin and microtubules (Ning et al., 2016); Phosphatidylinositol 4-Kinase (PI4K), regulating endocytic trafficking (Graham and Burd, 2011); Myosin Phosphatase-Targeting Subunit 1 and 2 (MyPT1 and MyPT2), myosin phosphatases regulating actomyosin contractility (Ito et al., 2004); Missing In Metastasis Protein (Mtss1), a cortactin-interacting protein (Bershteyn et al., 2010).

Afadin emerged as a prime candidate for follow up validation, as loss-of-function mutants in a kidney tubular cell line displayed defects in sphere formation and oriented cell division comparable to the *Tsc1* deficient cells (Gao et al., 2017). Antibodies recognizing the S6K1-dependent phospho-S1795 site of Afadin are commercially available, allowing site-specific validation of the LC-MS/MS data. Phospho-Afadin levels relative to actin loading control were increased in *Tsc1*-deficient mIMCD3 cells, while the levels in *Tsc1/S6k1*-deficient

cells were comparable to wild type (Fig. 7A and 7B). In addition, pharmacological inhibition of mTORC1 by rapamycin and of S6K1 by LY-2779964 and PF-4708671 decreased Afadin phosphorylation in TSC1 deficient cells after a two-hour treatment. The regulation of Afadin phosphorylation by TSC1 and S6K1 was also confirmed in knock-out mouse kidney extracts (Fig. 7C and 7D). To demonstrate whether S6K1 could directly phosphorylate Afadin in the cell, TSC1/S6K1 deficient mIMCD3 cells were transfected with a point-mutant of S6K1 conferring sensitivity to bulky ATP-analogs (Barilari et al., 2017). The analog-sensitive S6K1 (AS-S6K1) was able to thio-phosphorylate Afadin in a rapamycin-sensitive manner (Fig. 7E), thus demonstrating that Afadin is a novel direct S6K1 substrate in these cells. Since we observed that total Afadin levels correlated with the extent of phosphorylation (Fig. 7A and 7C), we asked whether its phosphorylation state might affect protein stability, as previously proposed (Elloul et al., 2014). As shown in Fig. 7F, cycloheximide treatment revealed that the half-life of Afadin was longer in *Tsc1* versus *Tsc1/S6k1* deficient cells, correlating with phosphorylation status.

To investigate its functional role, Afadin coding gene (*Afdn*) was disrupted using CRIPR-Cas9 in both wild type and TSC1 deficient mIMCD3 cells, followed by lentiviral transduction of wild type (wt) Afadin , serine- to alanine-1795 phosphomutant (S1795A) or vector control (Fig. 8A and supplementary Fig. S4A). Both Afadin constructs were expressed at similar levels and below endogenous levels. In addition, they were correctly localized at the membrane (Fig. 8B). *Afdn* KO and *Afdn/Tsc1* double KO cells had impaired formation of polarized spheres, similar to *Tsc1* KO cells (Fig. 8C, 8D, and supplementary Fig. S4B). Transduction with wt-Afadin and S1795A-Afadin had a similar rescue of sphere formation in *Afdn* KO cells (supplementary Fig. S4B), though the S1795A-Afadin phospho-mutant performed better than wt-Afadin in rescuing sphere formation in the *Afdn/Tsc1* double KO

cells (Fig. 8C and 8D). These data are consistent with the possibility that Afadin phosphorylation in TSC mutants impairs the adhesion system and promotes cell migration, as reported in other systems.

Since E-cadherin is the main adhesion protein in tubular epithelial cells and its function is also regulated by Afadin (Sato et al., 2006), immunofluorescence experiments were performed using E-cadherin and Afadin antibodies after sphere formation. In wild type cells, afadin staining was enriched in adherens junctions at apicolateral domain while E-cadherin staining was more abundant in lateral junctions (Fig. 8E). Strikingly, TSC1 deficient cells displayed an S6K1-dependent accumulation of both Afadin and E-cadherin at the apical domain, concomitant to an attenuation of these adhesion components at the lateral domains.

Discussion

Polycystic kidney disease is a common pathological consequence of hyperactive mTORC1, as observed in TSC and additional inherited diseases including Birt-Hogg-Dubé, Cowden and Peutz-Jeghers syndromes (Schmidt and Linehan, 2016). The mTORC1-driven polycystic kidney has distinctive features, as compared to ADPKD or ciliopathies (Armour et al., 2012; Ma et al., 2013; Pema et al., 2016). Here we identify S6K1 as a direct mTORC1 substrate required for cyst formation. S6K1 mutation affects the orientation but not the rate of cell division in TSC, thus disconnecting the origins of these two alterations of cell division as cause of TSC-related polycystic kidney disease. Centrosome mispositioning, as observed in interphase and in mitotic cells, underlies the defect in oriented cell division. This defect is revealed *in vivo* and in Matrigel-embedded cultures, when TSC cells mainly rely on cell junctions to correctly position the centrosome. By performing an unbiased and comprehensive S6K1-phosphoproteome in the TSC background, we highlight that the phosphopeptides whose expression is S6K1-dependent, mainly belong to the regulators of cell junctions and actomyosin cortex. One of these proteins, Afadin, is a direct S6K1 substrate involved in cell adhesion, migration and oriented cell division.

Previous studies in flies and fishes have already pointed out the involvement of S6K in the overgrowth phenotype of TSC mutants. In Drosophila flies, *S6k* deletion reduces the size of *Tsc1* or *Tsc2* deficient ommatidia to the level of wild type tissue, without causing the severe atrophy observed in TOR mutants (Gao et al., 2002). In Zebrafish Kupffer's vesicles (KV), morpholino-mediated *Tsc1* suppression increases cilia length while decreasing motility, an effect mimicked by S6K overexpression (Yuan et al., 2012). In addition, *Tsc1* mutation may also promote a senescence program, which is delayed by the combined deletion of *S6k1* in mouse embryonic fibroblasts (Barilari et al., 2017). Our data extend these observations to a

pathological condition, by showing that S6K1 regulates tubular kidney cell size and planar cell polarity in a context of TSC-driven cystogenesis. Interfering with other major outputs of mTORC1 activity, such as autophagy inhibition and the up-regulation of cap dependent translation, does not seem to affect cyst formation. The autophagy mutants and the 4E-BP1/4E-BP2 deficient mice do not recapitulate a polycystic kidney phenotype (Le Bacquer et al., 2019; Orhon et al., 2016). We can speculate that the S6K1-dependent phosphoproteome orchestrates a pleiotropic response required for the intense tissue remodeling in polycystic kidneys. S6Ks are the AGC family members that are exquisitely up-regulated in TSC conditions and could take over some of the functions of mTORC2-regulated kinases, such as Akt, SGK and PKC (Huang and Manning, 2009; Zhang et al., 2006). Accordingly, we show that Afadin is phosphorylated by S6K1 in TSC kidney cells, while Akt can regulate Afadin in different conditions (Elloul et al., 2014). In addition, S6Ks might have a specific role in centrosome positioning and planar cell polarity that is not shared by other mTOR targets. Interestingly, S6K2 has been proposed to localize at the centrosome (Rossi et al., 2007). Unfortunately, at this stage the lack of validated S6K1-specific antibodies for immunofluorescence has precluded the unambiguous assessment of S6K1 localization in TSC kidney cells.

In addition, S6K1 might have a prominent role in kidney physiology. S6K1 was shown to drive uninephrectomy (UNX)- and diabetes-induced renal hypertrophy (Chen et al., 2009). In both cases, a stimulation of RNA and protein synthesis and an increase in cell size, with minimum increase in cell number, occurs. Genetic inactivation of S6K1, with no alteration of 4E-BP1 phosphorylation, reverted the hypertrophy caused by both UNX and diabetes, comparable to rapamycin treatment (Chen et al., 2005) and to $RPS6^{P-/-}$ mice (Xu et al., 2015), although the latter would protect for a lesser extent. However, rpS6 phosphorylation did not seem to mediate the overgrowth in TSC kidney. Phospho-rpS6 mutant mice actually

exacerbated the polycystic phenotype of TSC mutants (Wu et al., 2016). Our phosphoproteome study suggests that novel S6K1 substrates, such as Afadin and additional proteins involved in actomyosin regulation and cell adhesion, might have a prominent role on the TSC-related cyst formation, as compared to rpS6. It will be interesting to determine whether S6K1 has a kidney cyst-specific involvement or also plays an important role in other severe pathological manifestations of TSC, such as seizures and autism.

Afadin is a 200 kDa F-actin-binding protein that acts as a crosslinker between the nectin-based adherens junctions (AJs) and the actin cortex (Mizutani and Takai, 2016). Afadin is essential for the formation of the AJs and for the interaction between nectins and E-cadherin. Afadin strengthens the association between the p120-catenin, a negative regulator of E-cadherin endocytosis, and E-cadherin, thus allowing a stabilization of the cadherin- and nectin-based junctions (Sato et al., 2006). Importantly, Afadin has been shown to participate in planar cell polarity and oriented cell division. Accumulation of Afadin at the cell cortex adjacent to the spindle pole contributes to oriented cell division in the renal tubular cells and mice lacking Afadin have misoriented mitosis (Gao et al., 2017). Moreover, during mitosis Afadin can bind to LGN, a protein present at the plasma membrane during mitotic round-up where it links the spindle motor protein NuMA to the actin cortex at the two cellular poles (Carminati et al., 2016). Afadin recruits LGN at the poles in metaphase, mediating its interaction with the cortex and other members of the spindle orienting machinery. These data are consistent with our evidence that Afadin and E-cadherin aberrantly localize at the apical membrane of TSC mutant cells that correlates with centrosome mispositioning in mitosis.

A previous study has revealed that in breast cancer cells, Afadin phosphorylation by Akt promotes Afadin stability and cell migration (Elloul et al., 2014). In addition, Afadin knock-down have demonstrated that one of the Afadin functions is the commitment of the cells to

adhere or to migrate (Elloul et al., 2014; Lorger and Moelling, 2006). In the present study, we show that Afadin phosphorylation by S6K1 in TSC mutant kidney cells also prolongs the protein half-life. It is tempting to speculate that Afadin phosphorylation may somehow represent a switch between migration and adhesion. TSC mutations result in loss of cell adhesion, in part through the control of ezrin and cadherin family members, as well as Rho signalling (Astrinidis et al., 2002; Barnes et al., 2010; Goncharova et al., 2004; Lamb et al., 2000). Afadin may represent an additional target downstream of activated mTORC1 in the regulation of adhesion. We demonstrate that the deregulation of the mTORC1-S6K1-Afadin axis on cell adhesion and centrosome positioning may represent a major contribution for kidney cyst formation.

Materials and Methods

Mice. *TSC1*$^{fl/fl}$ and *Ksp-Cre* mice were obtained from The Jackson Laboratory. The generation and genotyping of *S6k1*-mutant and *S6k1/S6k2*-double mutant mice are described elsewhere (Pende et al., 2004). *S6k1*-mutant mice were first crossed with *TSC1*$^{fl/fl}$ mice and then with *Ksp-Cre* mice. CAGGCre-ER mice were obtained from The Jackson Laboratory and crossed with *TSC1*$^{fl/fl}$ mice as described elsewhere (Liang et al., 2014). All animal studies were approved by the Direction Départementale des Services Véterinaires (Prefecture de Police, Paris, France; authorization number 75–1313) and the ethical committee of Paris Descartes University. Mice were housed in a 12-h light/dark cycle and fed a standard chow. Control mice were Cre-negative littermates of mutant mice.

Reagents. Pharmacological inhibitors were added to cells for the time and at the concentration, as specified. Rapamycin (#1292; Tocris) was dissolved in 100% ethanol (25 mg/ml), aliquoted and stored at -20°C. A 20 nM working solution was prepared in fresh media before use and cells were treated for the indicated time. PF-4708671 (#S2163) and LY2584702 Tosylate (#S7704) were purchased by Selleckchem and were dissolved in 100% DMSO, aliquoted and stored at -20°C. Respectively 10 µM and 1 µM working solution were prepared in fresh media before use and cells were treated for the indicated time.

For *in vivo* treatment, Temsirolimus (LC Laboratories) was dissolved in 100% ethanol (25 mg/ml), aliquoted, and stored at -20°C. 1 mg/ml working solution was prepared in 5% Tween-80, 5% PEG400, and 86% PBS before injection. Mice were injected i.p. with vehicle or temsirolimus (5 mg/kg) every other day for 2 weeks before sacrifice.

Antibodies. For immunoblotting: anti-Rictor (#2114), anti- phospho Rictor Thr1135 (#3806), anti-DNAJC2 (#12844), anti-phospho DNAJC2 (Ser47) (#12397), anti-CAD (#93925S), anti-phospho CAD (Ser1859) (#12662), anti-S6K1 (#2708), anti phospho S6K1 (Thr389) (#9234), anti-phospho Akt (#9271), anti-phospho RPS6 (Ser240/244) (#2215), anti-eIF4B (#3592), anti-phospho eIF4B (Ser422) (#3591), anti-phospho 4E-BP1 (Thr37/46) (#2855), anti-Afadin (for cells) (#13531), anti-phospho Afadin (Ser1795) (#5485) were purchased from Cell Signaling Technology; anti-TSC1 (#sc- 377386) was purchased from Santa Cruz Biotechnology, Inc; anti-β actin (#A5441), anti- α Tubulin (#T5168) and anti-FLAG M2® (1/1000; #F1804) were purchased from Sigma-Aldrich. For immunofluorescence, immunohistochemistry and immunocytofluorescence: anti-Afadin (1/500; #A0224), anti-BrdU (1/200; #BMC9318), anti-γ-Tubulin (1/500; #T5326) and Phalloidin-TRITC (1/500; #P1951) were purchased from Sigma-Aldrich; anti-phospho Histone H3 (Ser10) (1/400; #ab5176) and anti-NuMA (1/200; #ab109262) were purchased from Abcam; rhodamine labeled Dolichos Biflorus Agglutinin (DBA) (1/200; #RL-1032) was purchased from Vector Laboratories; anti-Arl13b (1/400; #17711-1-AP) was purchased from Proteintech; anti-LGN (1/200; #ABT174), anti-PAR3 (1/200; #07-330) were purchased from Merk Millipore; anti-aPKC (1/100; #sc-17781) from Santa Cruz Biotechnology, Inc; anti-FGFR1OP (FOP) (1/200; #H00011116-M01) was from Abnova.

For immunofluorescence after clearing: Fluorescein labeled, succinylated Wheat Germ Agglutinin (WGA) (1/200; # FL-1021S) was purchased from Vector Laboratories; anti-phospho Histone H3 (Ser10) (1/200); anti AQP2-Alexa Fluor ® 488 conjugated (1/200; # sc-515770) was purchased from Santa Cruz Biotechnology, Inc; TO-PRO™-3 Iodide (1/1000; #T3605) from Thermo Fisher Scientific.

Cell culture. The mIMCD3 cell line was purchased from ATCC and were cultured in DMEM (#10566032; Gibco) supplemented with 10% Fetal Bovine Serum, 20 U/ml Penicillin/Streptomycin (#15140122; Gibco) and 1mM Sodium Pyruvate (#11360070; Gibco). For spheroid formation, the protocol used is described elsewhere (Giles et al., 2014). Briefly, cells were trypsinized and dissociated into single cells by mechanically pipetting in trypsin and resuspending in medium. Cells were then diluted to 50,000/ml in 50% normal medium and 50% growth factor-reduced Matrigel (#356230; BD Biosciences) and plated on 8-well slides (LabTek-II #155409; Thermo Scientific) with normal medium added on top. On the following day, the medium was changed to FBS-free DMEM and left till fixation.

For the generation of *Tsc1* and *S6k1* knockout (KO) lines, sgRNA oligos were cloned into pX459 (Addgene #62988) which contains the Cas9 nuclease sequence and a puromycin resistance cassette. For the generation of the *Afadin* KO, sgRNA oligos were similarly cloned into a pGuide vector (containing the human U6 promoter and with a modified scaffold sequence to improve stability). mIMCD3 cells were transfected with 2µg of plasmid using *Trans*IT-X2® (MIR 6003; Mirus Bio). Forty-eight hours later, cells were trypsinized into puromycin (1 ug/ml) selection medium for 2 days and in regular medium thereafter. The colonies were allowed to grow until it was possible to pick them with a filtered tip and were transferred individually into a well of a 96-well-plate. Clones were expanded and verified for the loss of *TSC1*, *S6k1* and *Mllt4* by western blotting. The sgRNAs sequences used to generate the clones for this study are the following: *Tsc1*, 5'-TCT TTG GCC GTC TCT CGT CA-3' (PAM: TGG); *S6k1*, 5'-TTT GAG CTA CTT CGG GTA CT-3' (PAM: TGG); *Afdn*, 5'- CTG AAG TTG TCA TGA AAC GG-3' (PAM: CGG).

Cloning of constructs. The 3x-Flag tagged human Afadin (pCMV-3xAF6) construct was obtained from Dundee University. The mutation of serine 1795 to alanine was performed by

overlapping PCR using the following primers: Forward (5'-CAG AGA CTG TTC gCC CAG GGC CAA GAC GTG TCC AAC AAA G-3') and Reverse (5'-TGG GcG AAC AGT CTC TGC CGC TCT TTA AAG GTC AGG TTC TCT GG-3') and pCMV-3xAF6 as template. After digestion with DpnI, the resulting PCR reaction was transformed into competent *E. coli*. Clones were verified for the presence of the amino acid substitution by sequencing. The pLJM1-Rheb (Addgene) construct was used as the backbone to create the Flag-Neon and Flag-Afadin constructs. The pLJM1-Rheb construct was digested with Nhe1/EcoR1 and a 3x-flag mNeon cassette, amplified by PCR to contain the same restriction sites, was used to replace the Rheb insert. Amplification of the wild type and S1795A Afadin constructs was performed by PCR to include Nhe1 sites at both the 5' and 3' ends. The pLJM1-mNeon construct was digested with Nhe1/Xba1 and replaced with the Afadin PCR constructs. Orientation was verified by digesting.

Lentiviral production. Lentiviruses containing Neon-FLAG, Afadin WT-FLAG or Afadin S1795A-FLAG were generated by transient transfection of the lentiviral vector (plasmid) together with packaging plasmids (pBA.Rev, pTat, pGag/pol, pVSV-G) into HEK293T cells. The supernatant containing lentiviruses was collected, centrifuged, filtered through 0.45µm filter and stored in aliquots at -80°C, or immediately used to infect recipient cells. After two rounds of infection, cells were selected in puromycin (1µg/ml) and further passaged in culture as a bulk preparation for functional assays.

Immunoblotting. Cells and tissues were lysed in NP-40 lysis buffer (20 mM Tris pH 8.8; 138 mM NaCl; 5mM EDTA; 2.7 mM KCl; 20 mM NaF; 5% Glycerol; 1% NP-40- IGEPAL®; #CA-630; Sigma-Aldrich) supplemented with complete protease inhibitor and phosSTOP phosphatase

inhibitor cocktails (Roche). Protein extracts were resolved by SDS-PAGE, transferred to PVDF membranes and incubated with the primary antibodies.

Immunohistochemistry and immunofluorescence. Mouse tissues were fixed in 4% paraformaldehyde (PFA), embedded in paraffin and sectioned at 4 µm. Sections were deparaffinized and hydrated before being incubated in citrate buffer (pH6) till boiling for 3 minutes and then sub-boiling for 10 min. Sections were blocked in 3% normal goat serum, 1% BSA and 0.1% Triton X-100 for 30 min-1h and then incubated with the primary antibodies (or lectins) overnight at 4°C. Next, sections were incubated with biotinylated secondary antibodies and detected with the Vectastain Elite ABC kit (Vector) and DAB chromogen system (DAKO).

For in vivo BrdU pulsing, mice were injected i.p. with BrdU (50 mg/kg) 2 h before sacrifice. The percentage of BrdU incorporation was determined by counting BrdU-positive nuclei on the total number of nuclei among 10 distinct fields in 3 different animals for each condition.

For immunocytofluorescence, cells were grown on coverslips and fixed in 4% PFA (unless otherwise stated). The fixed cells were permeabilized with 0.3 % Triton in PBS; blocked with 5% normal goat serum, 3% BSA in PBS; and incubated with the primary antibodies.

Spheroids in chamber slides were washed twice with PBS containing calcium and magnesium and fixed in ice-cold 4% PFA for 30-45 min at 4°C under agitation. Once the Matrigel was dissolved, spheres were blocked and permeabilized in 7 mg/ml gelatin (porcine skin #G1890; Sigma-Aldrich) and 0.5% Triton in PBS with calcium and magnesium at RT for 1h and then incubated with the primary antibodies diluted in the same blocking/permeabilization buffer overnight at 4°C. Next, spheres were incubated with Alexa Fluor conjugated secondary

antibodies or Phalloidin-TRITC for 4h at RT and then DNA was stained by DAPI within the mounting medium (Vector Labs).

Immunofluorescence slides were analyzed using an ApoTome2 microscope (Zeiss) or a Confocal TCS SP5 (Leica). ImageJ software (National Institutes of Health) or Imaris v 9.2, ImarisXT, Bitplane AG was used for quantification.

Clearing and picture acquisition. Tissue clearing with CUBIC reagents was performed as described (Susaki et al., 2015). Briefly, mice were fixed by transcardial perfusion with 4% PFA, post-fixed at 4°C for 6h and included in agarose to be sectioned with a vibratome (Leica) sagittally at 1 mm. The sections were then incubated in CUBIC-reagent 1 at 37°C for 1 week, washed thoroughly in PBS and then incubated at 4°C for 30 days in primary antibody, lectin and DNA staining described in the text diluted in PBS containing 2% Triton X100 (PBS-2T), adding again the antibody after 2 weeks. Next, sections were incubated with Alexa Fluor ® secondary antibody 488 (1/200), lectin and DNA staining in PBS-T for 2 weeks at 4°. After staining the samples were cross-linked in PBS 4% PFA for 3 hours, then washed thoroughly in PBS before being transfer in Cubic-reagent 2 till acquisition.

Sections were imaged using a Lightsheet Z.1 (Carl Zeiss) with 20x objective.

Measurement of the angle of mitotic division. For analysis of the tissues after clearing the spindle vector VS and the tubular axis vector VT were generated from the coordinates (x, y, z) measured in ImageJ of the nuclei in anaphase and of the tubular staining respectively. Then the angle between the 2 vectors was measured in Excel and plotted using Prism 6 for Windows.

In mIMCD3's spheroids the spindle vector VS was generated from the coordinates of γ-Tubulin staining (x, y, z) of metaphase or anaphase mitosis measured in ImageJ. The midpoint (x^m, y^m, z^m) of Vs was calculated and the center (x^c, y^c, z^c) of each sphere was determined using ImageJ. A radial vector VC was generated from (x^c, y^c, z^c) and (x^m, y^m, z^m). The projected angle between VS and VC was eventually calculated using Excel.

TUNEL assay. TUNEL assays were performed using In Situ Cell Death Detection kit (Roche) according to the manufacturer's instructions.

Cystic index analysis. To quantify the number of cysts, whole kidney sections were scanned using a Nanozoomer 2.0 HT (Hamamatsu) after H&E staining; 4x images for each kidney section were selected. We used Image J to quantify the surface, expressed in pixels, covered by cysts in each kidney. We used a cut-off of 2,000 pixels as the minimum surface that a cyst should have to be included in the analysis. We next calculated the ratio between the obtained cystic area and the area of the entire kidney section and expressed it as the percentage of cysts for the given kidney.

Tubular cell surface measurement. For surface quantification, 4-µm kidney sections were stained with rhodamine labeled DBA, and an average of 80 tubular sections were measured for each genotype on 3 different mice using ImageJ. Briefly, the area of external profile of the tubule and the area of the lumen were measured and epithelial surface was calculated as the difference between the two areas.

Volume and mass live optical measurement. Volume and mass were analyzed with live imaging as previously described (Zlotek-Zlotkiewicz et al., 2015). Briefly, cells were trypsinized, counted and resuspended in medium supplemented with 1 mg/ml Alexa Fluor 488 Dextran (MW 10 kD; Life Technologies) at a concentration of 10^6 cells/ml before being injected in PDMS chips coated with fibronectin with a known height of 23 µm. Finally, the chamber was immersed in medium to prevent evaporation. Acquisitions were performed on a Ti inverted (Nikon) or an Axio Observer microscope (Carl Zeiss) at 37°C, with 5% CO2 atmosphere, using a 20× dry objective (NA 0.5 phase), or a SFluor 20× objective (NA 0.75 without phase ring) for the mass measurements. Images were acquired using MetaMorph (Molecular Devices). Images were acquired with a CoolSNAP HQ2 camera (Photometrics) for fluorescence or a PHA SICS camera (PHA SICS) for mass measurements. Images were analyzed with a custom-made MatLab program (MathWorks).

Phoshoproteome Enrichment and Mass Spectrometry. For phosphoproteomic analysis, cell lysates were prepared according to specifications from Cell Signaling Technology. Briefly, 2 x 10^8 cells of each genotype were starved for 2 hours in Earl's Balanced Salt Solution (EBSS; #24010043; Gibco) and then rinsed with ice-cold PBS. After carefully removing all PBS, cells were serially lysed in 10 ml of fresh urea lysis buffer (20 mM HEPES pH 8.0, 9 M urea) supplemented with phosphatase inhibitors (phosStop, Roche), to produce 20-40 mg of protein per condition. Lysates were frozen at -80 °C until processed for PTMScan analysis as previously described (Stokes et al., 2015) (Cell Signaling Technology).

Cellular extracts were sonicated, centrifuged, reduced with DTT, and alkylated with iodoacetamide. 15mg (antibody enrichment) or 500 (IMAC enrichment) total protein for each sample was digested with LysC (antibody) or trypsin (IMAC) and purified over C18

columns for enrichment with the Fe-IMAC (#20432) for total phosphopeptides and Akt substrate motif antibodies (#5561/#5563) for phospho-AGC-motif specific enrichment. Enriched peptides were purified over C18 STAGE tips (Rappsilber et al., 2003). Enriched peptides were subjected to secondary digest with trypsin and second STAGE tip prior to LC-MS/MS analysis.

Replicate injections of each sample were run non-sequentially for each enrichment. Peptides were eluted using a 90-minute or 150-minute linear gradient of acetonitrile in 0.125% formic acid delivered at 280 nL/min. Tandem mass spectra were collected in a data-dependent manner with a Thermo Orbitrap QExactive or Fusion™ Lumos™ Tribrid™ mass spectrometer using a top-twenty MS/MS method, a dynamic repeat count of one, and a repeat duration of 30 sec. Real time recalibration of mass error was performed using lock mass (Olsen et al., 2005) with a singly charged polysiloxane ion m/z = 371.101237**.**

MS/MS spectra were evaluated using SEQUEST and the Core platform from Harvard University (Eng et al., 1994; Huttlin et al., 2010; Villen et al., 2007). Files were searched against the most recent update of the UniProt *mus musculus* FASTA database. A mass accuracy of +/-5 ppm was used for precursor ions and 0.02 Da for product ions. Enzyme specificity was limited to trypsin, with at least one tryptic (K- or R-containing) terminus required per peptide and up to four mis-cleavages allowed. Cysteine carboxamidomethylation was specified as a static modification, oxidation of methionine and phosphorylation on serine, threonine, or tyrosine residues were allowed as variable modifications. Reverse decoy databases were included for all searches to estimate false discovery rates, and filtered using a 2.5% FDR in the Linear Discriminant module of Core. Peptides were also manually filtered using a -/+ 5ppm mass error range and presence of a phosphorylated residue (IMAC) or phosphorylated residue within an RXX(s/t) motif (Akt Substrate Motif antibodies). All quantitative results were generated using

Skyline (MacLean) to extract the integrated peak area of the corresponding peptide assignments in the MS1 channel. Accuracy of quantitative data was ensured by manual review in Skyline or in the ion chromatogram files.

Statistics. Standard Student T test or ANOVA two-tailed were used in the experiments unless otherwise stated.

Acknowledgements

We are grateful to the members of INSERM-U1151 for support, critically reading the manuscript and helpful discussions. We thank the histology, imaging, metabolomics and viral vector facilities at the SFR Necker for the technical help. This work was supported by grants from the European Research Council, Inserm Agemed, InCa and ARC to M.P.

References

Armour, E. A., Carson, R. P., and Ess, K. C. (2012). Cystogenesis and elongated primary cilia in Tsc1-deficient distal convoluted tubules. American journal of physiology Renal physiology *303*, F584-592.

Astrinidis, A., Cash, T. P., Hunter, D. S., Walker, C. L., Chernoff, J., and Henske, E. P. (2002). Tuberin, the tuberous sclerosis complex 2 tumor suppressor gene product, regulates Rho activation, cell adhesion and migration. Oncogene *21*, 8470-8476.

Barilari, M., Bonfils, G., Treins, C., Koka, V., De Villeneuve, D., Fabrega, S., and Pende, M. (2017). ZRF1 is a novel S6 kinase substrate that drives the senescence programme. The EMBO journal *36*, 736-750.

Barnes, E. A., Kenerson, H. L., Jiang, X., and Yeung, R. S. (2010). Tuberin regulates E-cadherin localization: implications in epithelial-mesenchymal transition. The American journal of pathology *177*, 1765-1778.

Ben-Sahra, I., Howell, J. J., Asara, J. M., and Manning, B. D. (2013). Stimulation of de novo pyrimidine synthesis by growth signaling through mTOR and S6K1. Science *339*, 1323-1328.

Bergmann, C., Guay-Woodford, L. M., Harris, P. C., Horie, S., Peters, D. J. M., and Torres, V. E. (2018). Polycystic kidney disease. Nat Rev Dis Primers *4*, 50.

Bershteyn, M., Atwood, S. X., Woo, W. M., Li, M., and Oro, A. E. (2010). MIM and cortactin antagonism regulates ciliogenesis and hedgehog signaling. Developmental cell *19*, 270-283.

Cadart, C., Zlotek-Zlotkiewicz, E., Le Berre, M., Piel, M., and Matthews, H. K. (2014). Exploring the function of cell shape and size during mitosis. Developmental cell *29*, 159-169.

Carminati, M., Gallini, S., Pirovano, L., Alfieri, A., Bisi, S., and Mapelli, M. (2016). Concomitant binding of Afadin to LGN and F-actin directs planar spindle orientation. Nature structural & molecular biology *23*, 155-163.

Chen, J. K., Chen, J., Neilson, E. G., and Harris, R. C. (2005). Role of mammalian target of rapamycin signaling in compensatory renal hypertrophy. J Am Soc Nephrol *16*, 1384-1391.

Chen, J. K., Chen, J., Thomas, G., Kozma, S. C., and Harris, R. C. (2009). S6 kinase 1 knockout inhibits uninephrectomy- or diabetes-induced renal hypertrophy. American journal of physiology Renal physiology *297*, F585-593.

di Pietro, F., Echard, A., and Morin, X. (2016). Regulation of mitotic spindle orientation: an integrated view. EMBO reports *17*, 1106-1130.

Elloul, S., Kedrin, D., Knoblauch, N. W., Beck, A. H., and Toker, A. (2014). The adherens junction protein afadin is an AKT substrate that regulates breast cancer cell migration. Molecular cancer research : MCR *12*, 464-476.

Eng, J. K., McCormack, A. L., and Yates, J. R. (1994). An approach to correlate tandem mass spectral data of peptides with amino acid sequences in a protein database. J Am Soc Mass Spectrom *5*, 976-989.

Gao, L., Yang, Z., Hiremath, C., Zimmerman, S. E., Long, B., Brakeman, P. R., Mostov, K. E., Bryant, D. M., Luby-Phelps, K., and Marciano, D. K. (2017). Afadin orients cell division to position the tubule lumen in developing renal tubules. Development *144*, 3511-3520.

Gao, X., Zhang, Y., Arrazola, P., Hino, O., Kobayashi, T., Yeung, R. S., Ru, B., and Pan, D. (2002). Tsc tumour suppressor proteins antagonize amino-acid-TOR signalling. Nature cell biology *4*, 699-704.

Giles, R. H., Ajzenberg, H., and Jackson, P. K. (2014). 3D spheroid model of mIMCD3 cells for studying ciliopathies and renal epithelial disorders. Nat Protoc *9*, 2725-2731.

Goncharova, E., Goncharov, D., Noonan, D., and Krymskaya, V. P. (2004). TSC2 modulates actin cytoskeleton and focal adhesion through TSC1-binding domain and the Rac1 GTPase. The Journal of cell biology *167*, 1171-1182.

Graham, T. R., and Burd, C. G. (2011). Coordination of Golgi functions by phosphatidylinositol 4-kinases. Trends in cell biology *21*, 113-121.

Henske, E. P., Jozwiak, S., Kingswood, J. C., Sampson, J. R., and Thiele, E. A. (2016). Tuberous sclerosis complex. Nat Rev Dis Primers *2*, 16035.

Huang, J., and Manning, B. D. (2009). A complex interplay between Akt, TSC2 and the two mTOR complexes. Biochemical Society transactions *37*, 217-222.

Huang, T. Y., DerMardirossian, C., and Bokoch, G. M. (2006). Cofilin phosphatases and regulation of actin dynamics. Current opinion in cell biology *18*, 26-31.

Huttlin, E. L., Jedrychowski, M. P., Elias, J. E., Goswami, T., Rad, R., Beausoleil, S. A., Villen, J., Haas, W., Sowa, M. E., and Gygi, S. P. (2010). A tissue-specific atlas of mouse protein phosphorylation and expression. Cell *143*, 1174-1189.

Ito, M., Nakano, T., Erdodi, F., and Hartshorne, D. J. (2004). Myosin phosphatase: structure, regulation and function. Mol Cell Biochem *259*, 197-209.

Kang, S. A., Pacold, M. E., Cervantes, C. L., Lim, D., Lou, H. J., Ottina, K., Gray, N. S., Turk, B. E., Yaffe, M. B., and Sabatini, D. M. (2013). mTORC1 phosphorylation sites encode their sensitivity to starvation and rapamycin. Science *341*, 1236566.

Lamb, R. F., Roy, C., Diefenbach, T. J., Vinters, H. V., Johnson, M. W., Jay, D. G., and Hall, A. (2000). The TSC1 tumour suppressor hamartin regulates cell adhesion through ERM proteins and the GTPase Rho. Nature cell biology *2*, 281-287.

Le Bacquer, O., Combe, K., Patrac, V., Ingram, B., Combaret, L., Dardevet, D., Montaurier, C., Salles, J., Giraudet, C., Guillet, C*., et al.* (2019). 4E-BP1 and 4E-BP2 double knockout mice are protected from aging-associated sarcopenia. J Cachexia Sarcopenia Muscle *10*, 696-709.

Liang, N., Zhang, C., Dill, P., Panasyuk, G., Pion, D., Koka, V., Gallazzini, M., Olson, E. N., Lam, H., Henske, E. P*., et al.* (2014). Regulation of YAP by mTOR and autophagy reveals a therapeutic target of tuberous sclerosis complex. The Journal of experimental medicine *211*, 2249-2263.

Lorger, M., and Moelling, K. (2006). Regulation of epithelial wound closure and intercellular adhesion by interaction of AF6 with actin cytoskeleton. Journal of cell science *119*, 3385-3398.

Ma, M., Tian, X., Igarashi, P., Pazour, G. J., and Somlo, S. (2013). Loss of cilia suppresses cyst growth in genetic models of autosomal dominant polycystic kidney disease. Nature genetics *45*, 1004-1012.

Menon, S., Dibble, C. C., Talbott, G., Hoxhaj, G., Valvezan, A. J., Takahashi, H., Cantley, L. C., and Manning, B. D. (2014). Spatial control of the TSC complex integrates insulin and nutrient regulation of mTORC1 at the lysosome. Cell *156*, 771-785.

Mizutani, K., and Takai, Y. (2016). Nectin spot: a novel type of nectin-mediated cell adhesion apparatus. The Biochemical journal *473*, 2691-2715.

Ning, W., Yu, Y., Xu, H., Liu, X., Wang, D., Wang, J., Wang, Y., and Meng, W. (2016). The CAMSAP3-ACF7 Complex Couples Noncentrosomal Microtubules with Actin Filaments to Coordinate Their Dynamics. Developmental cell *39*, 61-74.

Ohanna, M., Sobering, A. K., Lapointe, T., Lorenzo, L., Praud, C., Petroulakis, E., Sonenberg, N., Kelly, P. A., Sotiropoulos, A., and Pende, M. (2005). Atrophy of S6K1(-/-) skeletal muscle cells reveals distinct mTOR effectors for cell cycle and size control. Nature cell biology *7*, 286-294.

Olsen, J. V., de Godoy, L. M., Li, G., Macek, B., Mortensen, P., Pesch, R., Makarov, A., Lange, O., Horning, S., and Mann, M. (2005). Parts per million mass accuracy on an Orbitrap mass spectrometer via lock mass injection into a C-trap. Molecular & cellular proteomics : MCP *4*, 2010-2021.

Orhon, I., Dupont, N., Zaidan, M., Boitez, V., Burtin, M., Schmitt, A., Capiod, T., Viau, A., Beau, I., Kuehn, E. W.*, et al.* (2016). Primary-cilium-dependent autophagy controls epithelial cell volume in response to fluid flow. Nature cell biology *18*, 657-667.

Pearce, L. R., Komander, D., and Alessi, D. R. (2010). The nuts and bolts of AGC protein kinases. Nature reviews Molecular cell biology *11*, 9-22.

Pema, M., Drusian, L., Chiaravalli, M., Castelli, M., Yao, Q., Ricciardi, S., Somlo, S., Qian, F., Biffo, S., and Boletta, A. (2016). mTORC1-mediated inhibition of polycystin-1 expression drives renal cyst formation in tuberous sclerosis complex. Nature communications *7*, 10786.

Pende, M., Kozma, S. C., Jaquet, M., Oorschot, V., Burcelin, R., Le Marchand-Brustel, Y., Klumperman, J., Thorens, B., and Thomas, G. (2000). Hypoinsulinaemia, glucose intolerance and diminished beta-cell size in S6K1-deficient mice. Nature *408*, 994-997.

Pende, M., Um, S. H., Mieulet, V., Sticker, M., Goss, V. L., Mestan, J., Mueller, M., Fumagalli, S., Kozma, S. C., and Thomas, G. (2004). S6K1(-/-)/S6K2(-/-) mice exhibit perinatal lethality and rapamycin-sensitive 5'-terminal oligopyrimidine mRNA translation and reveal a mitogen-activated protein kinase-dependent S6 kinase pathway. Molecular and cellular biology *24*, 3112-3124.

Rappsilber, J., Ishihama, Y., and Mann, M. (2003). Stop and go extraction tips for matrix-assisted laser desorption/ionization, nanoelectrospray, and LC/MS sample pretreatment in proteomics. Analytical chemistry *75*, 663-670.

Rossi, R., Pester, J. M., McDowell, M., Soza, S., Montecucco, A., and Lee-Fruman, K. K. (2007). Identification of S6K2 as a centrosome-located kinase. FEBS letters *581*, 4058-4064.

Rush, J., Moritz, A., Lee, K. A., Guo, A., Goss, V. L., Spek, E. J., Zhang, H., Zha, X. M., Polakiewicz, R. D., and Comb, M. J. (2005). Immunoaffinity profiling of tyrosine phosphorylation in cancer cells. Nat Biotechnol *23*, 94-101.

Sarbassov, D. D., Guertin, D. A., Ali, S. M., and Sabatini, D. M. (2005). Phosphorylation and regulation of Akt/PKB by the rictor-mTOR complex. Science *307*, 1098-1101.

Sato, T., Fujita, N., Yamada, A., Ooshio, T., Okamoto, R., Irie, K., and Takai, Y. (2006). Regulation of the assembly and adhesion activity of E-cadherin by nectin and afadin for the formation of adherens junctions in Madin-Darby canine kidney cells. The Journal of biological chemistry *281*, 5288-5299.

Saxton, R. A., and Sabatini, D. M. (2017). mTOR Signaling in Growth, Metabolism, and Disease. Cell *169*, 361-371.

Schmidt, L. S., and Linehan, W. M. (2016). Genetic predisposition to kidney cancer. Semin Oncol *43*, 566-574.

Shao, X., Somlo, S., and Igarashi, P. (2002). Epithelial-specific Cre/lox recombination in the developing kidney and genitourinary tract. J Am Soc Nephrol *13*, 1837-1846.

Sharma, N., Malarkey, E. B., Berbari, N. F., O'Connor, A. K., Vanden Heuvel, G. B., Mrug, M., and Yoder, B. K. (2013). Proximal tubule proliferation is insufficient to induce rapid cyst formation after cilia disruption. J Am Soc Nephrol *24*, 456-464.

Shima, H., Pende, M., Chen, Y., Fumagalli, S., Thomas, G., and Kozma, S. C. (1998). Disruption of the p70(s6k)/p85(s6k) gene reveals a small mouse phenotype and a new functional S6 kinase. The EMBO journal *17*, 6649-6659.

Stokes, M. P., Farnsworth, C. L., Gu, H., Jia, X., Worsfold, C. R., Yang, V., Ren, J. M., Lee, K. A., and Silva, J. C. (2015). Complementary PTM Profiling of Drug Response in Human Gastric Carcinoma by Immunoaffinity and IMAC Methods with Total Proteome Analysis. Proteomes *3*, 160-183.

Susaki, E. A., Tainaka, K., Perrin, D., Yukinaga, H., Kuno, A., and Ueda, H. R. (2015). Advanced CUBIC protocols for whole-brain and whole-body clearing and imaging. Nat Protoc *10*, 1709-1727.

Treins, C., Warne, P. H., Magnuson, M. A., Pende, M., and Downward, J. (2010). Rictor is a novel target of p70 S6 kinase-1. Oncogene *29*, 1003-1016.

Villen, J., Beausoleil, S. A., Gerber, S. A., and Gygi, S. P. (2007). Large-scale phosphorylation analysis of mouse liver. Proceedings of the National Academy of Sciences of the United States of America *104*, 1488-1493.

Wu, H., Chen, J., Xu, J., Dong, Z., Meyuhas, O., and Chen, J. K. (2016). Blocking rpS6 Phosphorylation Exacerbates Tsc1 Deletion-Induced Kidney Growth. J Am Soc Nephrol *27*, 1145-1158.

Xu, J., Chen, J., Dong, Z., Meyuhas, O., and Chen, J. K. (2015). Phosphorylation of ribosomal protein S6 mediates compensatory renal hypertrophy. Kidney international *87*, 543-556.

Yeung, R. S., Xiao, G. H., Jin, F., Lee, W. C., Testa, J. R., and Knudson, A. G. (1994). Predisposition to renal carcinoma in the Eker rat is determined by germ-line mutation of the tuberous sclerosis 2 (TSC2) gene. Proceedings of the National Academy of Sciences of the United States of America *91*, 11413-11416.

Yuan, S., Li, J., Diener, D. R., Choma, M. A., Rosenbaum, J. L., and Sun, Z. (2012). Target-of-rapamycin complex 1 (Torc1) signaling modulates cilia size and function through protein synthesis regulation. Proceedings of the National Academy of Sciences of the United States of America *109*, 2021-2026.

Zhang, H. H., Lipovsky, A. I., Dibble, C. C., Sahin, M., and Manning, B. D. (2006). S6K1 regulates GSK3 under conditions of mTOR-dependent feedback inhibition of Akt. Molecular cell *24*, 185-197.

Zhou, J., Brugarolas, J., and Parada, L. F. (2009). Loss of Tsc1, but not Pten, in renal tubular cells causes polycystic kidney disease by activating mTORC1. Human molecular genetics *18*, 4428-4441.

Zlotek-Zlotkiewicz, E., Monnier, S., Cappello, G., Le Berre, M., and Piel, M. (2015). Optical volume and mass measurements show that mammalian cells swell during mitosis. The Journal of cell biology *211*, 765-774.

Figure Legend

Figure 1. **S6K1 deletion protects from cyst formation in a mouse model of renal TSC without affecting proliferation.** (a) Macroscopic photos of BrdU staining at post-natal day 90 of the different genotypes indicated. Scale bar, 1mm. (b) Kidney/body weight ratio of the indicated phenotypes at post-natal day 90. Mean ± SEM. n= 12 mice/group. (c) Cystic index of mice of indicated genotypes. Mean ± SEM. n= 3 mice/group. (d) Plasmatic urea concentrations (mmol/l) were determined in the indicated genotypes at pre-cystic age (post-natal day 20). Mean ± SEM. n= 3 mice/group. (e) Representative pictures and (f) relative quantifications of BrdU staining at post-natal day 90 of the different genotypes indicated. The percentage of BrdU-positive cells on the total number of tubular cells was counted in 10 different fields of each section. Empty arrows point at positive cells. Mean ± SEM. n= 3 mice/group. Scale bar, 20µm. (g) Representative pictures and (h) relative quantifications of $pH3^{S10}$ staining at post-natal day 90 of the different genotypes indicated. The percentage of $pH3^{S10}$-positive cells on the total number of tubular cells was counted in 10 different fields of each section. Empty arrows point at positive cells. Mean ± SEM. n= 3 mice/group. Scale bar, 20µm.

Figure 2. **S6K1 hyperactivation is responsible for the aberrant orientation of cell division in TSC renal disease.** (a) Western blots of mouse whole-kidney extracts at pre-cystic age (post-natal day 20), randomly fed, showing an induction of mTORC1 activity in *Tsc1*-deleted animals and an effect of *S6k1* concomitant deletion on some of the known substrates of the kinase. (b) Densitometry analysis and relative quantification of the phosphorylated forms of the indicated proteins. Actin was used as a loading control. (c) Representative pictures and (d) relative measurements of tubular cell surface area

at post-natal day 10 of the different genotypes indicated. Roughly n=50 tubular sections from five different fields of each section were measured. Mean ± SEM. n= 3 mice/group. Scale bar, 10 µm. (e) Representative 3D reconstructed images of mitotic divisions (anaphase) of renal tubular cells, longitudinally oriented in *Tsc1*$^{fl/fl}$ and *Ksp-Cre; Tsc1*$^{fl/fl}$*; S6k1*$^{-/-}$ mice and aberrantly oriented in the *Ksp-Cre; Tsc1*$^{fl/fl}$ mice. The tubular axis orientation is marked with a cyan dotted line, the mitosis orientation with a yellow dotted line. (f) Quantification of the mitotic division orientation at post-natal day 20 of the different genotypes indicated. A minimum of n=30 mitotic events for each genotype were measured. To assess the significance of the data, a Mann-Whitney U test was used. Mean ± SEM. n= 4 mice/group.

Figure 3. **Characterization of CRISPR/Cas9-mediated deletion of *Tsc1* and *S6k1* in mIMCD3 cells**. (a) Cells were serum starved overnight and subsequently amino acid starved with EBSS (Earle's Balanced Salt Solution) for 1.5h. They were then either collected in starvation or stimulated with complete medium for 0.5h and collected or treated with 20nM rapamycin for 0.5h and then collected. Cell lysates were probed with the indicated antibodies to characterize the effects of the loss of *Tsc1* and *Tsc1/S6k1* on mTORC1 signaling pathways in the cell lines. Densitometry analysis and relative quantification of the phosphorylated forms of the indicated proteins are reported under each blot. Actin was used as a loading control. (b) Cells were trypsinized, plated as single cells in Matrigel and cultured for 5 days before being fixed wth 4% PFA and stained with DAPI to quantify the number of cells per sphere derived from a single cell. An average of 100 spheres pooled from 3 independent experiments were quantified for each genotype. Horizontal lines represent the mean ± SEM. (c) Volume and (d) mass were analyzed by optical measurement at G1 (2.5 h after mitotic division) for the

different genotypes. A minimum of 100 cells pooled from 3 independent experiments were quantified for each genotype. Horizontal lines represent the mean ± SEM. (e) Representative pictures and (f) quantifications of primary cilia length in the different genotypes. Cells were plated on coverslips, left to adhere and serum starved overnight before fixation. Primary cilia axonemes and basal bodies were stained with Arl13b and γ-Tubulin antibodies, respectively. Z-stack images were analyzed with FIJI software. 3D cilia length was measured using the Neurite Tracer plugin in FIJI. A minimum of 100 cilia pooled from 3 independent experiments were quantified for each genotype. Horizontal lines represent the mean ± SEM. Scale bar, 10 µm.

Figure 4. **Hyperactive S6K1 leads to centrosome mislocalization in mIMCD3 3D cultures and *in vivo* both during mitosis and in interphase.** (a) Representative images of 5-day mIMCD3s spheres immunolabeled with γ-Tubulin, Arl13b and nuclei to quantify spheres with polarized centrosomes and primary cilia. Only spheres with a visible lumen and with all the centrosomes and primary cilia correctly localized on the luminal (apical) side were considered as normal. Scale bar, 10 µm. (b) Quantification of the percentage of spheres with polarized primary cilia on total number of spheres per genotype. The ratio was calculated on roughly n=70 spheres per experiment. The histograms are an average of 3 independent experiments. Mean ± SEM. (c) Representative images of 5-day mIMCD3s spheres immunolabeled with γ-tubulin and nuclei to measure spindle orientation. Yellow dotted lines indicate the spindle vectors. A schematic of how the spindle angle was measured is shown in the first figure. Scale bar, 10 µm. (d) Quantification of spindle angles relative to the apical-basal axis in 5-day spheres. Each dot represents a mitotic event, 3 independent experiments were

analyzed. Horizontal lines represent the mean ± SEM. (e) Representative pictures of kidney sections at post-natal day 20 of the indicated genotypes immunolabeled with FOP and γ-Tubulin to highlight the centrosome in renal tubular cells. Scale bar, 5 µm. (g) Quantification of angle α contained by normal to cell base and nucleus-centrosome vector and (f) schematic representation of how the angle α was measured. More than n=150 centrosome positions from five different fields of each section were measured. Mean ± SEM. n= 3 mice/group.

Figure 5. **Centrosome mispositioning in TSC1 mutant cells is not due to intrinsic or apico/basal polarity issues** (a) Representative images of 5-day mIMCD3s spheres immunolabeled with γ-tubulin, Par3 and nuclei to show the localization of the centrosomes compared to the apical markers. Scale bar, 10 µm. (b) Representative images of 5-day mIMCD3s spheres immunolabeled with Arl13b, aPKC and nuclei to show the localization of the primary cilia compared to the apical markers. Scale bar, 5 µm. (c) Representative images of cells cultured on L shape patterns and recorded by time-lapse microscopy for the different genotypes. (d) Distribution of mitotic spindle angles relative to pattern orientation (α^b - α^a) at anaphase onset. A minimum of 100 angles from 3 independent experiments were quantified for each genotype. Horizontal lines represent the mean ± SEM. Scale bar, 5 µm.

Figure 6. **Phosphoproteomic screening of *TSC1* single knockout versus *TSC1/S6k1* double knockout cells.** (a) Volcano plots of AGC kinase-motif antibody enrichment and (b) IMAC enrichment. The x-axis shows log2-ratio for phosphopeptides between samples and the y-axis shows the -log10 p-value. The horizontal blue bar represents the statistical cut-off of significance (p value of 0.05). Red dots represent downregulated

phospho-peptides and green dots represent up-regulated phospho-peptides. The numbers in the chart represent the number of statistically-significant differentially enriched peptides. Representative peptides and their sites of modification are shown. (c) Gene ontology analysis, using DAVID, showing statistically significant gene set enrichments comparing the IMAC statistically-significant differentially phosphorylated proteins versus the entire IMAC enrichment set.

Figure 7. Afadin is phosphorylated by S6K1 in Tsc1-mutant conditions both in culture and *in vivo*. (a) Cells were serum starved overnight and subsequently amino acid starved with EBSS (Earle's Balanced Salt Solution) for 1.5h with or without the indicated treatments. They were then collected and cell lysates were probed with the indicated antibodies. * represents a non-specific cross reactive band. (b) Densitometry analysis and relative quantification of the phosphorylated forms of the indicated proteins. Actin was used as a loading control. (c) Western blots of mouse whole-kidney extracts at pre-cystic age (post-natal day 20), randomly fed, showing an induction of Afadin phosphorylation in *Tsc1*-deleted animals and an effect of *S6k1* concomitant deletion. (d) Densitometry analysis and relative quantification of the phosphorylated form of Afadin. Actin was used as a loading control. (e) AS-S6K1 was transfected in *Tsc1/S6k1* dKO mIMCD3 cells with FLAG-Afadin-WT. An *in vivo* kinase assay was performed in the presence of 6-Bn-ATP-γ-S both in presence and in absence of 20nM rapamycin. After immunoprecipitation using an anti-FLAG antibody, the thio-phosphorylation of Afadin was revealed by Western blot using an anti-thiophosphate ester antibody. Expression levels of Afadin, phospho-S1795-Afadin, FLAG and phospho-RPS6 were revealed by Western blot on total extracts using the indicated antibody. (f) *Tsc1* KO and *Tsc1/S6k1*

dKO mIMCD3s were plated and treated at the same time with 20 µg/ml of cycloheximide (CHX) in normal medium, to block protein translation. Cells were then collected at the different times indicated and protein lysates were probed with the indicated antibody to compare the stability of Afadin in the two genotypes. Ubiquitin was probed to evaluate the efficacy of the CHX treatment.

Figure 8. Afadin phosphorylation is involved in the regulation of centrosome positioning in *Tsc1* KO cells. (a) Cells *Tsc1/Afdn* dKO were transduced with lentivirus FLAG-Neon, FLAG-Afadin-WT or FLAG-Afadin-S1795A. Cells were plated then serum starved overnight and subsequently amino acid starved with EBSS (Earle's Balanced Salt Solution) for 2h. They were then collected and cell lysates were probed with the indicated antibodies. * represents a non-specific cross-reactive band. (b) The same cells were plated on coverslips, fixed with 4% PFA and probed with anti-Afadin antibody to confirm the correct localization of the constructs. (c) Representative images of 5-day spheres from cells *Tsc1/Afdn* dKO transduced with lentivirus FLAG-Neon, FLAG-Afadin-WT or FLAG-Afadin-S1795A. After fixation, spheres were immunolabeled with γ-Tubulin, Arl13b and nuclei to quantify spheres with polarized centrosomes and primary cilia. Scale bar, 5 µm. (d) Quantification of the fold-rescue in sphere formation assays with polarized primary cilia. The ratio was calculated on roughly n=70 spheres per experiment. The histograms are an average of 3 independent experiments normalized on the FLAG-Neon transduced-derived spheres. Mean ± SEM. (e) Representative images of 5-day mIMCD3s spheres immunolabeled with Afadin, E-cadherin and nuclei to show the relative localization of the two proteins. Scale bar, 10 µm.

Figure S1 (a) Kidney/body weight ratio of the indicated phenotypes at post-natal day 90. Mean ± SEM. n= 3/4 mice/group. (b) Quantification and (c) representative images of BrdU staining at post-natal day 90 of the different genotypes indicated. The percentage of BrdU-positive cells on the total number of tubular cells was counted in 10 different fields of each section. Mean ± SEM. n= 3 mice/group. Scale bar, 20µm.

Figure S2 (a) mIMCD3 cells were mutated for either *Tsc1* or *Tsc1/S6k1* by CRISPR/Cas9. After selection, cells were plated and protein extracts were tested for the expression of TSC1 and S6K1 proteins and for targets of the activation of the pathway. (b) Cell density was analyzed as the ratio of mass to volume measured for the same cells by optical measurement at G1 (2.5 h after mitotic division) for the different genotypes. A minimum of 50 cells pooled from 3 independent experiments were quantified for each genotype. Horizontal lines represent the mean ± SEM. (c) With the same optical measurement, the volume of cells in mitosis was analyzed. The volume was measured just before metaphase round-up and during the metaphase round-up for the different genotypes. (d) The volume of two daughter cells after mitosis was analyzed to calculate the relative ratio. A minimum of 100 cells pooled from 3 independent experiments were quantified for each genotype. Horizontal lines represent the mean ± SEM.

Figure S3 (a) Western blot of total cell extracts from the indicated genotypes, collected after 1.5h starvation in EBSS. Membranes were probed with two different AGC kinase-motif antibodies (anti-RXXS*/T* or anti-RXRXXS*/T*) used in the phosphoproteomic screening.

Figure S4 (a) Cells *Afdn* KO were transduced with lentivirus FLAG-Neon, FLAG-Afadin-WT or FLAG-Afadin-S1795A. Cells were plated then serum starved overnight and subsequently amino acid starved with EBSS (Earle's Balanced Salt Solution) for 2h. They

were then collected and cell lysates were probed with the indicated antibodies. (b) Quantification of the fold-rescue in sphere formation assay with polarized primary cilia. The ratio was calculated on roughly n=70 spheres per experiment. The histograms are an average of 3 independent experiments normalized on the FLAG-Neon transduced-derived spheres. Mean ± SEM.

Figure 1

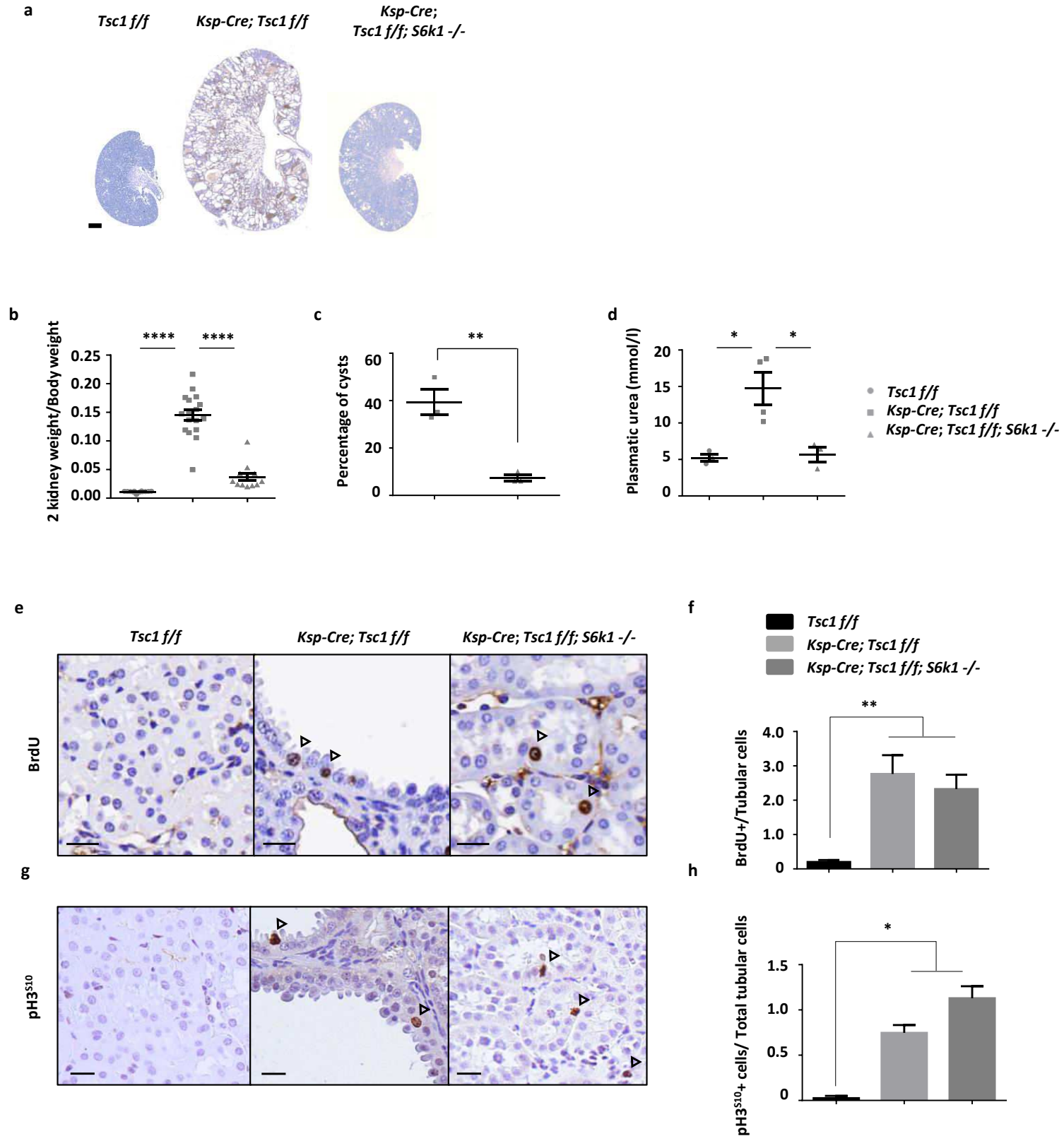
a
Tsc1 f/f
Ksp-Cre; Tsc1 f/f
Ksp-Cre; Tsc1 f/f; S6k1 -/-
b
2 kidney weight/Body weight
0.25
0.20
0.15
0.10
0.05
0.00
****
****
c
Percentage of cysts
60
40
20
0
**
d
Plasmatic urea (mmol/l)
20
15
10
5
0
*
*
Tsc1 f/f
Ksp-Cre; Tsc1 f/f
Ksp-Cre; Tsc1 f/f; S6k1 -/-
e
Tsc1 f/f
Ksp-Cre; Tsc1 f/f
Ksp-Cre; Tsc1 f/f; S6k1 -/-
BrdU
f
Tsc1 f/f
Ksp-Cre; Tsc1 f/f
Ksp-Cre; Tsc1 f/f; S6k1 -/-
**
BrdU+/Tubular cells
4.0
3.0
2.0
1.0
0
g
pH3S10
h
*
pH3S10+ cells/ Total tubular cells
1.5
1.0
0.5
0

Figure 2

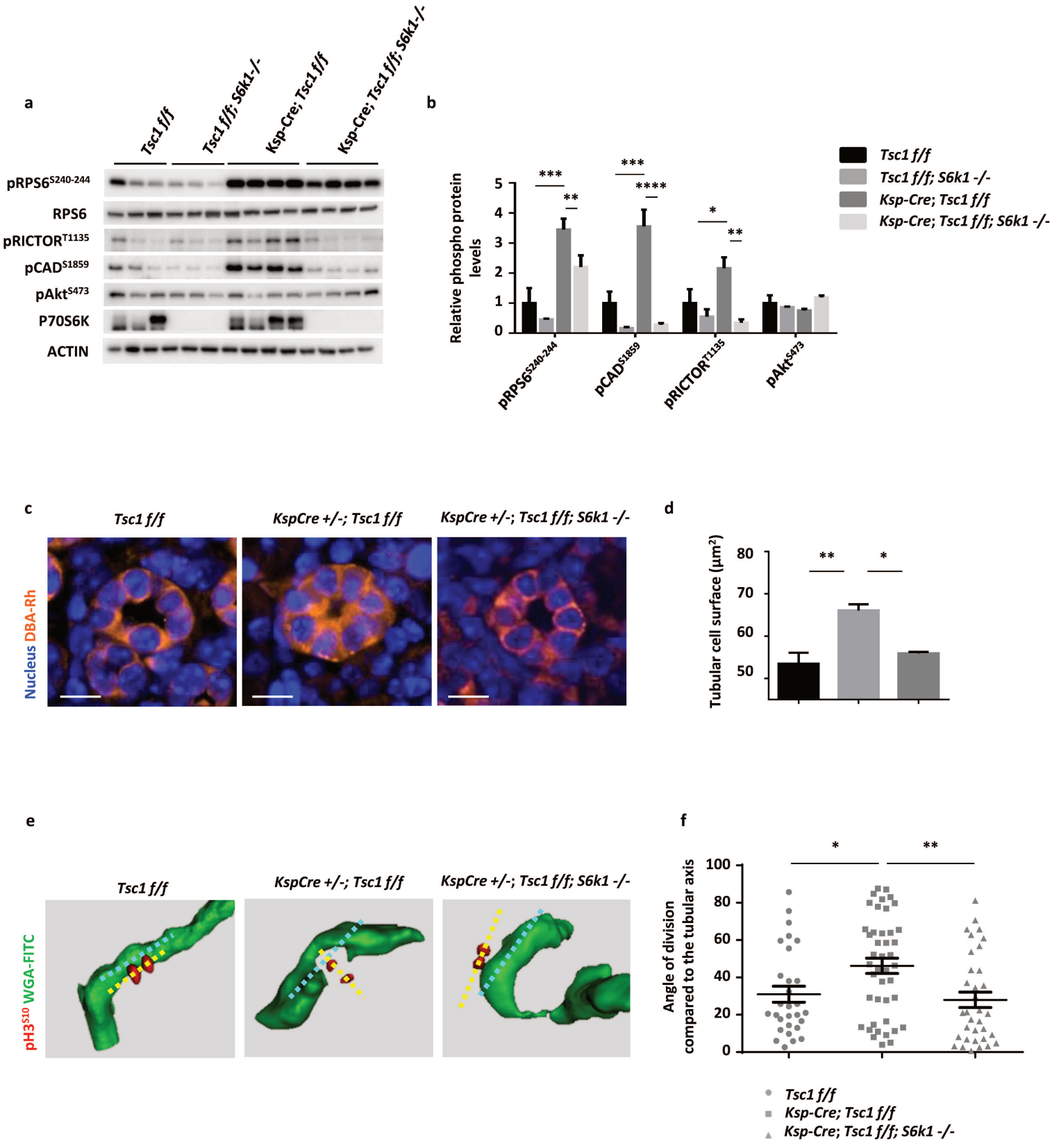
a
Tsc1 f/f
Tsc1 f/f; S6k1-/-
Ksp-Cre; Tsc1 f/f
Ksp-Cre; Tsc1 f/f; S6k1-/-
pRPS6S240-244
RPS6
pRICTORT1135
pCADS1859
pAktS473
P70S6K
ACTIN
b
Relative phospho protein levels
Tsc1 f/f
Tsc1 f/f; S6k1 -/-
Ksp-Cre; Tsc1 f/f
Ksp-Cre; Tsc1 f/f; S6k1 -/-
pRPS6S240-244
pCADS1859
pRICTORT1135
pAktS473
c
Tsc1 f/f
KspCre +/-; Tsc1 f/f
KspCre +/-; Tsc1 f/f; S6k1 -/-
Nucleus DBA-Rh
d
Tubular cell surface (µm²)
e
Tsc1 f/f
KspCre +/-; Tsc1 f/f
KspCre +/-; Tsc1 f/f; S6k1 -/-
pH3S10 WGA-FITC
f
Angle of division compared to the tubular axis
Tsc1 f/f
Ksp-Cre; Tsc1 f/f
Ksp-Cre; Tsc1 f/f; S6k1 -/-

Figure 3

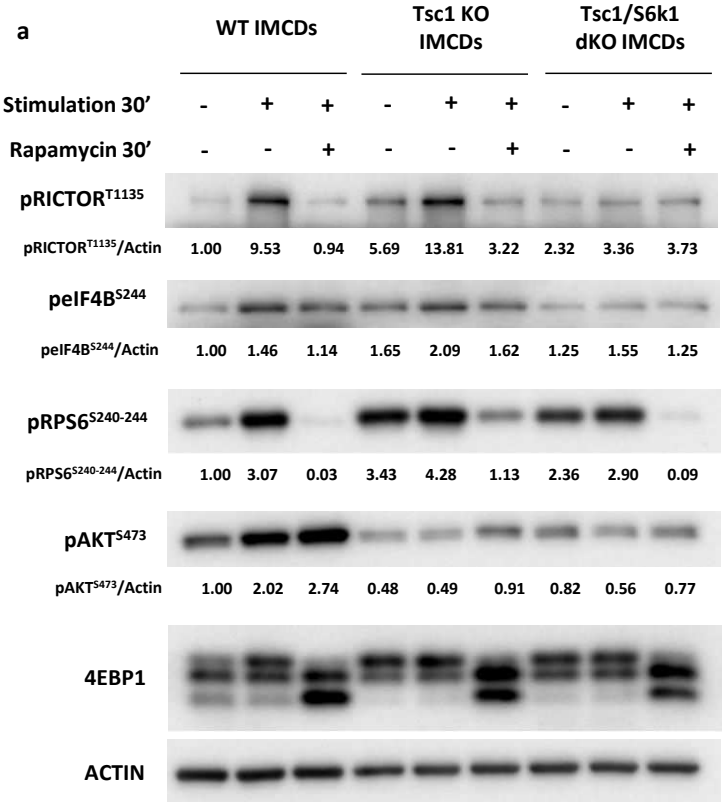
a
WT IMCDs
Tsc1 KO IMCDs
Tsc1/S6k1 dKO IMCDs
Stimulation 30'
Rapamycin 30'
pRICTOR T1135
pRICTOR T1135/Actin 1.00 9.53 0.94 5.69 13.81 3.22 2.32 3.36 3.73
peIF4B S244
peIF4B S244/Actin 1.00 1.46 1.14 1.65 2.09 1.62 1.25 1.55 1.25
pRPS6 S240-244
pRPS6 S240-244/Actin 1.00 3.07 0.03 3.43 4.28 1.13 2.36 2.90 0.09
pAKT S473
pAKT S473/Actin 1.00 2.02 2.74 0.48 0.49 0.91 0.82 0.56 0.77
4EBP1
ACTIN

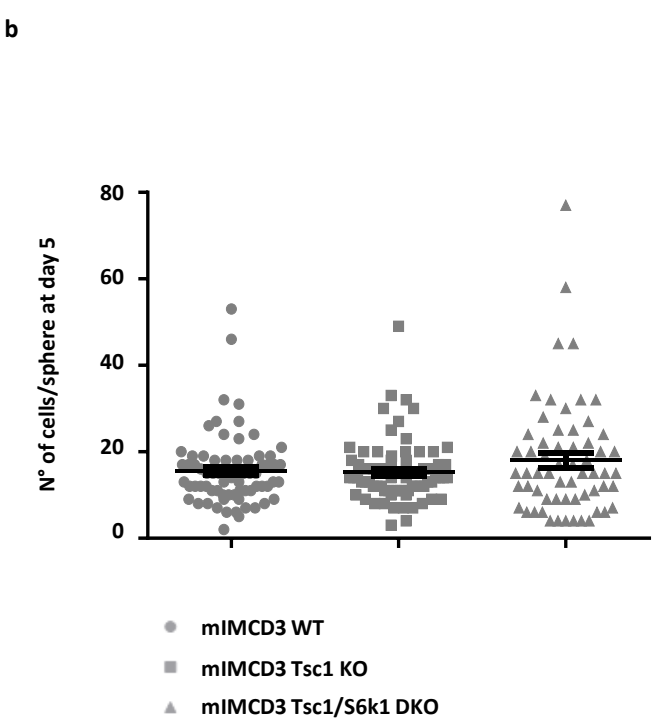
b
N° of cells/sphere at day 5
mIMCD3 WT
mIMCD3 Tsc1 KO
mIMCD3 Tsc1/S6k1 DKO

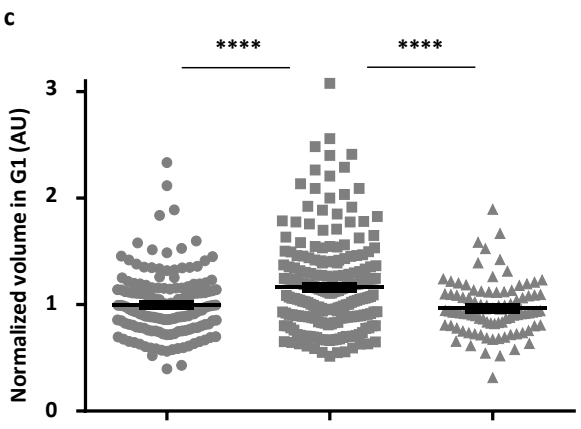
c
Normalized volume in G1 (AU)
****
****

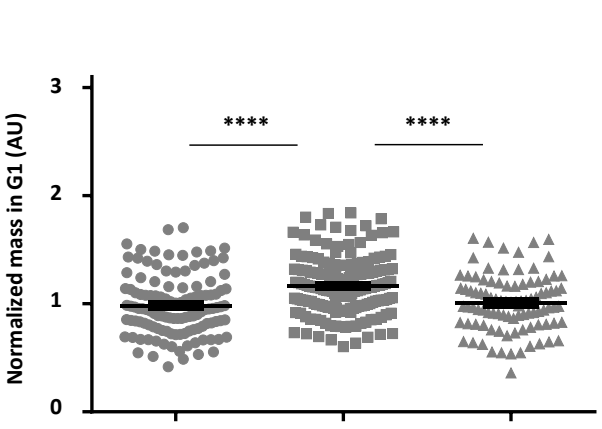
d
Normalized mass in G1 (AU)
****
****

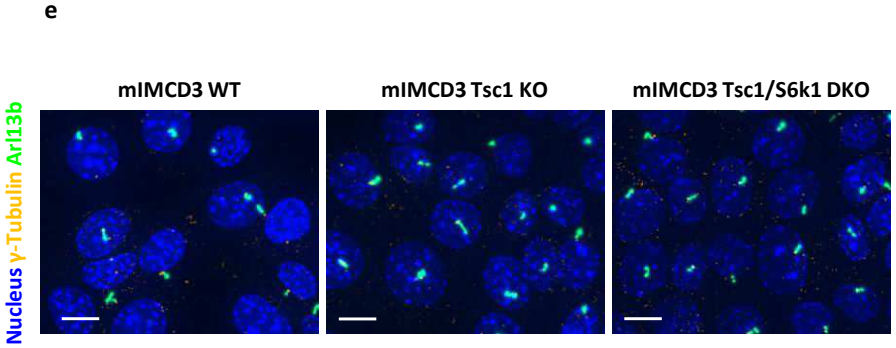
e
mIMCD3 WT
mIMCD3 Tsc1 KO
mIMCD3 Tsc1/S6k1 DKO
Nucleus γ-Tubulin Arl13b

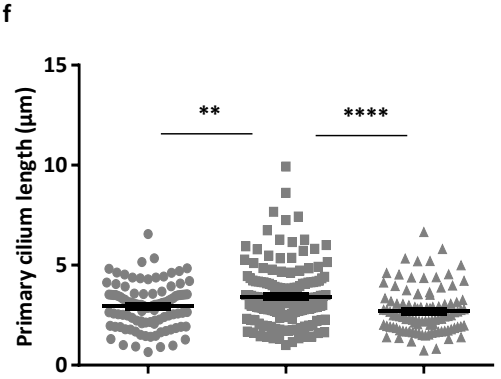
f
Primary cilium length (µm)
**
****

Figure 4

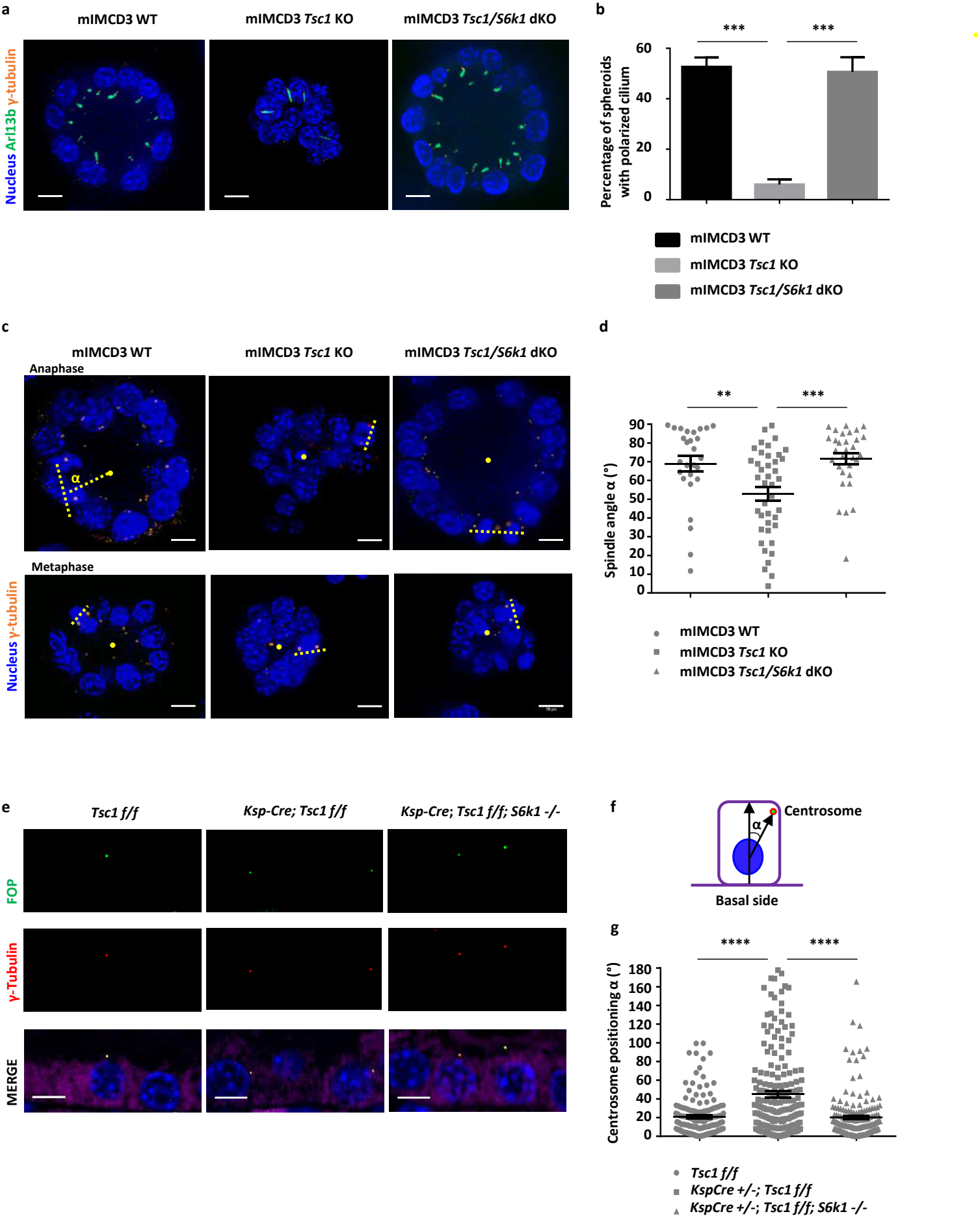
a
mIMCD3 WT
mIMCD3 Tsc1 KO
mIMCD3 Tsc1/S6k1 dKO
Nucleus Arl13b γ-tubulin
b
***
***
Percentage of spheroids with polarized cilium
60
40
20
0
mIMCD3 WT
mIMCD3 Tsc1 KO
mIMCD3 Tsc1/S6k1 dKO
c
mIMCD3 WT
mIMCD3 Tsc1 KO
mIMCD3 Tsc1/S6k1 dKO
Anaphase
α
Metaphase
Nucleus γ-tubulin
d
**
***
Spindle angle α (°)
90
80
70
60
50
40
30
20
10
0
mIMCD3 WT
mIMCD3 Tsc1 KO
mIMCD3 Tsc1/S6k1 dKO
e
Tsc1 f/f
Ksp-Cre; Tsc1 f/f
Ksp-Cre; Tsc1 f/f; S6k1 -/-
FOP
γ-Tubulin
MERGE
f
α
Centrosome
Basal side
g
****
****
Centrosome positioning α (°)
180
160
140
120
100
80
60
40
20
0
Tsc1 f/f
KspCre +/-; Tsc1 f/f
KspCre +/-; Tsc1 f/f; S6k1 -/-

Figure 5

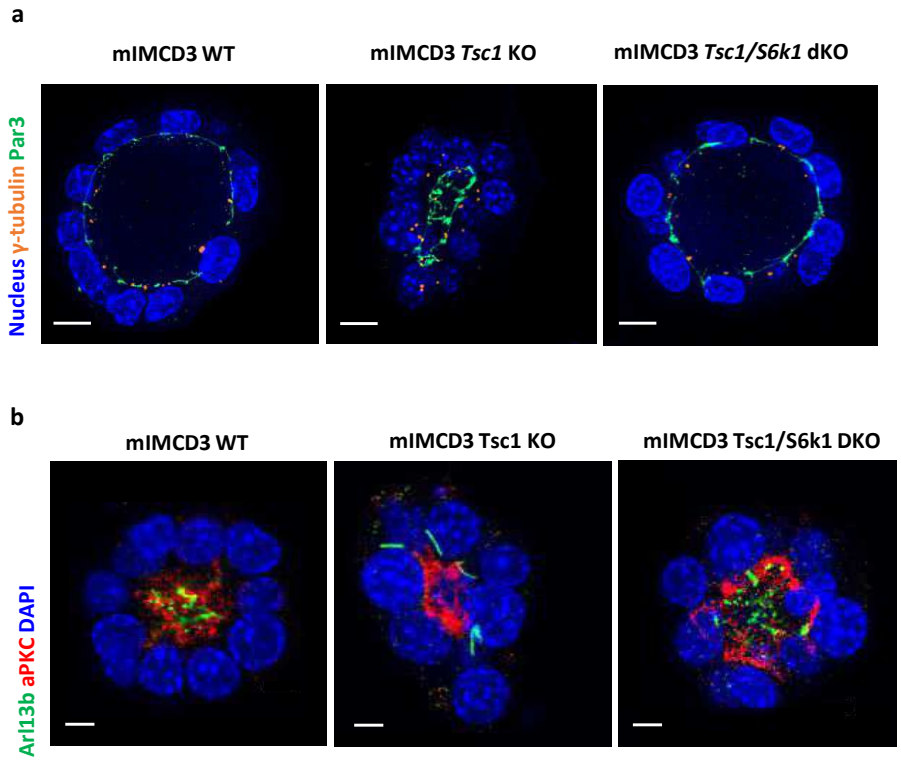
a
mIMCD3 WT
mIMCD3 Tsc1 KO
mIMCD3 Tsc1/S6k1 dKO
Nucleus γ-tubulin Par3
b
mIMCD3 WT
mIMCD3 Tsc1 KO
mIMCD3 Tsc1/S6k1 DKO
Arl13b aPKC DAPI

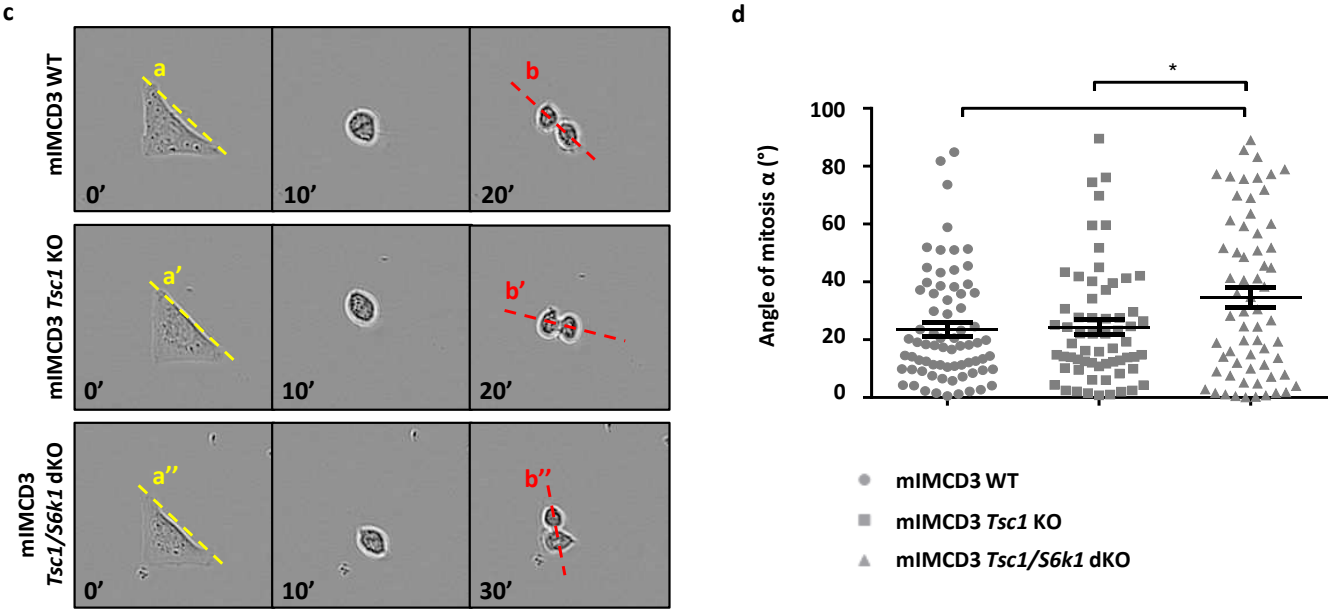
c
mIMCD3 WT
mIMCD3 Tsc1 KO
mIMCD3 Tsc1/S6k1 dKO
a
b
a'
b'
a''
b''
0'
10'
20'
30'
d
Angle of mitosis α (°)
100
80
60
40
20
0
*
mIMCD3 WT
mIMCD3 Tsc1 KO
mIMCD3 Tsc1/S6k1 dKO

Figure 6

a

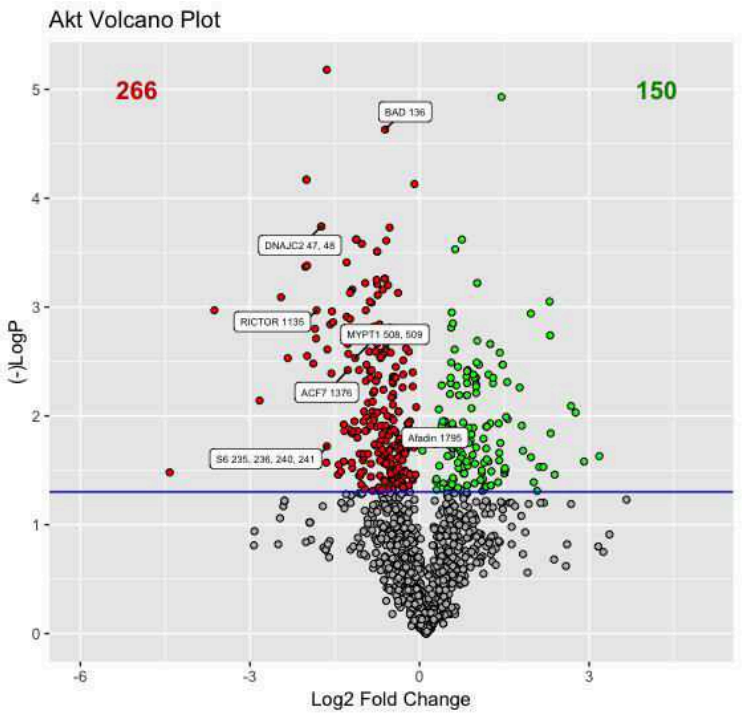
Akt Volcano Plot
266
150
BAD 136
DNAJC2 47, 48
RICTOR 1135
MYPT1 508, 509
ACF7 1376
Afadin 1795
S6 235, 236, 240, 241
(-)LogP
Log2 Fold Change

b

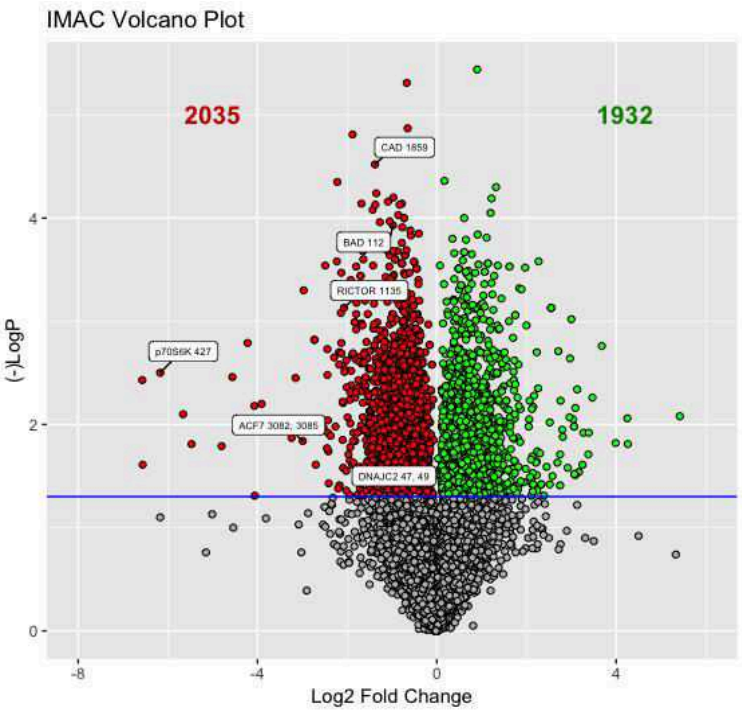
IMAC Volcano Plot
2035
1932
CAD 1859
BAD 112
RICTOR 1135
p70S6K 427
ACF7 3082, 3085
DNAJC2 47, 49
(-)LogP
Log2 Fold Change

c

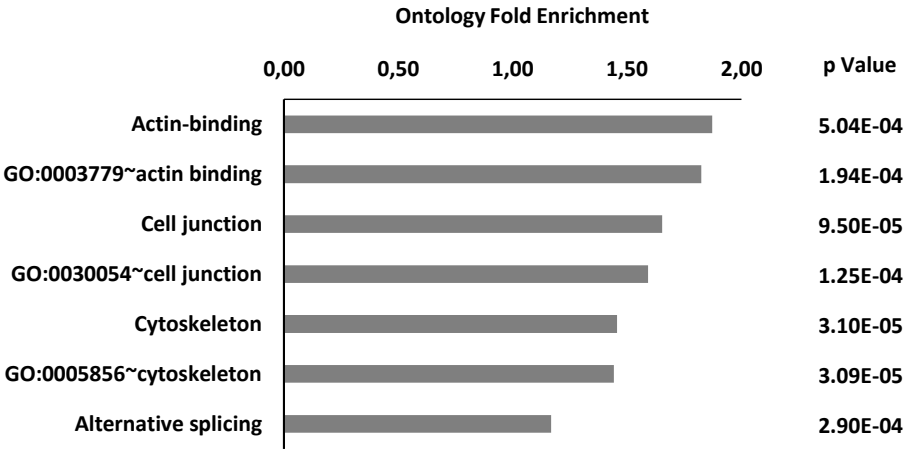
Ontology Fold Enrichment
0,00
0,50
1,00
1,50
2,00
p Value
Actin-binding
5.04E-04
GO:0003779~actin binding
1.94E-04
Cell junction
9.50E-05
GO:0030054~cell junction
1.25E-04
Cytoskeleton
3.10E-05
GO:0005856~cytoskeleton
3.09E-05
Alternative splicing
2.90E-04

Figure 7

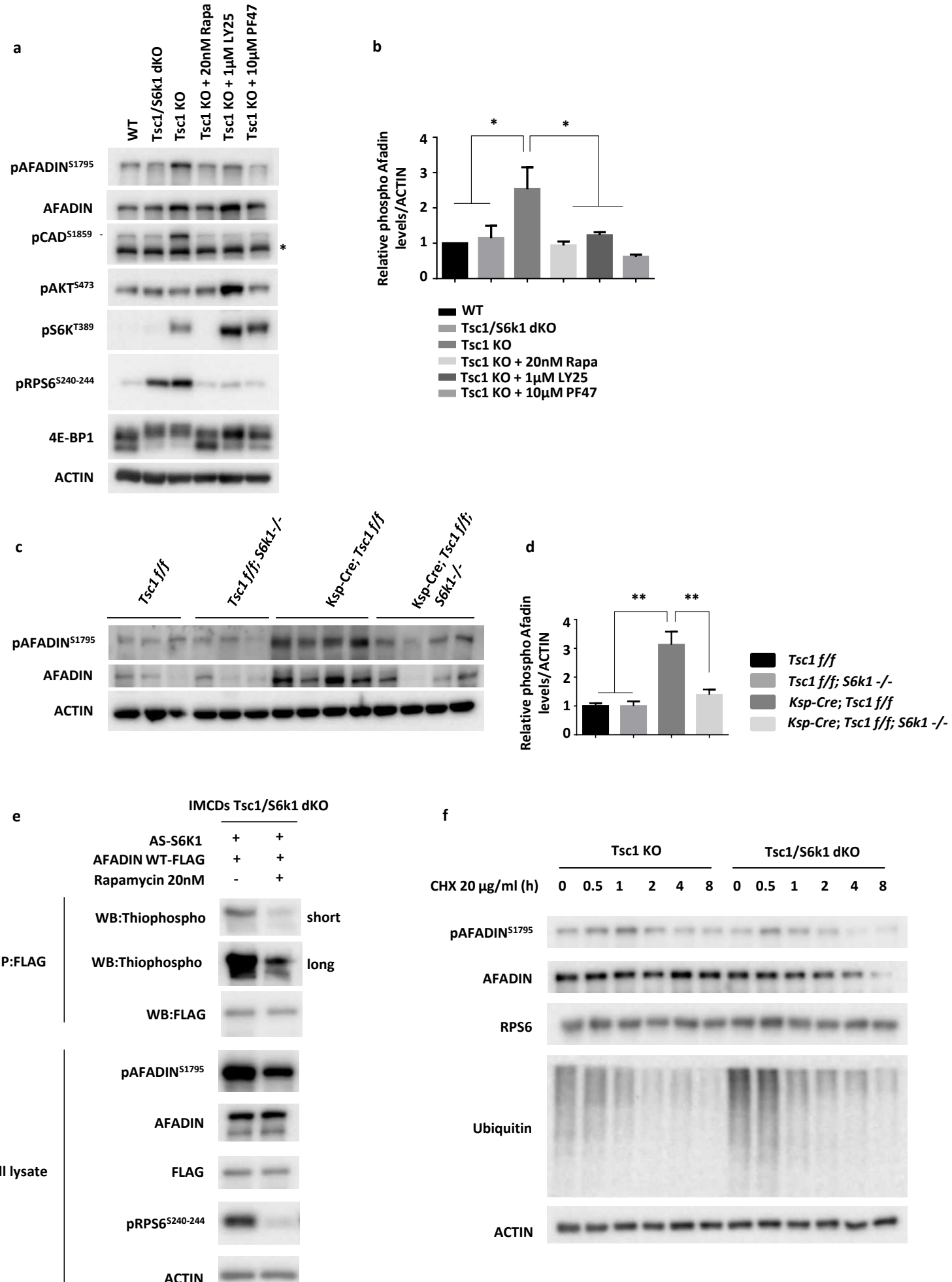
a
WT
Tsc1/S6k1 dKO
Tsc1 KO
Tsc1 KO + 20nM Rapa
Tsc1 KO + 1µM LY25
Tsc1 KO + 10µM PF47
pAFADIN S1795
AFADIN
pCAD S1859
pAKT S473
pS6K T389
pRPS6 S240-244
4E-BP1
ACTIN
b
Relative phospho Afadin levels/ACTIN
WT
Tsc1/S6k1 dKO
Tsc1 KO
Tsc1 KO + 20nM Rapa
Tsc1 KO + 1µM LY25
Tsc1 KO + 10µM PF47
c
Tsc1 f/f
Tsc1 f/f; S6k1-/-
Ksp-Cre; Tsc1 f/f
Ksp-Cre; Tsc1 f/f; S6k1-/-
pAFADIN S1795
AFADIN
ACTIN
d
Relative phospho Afadin levels/ACTIN
Tsc1 f/f
Tsc1 f/f; S6k1 -/-
Ksp-Cre; Tsc1 f/f
Ksp-Cre; Tsc1 f/f; S6k1 -/-
e
IMCDs Tsc1/S6k1 dKO
AS-S6K1
AFADIN WT-FLAG
Rapamycin 20nM
IP:FLAG
WB:Thiophospho
short
WB:Thiophospho
long
WB:FLAG
Cell lysate
pAFADIN S1795
AFADIN
FLAG
pRPS6 S240-244
ACTIN
f
Tsc1 KO
Tsc1/S6k1 dKO
CHX 20 µg/ml (h)
pAFADIN S1795
AFADIN
RPS6
Ubiquitin
ACTIN

Figure 8

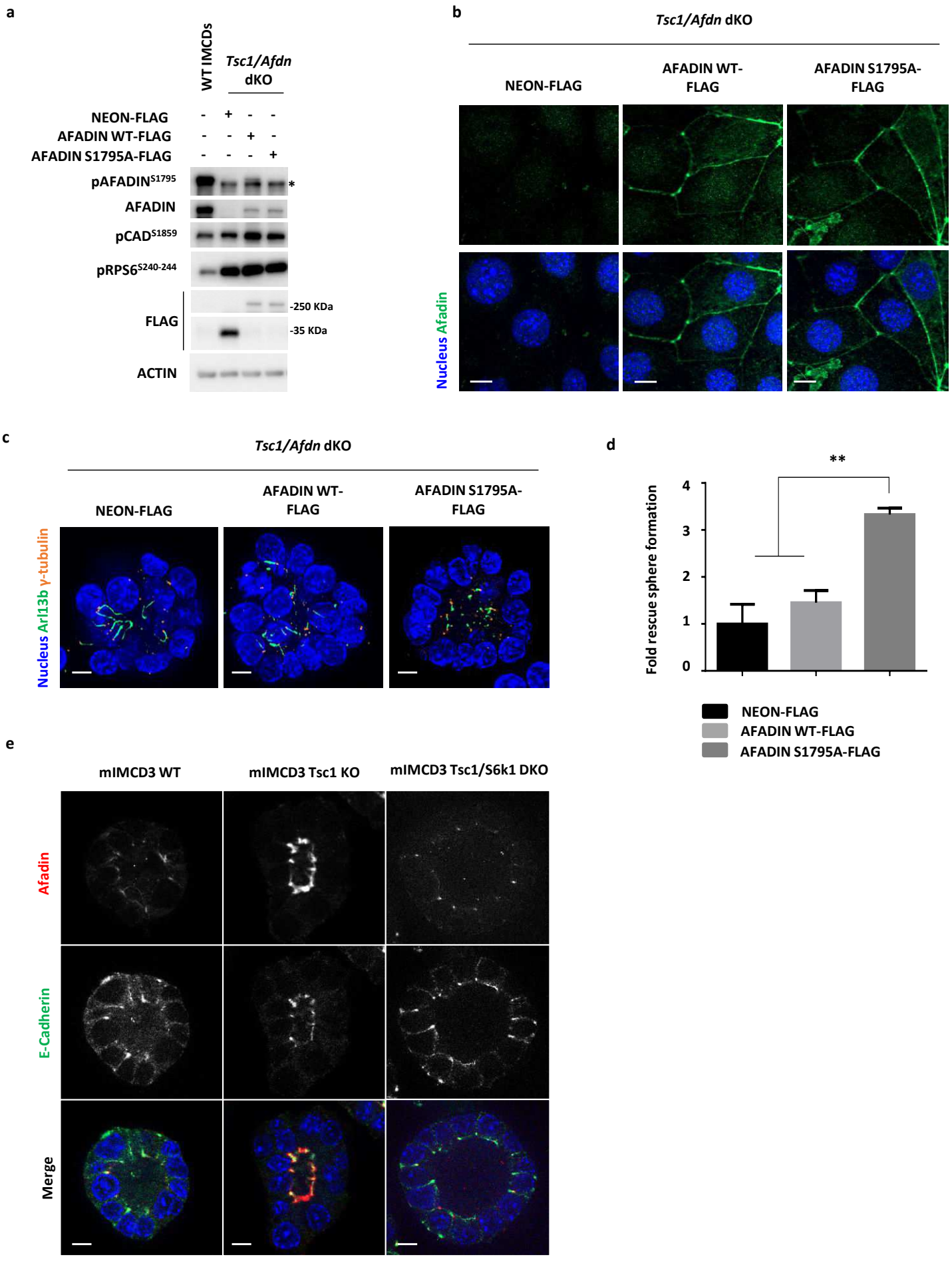
a
WT IMCDs
Tsc1/Afdn dKO
NEON-FLAG
AFADIN WT-FLAG
AFADIN S1795A-FLAG
pAFADIN S1795
AFADIN
pCAD S1859
pRPS6 S240-244
FLAG
-250 KDa
-35 KDa
ACTIN
b
Tsc1/Afdn dKO
NEON-FLAG
AFADIN WT-FLAG
AFADIN S1795A-FLAG
Nucleus Afadin
c
Tsc1/Afdn dKO
NEON-FLAG
AFADIN WT-FLAG
AFADIN S1795A-FLAG
Nucleus Arl13b γ-tubulin
d
**
Fold rescue sphere formation
0
1
2
3
4
NEON-FLAG
AFADIN WT-FLAG
AFADIN S1795A-FLAG
e
mIMCD3 WT
mIMCD3 Tsc1 KO
mIMCD3 Tsc1/S6k1 DKO
Afadin
E-Cadherin
Merge

Figure S1

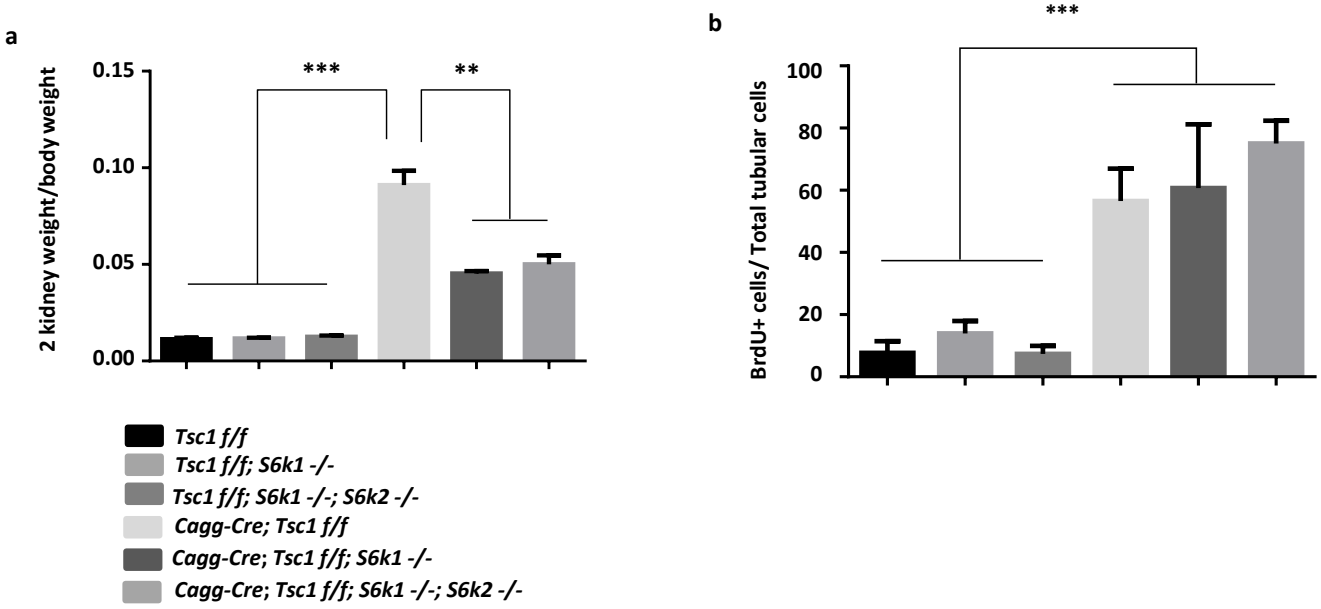
a
2 kidney weight/body weight
0.15
0.10
0.05
0.00
***
**
b
BrdU+ cells/ Total tubular cells
100
80
60
40
20
0
***
Tsc1 f/f
Tsc1 f/f; S6k1 -/-
Tsc1 f/f; S6k1 -/-; S6k2 -/-
Cagg-Cre; Tsc1 f/f
Cagg-Cre; Tsc1 f/f; S6k1 -/-
Cagg-Cre; Tsc1 f/f; S6k1 -/-; S6k2 -/-

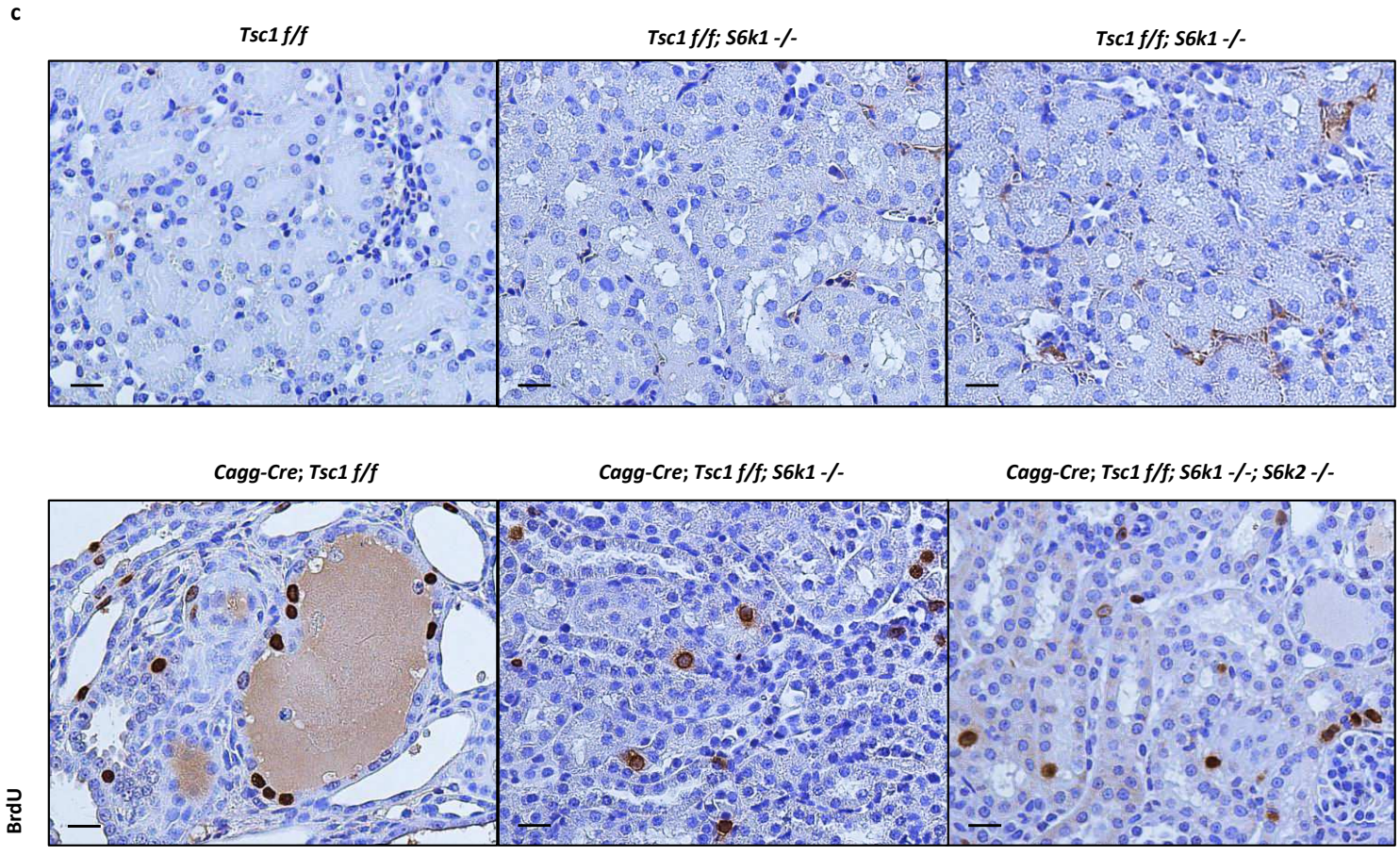
c
Tsc1 f/f
Tsc1 f/f; S6k1 -/-
Tsc1 f/f; S6k1 -/-
Cagg-Cre; Tsc1 f/f
Cagg-Cre; Tsc1 f/f; S6k1 -/-
Cagg-Cre; Tsc1 f/f; S6k1 -/-; S6k2 -/-
BrdU

Figure S2

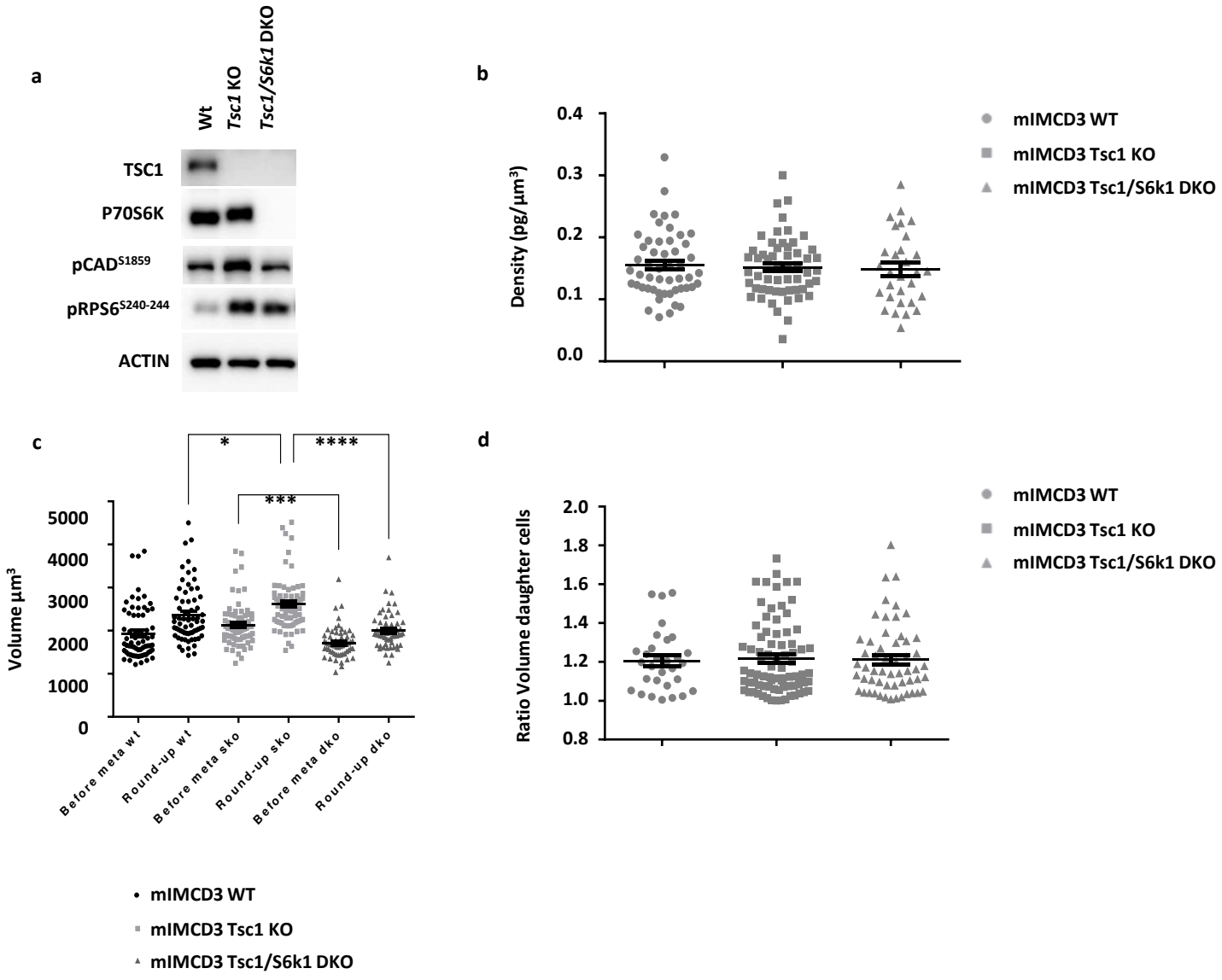
a
Wt
Tsc1 KO
Tsc1/S6k1 DKO
TSC1
P70S6K
pCAD S1859
pRPS6 S240-244
ACTIN
b
Density (pg/µm³)
0.4
0.3
0.2
0.1
0.0
mIMCD3 WT
mIMCD3 Tsc1 KO
mIMCD3 Tsc1/S6k1 DKO
c
*
****
***
Volume µm³
5000
4000
3000
2000
1000
0
Before meta wt
Round-up wt
Before meta sko
Round-up sko
Before meta dko
Round-up dko
mIMCD3 WT
mIMCD3 Tsc1 KO
mIMCD3 Tsc1/S6k1 DKO
d
Ratio Volume daughter cells
2.0
1.8
1.6
1.4
1.2
1.0
0.8
mIMCD3 WT
mIMCD3 Tsc1 KO
mIMCD3 Tsc1/S6k1 DKO

Figure S3

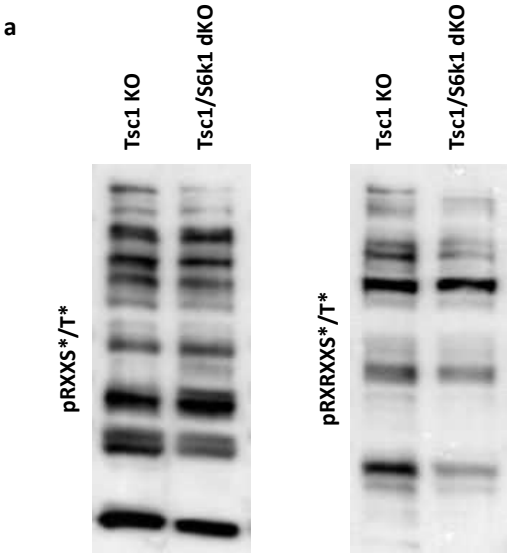

Figure S4

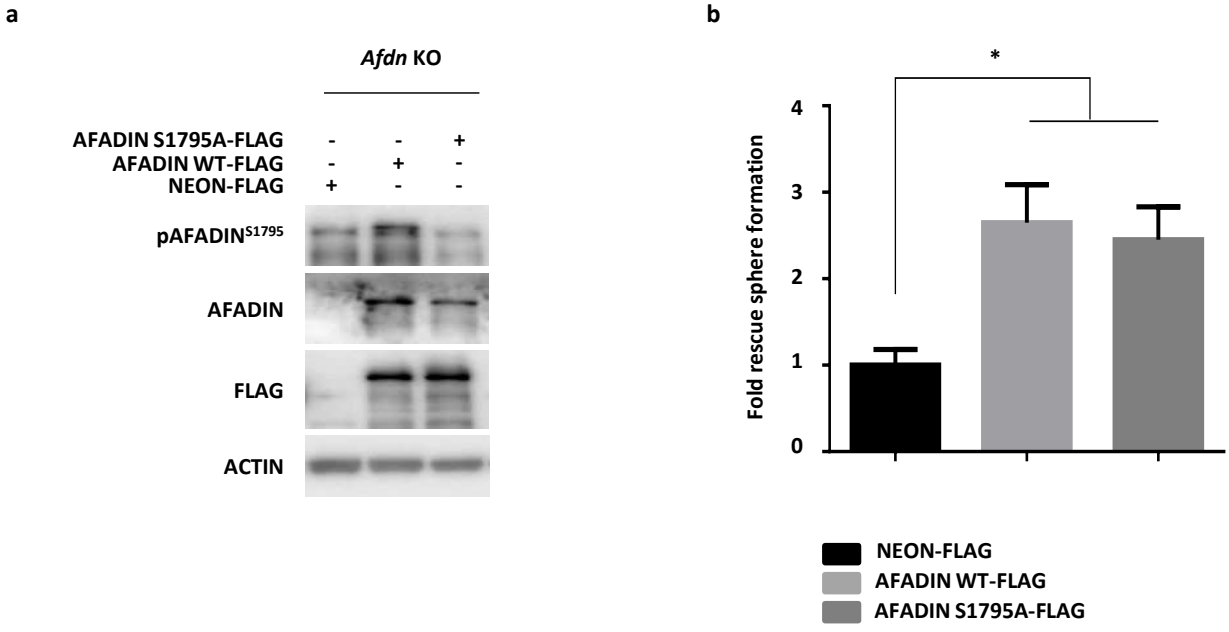

ANNEXES

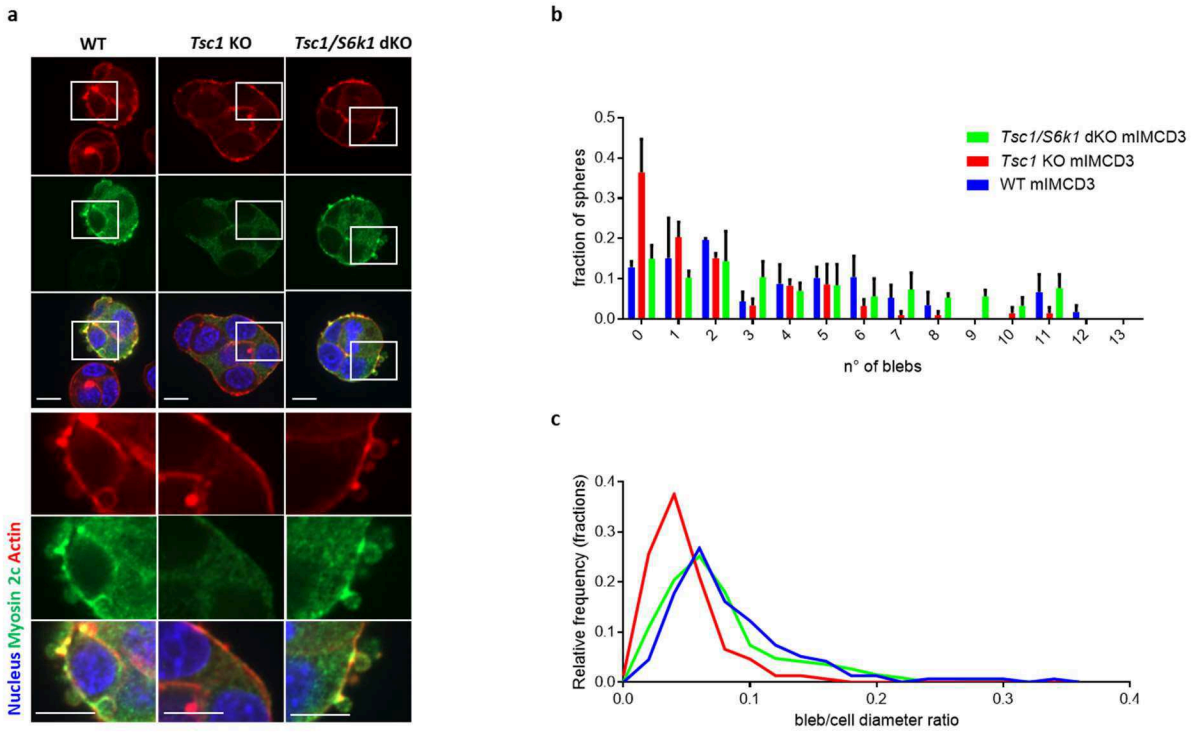

Figure W. Hyperactive S6K1 affects cortical tension in 3D culture

(a) Cells were trypsinized, plated as single cells in Matrigel and cultured for 24 hours before being fixed wth 4% PFA. Immunofluorescence for detection of Myosin-2c and staining of F-actin were then performed to visualize the cortical blebs in the indicated genotypes. Scale bar, 10µm. (b) Graphical representation of the fraction of spheres that possess the indicated number of blebs; spheres Tsc1 KO form less blebs than the controls and the Tsc1/S6K1 dKO. The number of blebs per sphere was calculated on roughly n=70 spheres per experiment. The histograms are an average of 3 independent experiments. Mean ± SEM. (c) Distribution of the bleb-to-cell diameter ratio in the different genotypes expressed as fraction of the totality; spheres Tsc1 KO form smaller blebs than the controls and the Tsc1/S6K1 dKO. The ratio was calculated on roughly n=70 spheres per experiment. The curves have been generated by pulling 3 independent experiments.

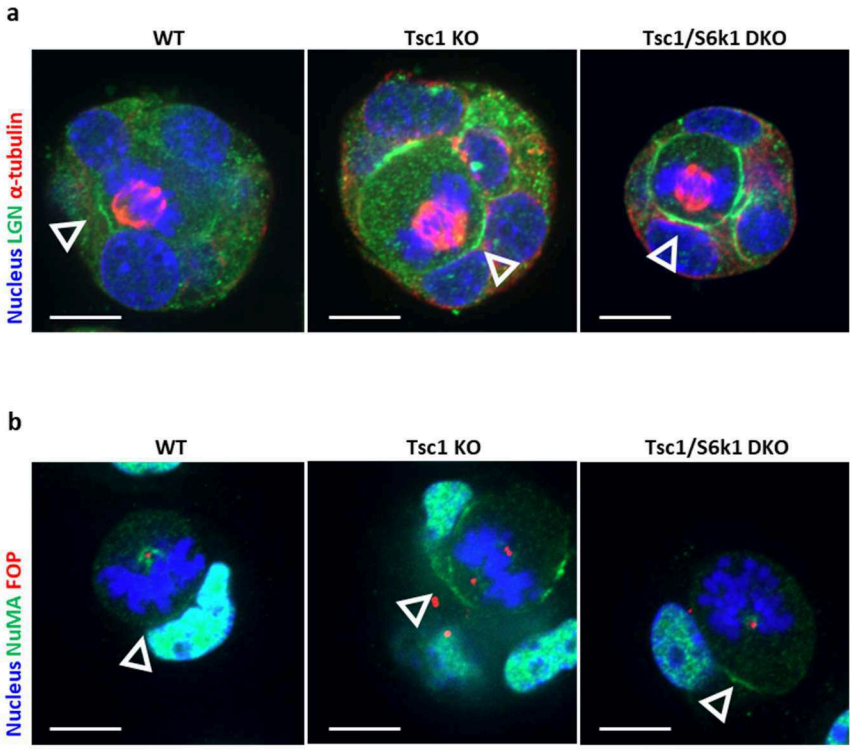

Figure X. LGN and NuMA localize at the membrane in *Tsc1* KO cells

Cells were trypsinized, plated as single cells in Matrigel and cultured for 24 hours before being fixed wth 4% PFA. (a) Representative images of immunofluorescent detection of LGN and α-tubulin were then performed to visualize the presence of LGN at the membrane adjacent to the mitotic spindle. Arrows point to the crescent-shaped membrane localization of LGN. Scale bar, 10μm. (b) representative images of immunofluorescent detection of NuMA and FOP were then performed to visualize the presence of NuMA at the membrane adjacent to the mitotic spindle. Arrows point to the crescent-shaped membrane localization of NuMA. Scale bar, 10μm.

DISCUSSION

Upregulation of mTOR has been reported in many renal diseases, as hamartoma syndromes (Peutz–Jeghers syndrome, Birt-Hogg-Dubé syndrome and, obviously, Tuberous Sclerosis Complex), diabetic nephropathies, polycystic kidney diseases (PKDs) and ciliopathies (Torres et al., 2010; Grahammer et al., 2014; Boehlke et al., 2010). In these diseases mTOR is activated by many mechanisms that trigger different pathological outcomes, but interestingly, cyst formation is a common feature shared by all of them. Many questions arise from the study of mTOR activation in such pathologies, as: what are the molecular basis of the phenotypic differences and similarities? Are some branches of the mTOR pathway specifically involved in one phenotype?

Our data show how the S6K1 axis of the mTOR signaling is crucial for the formation of renal cysts by selectively perturbing the orientation of division of the abnormally-growing tubular cells. Moreover, the phosphoproteomic screening revealed that mTORC1/S6K1 pathway predominantly regulate proteins associated with the cytoskeleton and the cell-to-cell junctions. Finally, we could validate a protein of the cell junctions, Afadin, as a target of S6K1 important in the regulation of oriented cell division.

As detailed in the introduction, mTOR programs cells to proceed in their cell cycle, to grow in size and to produce macromolecules. To generate all these different outcomes, many substrates are under its control. Persistent autophagy inhibition by hyperactive mTORC1 can drive degenerative neurological diseases (Nixon, 2013), hypertrophies (Komatzu et al., 2005) and kidney fibrosis (Li et al., 2016). However, specific deletion of autophagy-driver genes has never shown cystic phenotype (Li et al., 2016; Jiang et al., 2012; Kuma et al., 2017). The deletion of 4E-BP1/2, mTORC1 substrates involved in the control of cap-dependent translation, alters cell senescence, proliferation, insulin resistance and the sensitivity to HFD-induced obesity, but it does not display any particular renal phenotype (Le Bacquer et al., 2007).

S6K1 was shown to drive uninephrectomy (UNX)- and diabetes-induced renal hypertrophy. In both cases an increase in cell size, with minimum increase in cell number, occurs. Genetic inactivation of S6K1 reverted the hypertrophy caused by both UNX and diabetes, with no

alteration of 4E-BP1 phosphorylation (Chen et al., 2009), comparable to rapamycin treatment (Chen et al., 2005) and to $RPS6^{P-/-}$ mice (Xu et al., 2014).

S6K1 is the most active AGC kinase in context of TSC. As I detailed earlier, it has been shown by multiple studies that S6K1 does not participate to the increase in cell number promoted by mTOR activation, but rather to cell size. Our results confirm this and demonstrate that S6K1 does not control cell proliferation in TSC-driven mTORC1 hyperactivation, where both increase in cell number and in cell size occur.

Conversely, our results reveal a role of S6K1 in control of oriented cell division, shown here for the first time. Thus, the mTORC1/S6K1 axis is a central regulator of oriented cell division in post-natal kidney tubular cells. It will be interesting to study its participation in this process of mitotic orientation also in other PKDs where mTOR is upregulated.

Our data are also an important evidence in the PKD field, because they show that oriented cell division (OCD) is necessary to trigger cystogenesis. Since the first report of defective OCD in polycystic kidney (Fischer et al., 2006), the scientific community has been trying to understand the cause-effect relationship between these two processes. Defective OCD has been described before cyst onset in many PKD murine models (Fischer et al., 2006; Luyten et al., 2010; Simons et al., 2005; Bonnet et al., 2009). This led to the assumption that defective OCD is a cause of renal cysts. OCD is controlled by the planar cell polarity (PCP) pathway, a complex system of oriented arrangement of proteins within each cell that allows an organization of the tissue in a plane perpendicular to the apico-basal axis. Briefly, two members of the family of the transmembrane protein cadherins, Fat and Dachsous, are localized asymmetrically at the lateral membrane of epithelial cells, due to reciprocal cross-inhibition (McNeil, 2009). This activates a complex signal transduction in which different proteins of the core PCP signaling are consequently asymmetrically distributed to regulate the planar polarity of the cell in communication with the neighboring cells. In this regard, kidney specific deletion of *Fat4*, member of the Fat cadherins, causes tubule dilatation and cyst formation through randomization of the mitotic spindle orientation (Saburi et al., 2008). Moreover, kidney-specific inactivation of *Wnt9b*, ligand of the Wnt family that signals through the non-canonical pathway, leads to loss of OCD and PKD (Karner et al., 2009).

Nevertheless, it is still debated whether loss of PCP and OCD occurs before or after cystogenesis. Two studies in the same year reported opposite results, one showing that loss

of OCD occurs before cystogenesis in *Pkd1/Pkd2* mutant kidneys (Luyten et a., 2010) and the other showing that loss of OCD is just an effect of tubular enlargement (Nishio et al., 2010). Moreover, disruption of PCP proteins in renal epithelium induces loss of planar polarization but do not cause cysts (Kunimoto et al., 2017).

Our results prove that loss of OCD is necessary to cause cystogenesis because of two main evidences. First, *Tsc1* single mutants display misoriented cell division before cyst onset. Second, the double mutants *Tsc1/S6k1* show repristinated orientation of mitotic spindle and a protection from cyst formation compared to the *Tsc1* single mutants. Of note, the defective OCD in *Tsc1*-mutant kidneys occurs in combination with increased proliferation. The interpretation of our results on the base of the previous data suggests that defects in OCD are necessary but not sufficient to trigger cystogenesis but have to be accompanied by an abnormal growth stimulus, in our case the upregulation of mTORC1. In fact, embryonic deletion of *HNF1β* triggers a very severe PKD with early onset, while post-natal deletion does not cause any cystic phenotype, unless a stress as ischemia/reperfusion (IR) is inflicted (Verdeguer et al., 2010). Thus, PKD onset depends on the proliferation status of the cells that are mutated: cells that are in active proliferation (in this case triggered by IR) and have defective PCP (due to *HNF1β* inactivation) will develop cysts, while IR-driven proliferation *per se* does not induce cyst.

In conclusion, upregulation of mTORC1 in *Tsc1*-mutant kidneys provokes an S6K1-independent induction of cell proliferation and an S6K1-dependent perturbation of OCD, that combined trigger cyst formation.

Defective OCD is due to misoriented mitotic spindle orientation. The orientation of the spindle during mitosis follows the orientation of the centrosomes, the microtubule organizing center (MTOC) organelles. During G1, each epithelial cell possesses one centrosome, localized apically, where it forms the basal body of the primary cilium. In S-phase the centrosome is duplicated to allow, during mitosis, the migration of each centrosomes at the lateral poles to form the mitotic spindle. To assure a correct orientation of cell division, the spindle positioning is regulated by internal and external cues (Di Pietro et al., 2016):

- the LGN/NuMA complex, that during mitosis localizes to the cell cortex at the lateral poles and directs the orientation and positioning of the spindle;

- the PCP pathway and the intercellular junctions, network that orchestrates the orientation of division of single cells relative to the tissue axis and accordingly to mechanical forces;
- the actin cytoskeleton, which forms a network under the membrane (the cortex) in control of cell deformation and force transmission to orient the spindle;

Between these factors an extensive cross-talk exists (Di Pietro et al., 2016). In order to understand which aspects are perturbed in *Tsc1*-mutant renal cells, we evaluated these mechanisms in our models. Loss of LGN or NuMA precludes the correct localization of the spindle poles at the lateral cortex both *in vivo* and in culture (Peyre et al., 2011). For instance, when single cells are cultured on micro adhesive surfaces, the geometry of the surface dictates a specific shape and adhesion pattern to the cells, which determines the axis of division guided by the integrin signaling (Théry et al., 2005). In this condition, if the LGN/NuMA complex is perturbed, the cells will not be able to correctly orient their spindle with the direction imposed by the pattern and will be misoriented in anaphase (Wolf et al., 2019). We cultured our cells on L-shaped micropattern and we measured the angle of cell division relative to the theoretical axis (Figure 5c and d). We observed that mitosis in *Tsc1* KO mIMCD3 cells orients as in the control cells, therefore suggesting that *Tsc1* mutation does not perturb the targeting of the LGN/NuMA complex to the cortex. In this set up, the *Tsc1/S6k1* dKO cells showed a slight defect in cell orientation, probably because their smaller size (Figure 3c) reduces the cellular surface in contact with the fibronectin pattern. In fact it has been shown that kidney cells deriver from dog plated on bigger micropattern have a spread actin cytoskeleton that modifies their contractility and impacts the centrosome polarization and lumen formation compared to smaller micropatterns (Rodríguez-Fraticelli et al., 2012). To go further, we evaluated whether LGN and NuMA could be correctly targeted to the cortex at mitosis by immunofluorescence in early-stage 3D cultures of mIMCD3s. We could observe the presence of cortical crescents of these proteins at the side of the spindle with no significant differences between the genotypes (Figure X). We then concluded that misorientation of cell division in *Tsc1*-mutant is not connected with defects in the mere membrane targeting of LGN and Numa. mTORC1/S6K1 hyperactivation rather prevents the spindle to be aligned to the axis of the tissue.

Very interestingly, the phosphoproteomic screening showed us that proteins related to the cytoskeleton, to the cell junctions and involved in actin binding are the most differentially phosphorylated between *Tsc1* KO and *Tsc1/S6K1* dKO (Figure 6c).

For these reasons we focused on the extrinsic cues that regulate oriented cell division, such as the intercellular junctions and the PCP. During organ morphogenesis a tight crosstalk between the PCP pathway, the cytoskeleton and the cell junctions must be in place in order to assure the correct formation of the organ (Costantini et Kopan, 2010). For example, during embryonic kidney development, the diameter of the nascent tubule is regulated by the process of convergent extension, in which a change of shape, mediated by the actin cytoskeleton and the remodeling of the cell junctions, promotes the elongation of the cells perpendicularly to the longitudinal axis of the tubule, and the consequent intercalation by migration (Figure Y).

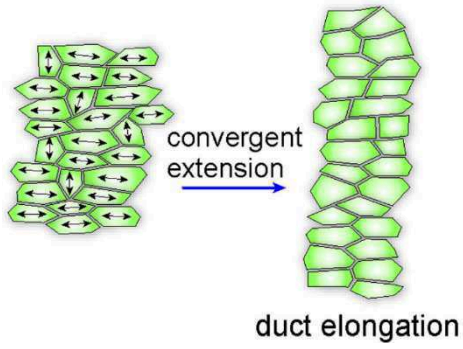

From Costantini et Kopan, 2010

Figure Y. Convergent extension

Scheme of the process of convergent extension for tubule elongation during embryogenesis.

Aderehns junctions (AJs) are composed primarily by the transmembrane cadherins and nectins. These proteins are connected to the actin cytoskeleton through respectively catenins and Afadin. They form intercellular connection systems at the lateral membrane that also serve as hub for signal transduction (Pinheiro et Bellaïche, 2018). Importantly, AJs are very dynamic and capable of responding to mechanical cues by triggering their own remodeling, which is translated into cell reshaping.

The position, the length and the stability of the AJs are crucial to ensure a correct OCD (Gloerich et al., 2017; Hart et al., 2017; Bosveld et al., 2016). Of note, AJs are able to sense external mechanical cues to regulate the adhesive force through changes in actin cortex tension and shape (Buckley et al., 2014; Bardet et al., 2013).

To enter mitosis, cells need to increase their volume and to remodel their actin cytoskeleton to assume a round shape, by establishing a stiff actin cortex (Clark et al., 2013; Chugh et al., 2016). Perturbation of the actin cortex by latrunculin treatment (that prevents actin polymerization) generates spindle orientation defects in cultured cells and *in vivo* (Zheng et al., 2013; Luxenburg et al., 2011) and perturbs LGN cortical localization (Zheng et al., 2013). A stiff and intact actin cortex is therefore crucial for a correct division, probably because it counteracts the pulling forces exerted on the spindle to segregate the microtubules (Redemann et al., 2010). However, it is still not clear how F-actin influences the spindle orientation. Taken together, this data point to an important link between AJs, PCP, actin cytoskeleton and mechanical tension in determining cell shape and cell division orientation.

Tumor suppressor PTEN, a negative regulator of the PI3K/Akt signaling pathway, controls the cortical tension and the AJs rearrangement (Bardet et al., 2013). Briefly, *pten* mosaic invalidation in Drosophila pupal epithelium leads to a heterogeneity in the length of the newly formed cadherin-based AJs that become unstable and cause a decrease in the cortical tension. This eventually perturbs the epithelial organization and rearrangements resulting in defective tissue morphogenesis and polarization. Thus, these results show the implication of the PI3K/Akt signaling pathway, one of the major regulators of mTOR activation, in the dynamic arrangement of cortical tension, AJs and PCP. Therefore, we investigated whether mTORC1 and S6K1 play a role in this regulation too.

We observed that *Tsc1* loss causes a mispositioning of E-cadherin and Afadin correlated with an incorrect localization of the centrosomes (Fig. 4 and 8). Moreover, we have preliminary data showing a decrease in the cortical tension in 3D cultured mIMCD3s depleted of *Tsc1* (Figure W-a), visualized as a decrease in both number (Figure W-b) and size (Figure W-c) of cortical blebs, which are dynamic and localized membrane swelling generated by the cell to relieve excessive cortical tension (Tinevez et al., 2009).

These results favor the hypothesis that an upregulation of mTORC1/S6K1 activity causes an instability of the AJs and of the actin cortex. This may result in loss of cell shape control,

decrease in tension and, therefore, defective orientation of the cells in the tissue with consequential loss of oriented cell division and centrosome delocalization.

For these reasons, the fact that Afadin is an S6K1 substrate upregulated in *Tsc1*- KO kidney (Fig 7 of the manuscript), has risen interesting perspectives in the mechanism of action. Although Afadin is likely not the only substrate of S6K1 involved in this regulation, it has been reported to be a player in OCD control. Afadin is a 200 kDa F-actin-binding protein that acts as a crosslinker between the nectin-based AJs and the actin cortex. It interacts with many proteins as nectins, F-actin, α-catenin, and Rap1 (Mandai et al., 2013). Afadin is essential for the formation of the AJs and for the interaction between nectins and E-cadherin (Figure Y). Briefly, trans-interaction of nectins at the cell-to-cell contact site induces the activation of Rap1 and CDC42 GTPases through the Tyrosine kinase c-Src. Activated Rap1 and CDC42 reorganize the cytoskeleton and help the recruitment of the cadherin-catenin system, in part by Afadin-mediated association between the p120-catenin and E-cadherin. This allows a p120-dependent inhibition of E-cadherin endocytosis and a stabilization of the cadherin- and nectin-based junctions (Hoshino et al., 2005). In fact, downregulation of Afadin impairs the formation of AJs (Sato et al., 2006).

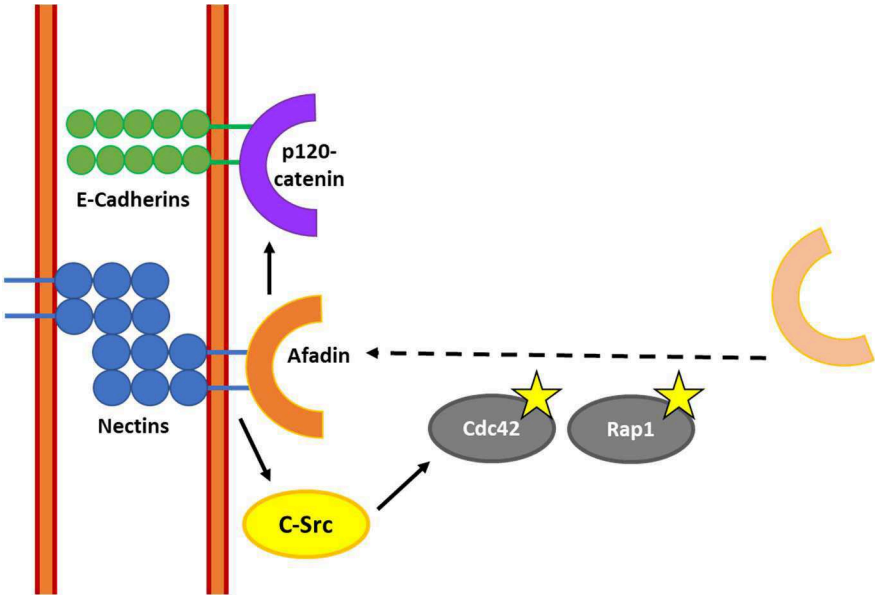

Adapted from Manday et al., 2013

Figure Z. Formation of adherens junctions

Schematic representation of the sequence of events governing the formation of the adherens junctions and role of Afadin.

Canoe, the *Drosophila* orthologue of Afadin, is also localized at the AJs and is required for PCP regulation during embryogenesis (Boettner et al., 2003; Sawyer et al., 2011) by directly regulating the PCP pathway (O'Keefe et al., 2009). Involvement of Afadin in PCP and OCD regulation has also been shown in mammals. For example, polarized accumulation of Afadin at the cell cortex orients the spindle pole and participates in orienting cell division. Mice lacking Afadin in the renal tubular cells have, indeed, misoriented mitosis and tubular abnormalities (Gao et al., 2017). Moreover, during mitosis Afadin can bind to LGN at the plasma membrane, where it links the spindle-associated protein NuMA to the actin cortex at the two cellular poles (Carminati et al., 2016). Carminati and colleagues discovered that Afadin recruits LGN at the poles in metaphase, mediating its interaction with the cortex and other members of the spindle orienting machinery. This then allows the correct recruitment of NuMA at the spindle pole. Of note, this network of interactions is also conserved in *Drosophila*, establishing Afadin/Canoe as the first physical link between cortical actin and the spindle machinery.

Moreover, Afadin has already been reported to be subjected to phosphorylation. The Ser^{1795} has been described as targeted by Akt-mediated phosphorylation upon growth factor's stimulation to mediate the entrance of Afadin into the nucleus and induce a migratory phenotype in breast cancer cells (Elloul et al., 2014). Recently, a group reported that upon insulin stimulation, Akt-mediated phosphorylation of Afadin's Ser^{1795} negatively regulates the insulin signaling in adipocytes. This phosphorylation event is impaired in obesity and insulin resistance conditions (Lundh et al., 2019). Thus, Afadin is placed under the control of the Insulin/PI3K pathway.

Indeed, we demonstrated that S6K1-mediated phosphorylation of the Ser^{1795} of Afadin occurs in TSC conditions when Akt is inhibited and that this event has a role in the regulation of OCD in the kidney downstream of mTORC1 activation (Fig. 7 and 8 of the manuscript). This likely suggests that this phosphorylation event is an important step into the pathogenesis of PI3K/mTOR related pathologies.

To speculate on the role of Afadin phosphorylation in relation to OCD deregulation by hyperactive S6K1, we can make different observation:

- The Ser^{1795} is actually located in the actin-binding domain, just after the Actin- and LGN-binding sites. To date, no one studied the effect of this phosphorylation, or any

phosphorylation, on the ability of Afadin to bind F-actin or LGN and how it can impact the mitotic spindle orientation. It will be therefore interesting to assess it by performing co-immunoprecipitation of LGN and co-sedimentation of F-actin with phospho-mutant (S195A) and phospho-mimetic (S1795E) forms of Afadin.

- The phosphorylated form of Afadin has a higher stability (Fig. 7f of the manuscript) and this might cause a decrease in the dynamics of the AJs (both nectin- and cadherin-based). This defect may lead to abnormal localization of the AJs that would not be able to install a correct planar polarization. In 3D culture of *Tsc1* KO mIMCD3s we actually observed aggregates of Afadin at the apical membrane that strongly colocalize with E-cadherin. Hence, E-cadherin becomes abnormally localized at the apical surface to the detriment of lateral membranes, concomitant with centrosome mispositioning (Fig.8c and 4a of the manuscript).
- Afadin is involved, as other proteins of the AJs, in the generation and response to tissue tension of the epithelial cells. Lack of Canoe disrupts spindle orientation in Drosophila egg chamber by disorganization of myosin, thus perturbing the apical cortical tension and resulting in disproportion of the cells in the tissue (Finegan et al., 2018). Moreover, Afadin has been shown to maintain AJs integrity in response to elevated contractility (Choi et al., 2016). It is, therefore, tempting to hypothesize that the decrease in tissue tension of *Tsc1* KO cells (Fig. X discussion) and the defect in AJs formation (Fig. 8e) are related to Afadin phosphorylation . For instance, phosphorylated Afadin might not be able to respond and help the generation of tension, while promoting migration.

It would be interesting to further investigate the role of mTORC1/S6K1/Afadin in all these aspects and to explore other possible targets that were revealed by the phosphoproteomic screening and may concur in the regulation of PCP, OCD and actin cytoskeleton regulation.

According to our results we can propose the following model: in case of *Tsc1* inactivation, mTORC1 is constitutively activated and promotes multiple changes in the cells mediated by its substrates. Through set of targets, mTORC1 triggers increase in proliferation rate. Conversely, through S6K1 hyperactivation, it induces an increase in cell size. S6K1 also phosphorylates different proteins that are involved in cytoskeleton rearrangement and intercellular junctions, perturbing the shape and the tension of the actin cortex. Moreover, it alters the oriented cell

division by phosphorylation-dependent increased stability of Afadin, that perturbs the E-cadherin localization and the centrosome positioning. For these reasons, S6K1 might be considered as an interesting downstream of mTORC1 to target in therapy, to restore the correct polarization of the cells in the tissue caused in context of mTOR hyperactivation.

REFERENCES

Abe, Y., Yoon, S.O., Kubota, K., Mendoza, M.C., Gygi, S.P., Blenis, J., 2009. p90 ribosomal S6 kinase and p70 ribosomal S6 kinase link phosphorylation of the eukaryotic chaperonin containing TCP-1 to growth factor, insulin, and nutrient signaling. Journal of Biological Chemistry 284, 14939–14948. https://doi.org/10.1074/jbc.M900097200

Aguilar, V., Alliouachene, S., Sotiropoulos, A., Sobering, A., Athea, Y., Djouadi, F., Miraux, S., Thiaudière, E., Foretz, M., Viollet, B., Diolez, P., Bastin, J., Benit, P., Rustin, P., Carling, D., Sandri, M., Ventura-Clapier, R., Pende, M., 2007. S6 Kinase Deletion Suppresses Muscle Growth Adaptations to Nutrient Availability by Activating AMP Kinase. Cell Metabolism 5, 476–487. https://doi.org/10.1016/j.cmet.2007.05.006

Alimonti, A., Nardella, C., Chen, Z., Clohessy, J.G., Carracedo, A., Trotman, L.C., Cheng, K., Varmeh, S., Kozma, S.C., Thomas, G., Rosivatz, E., Woscholski, R., Cognetti, F., Scher, H.I., Pandolfi, P.P., 2010. A novel type of cellular senescence that can be enhanced in mouse models and human tumor xenografts to suppress prostate tumorigenesis. Journal of Clinical Investigation 120, 681–693. https://doi.org/10.1172/JCI40535

Arif, A., Terenzi, F., Potdar, A.A., Jia, J., Sacks, J., China, A., Halawani, D., Vasu, K., Li, X., Brown, J.M., Chen, J., Kozma, S.C., Thomas, G., Fox, P.L., 2017. EPRS is a critical mTORC1-S6K1 effector that influences adiposity in mice. Nature 542, 357–361. https://doi.org/10.1038/nature21380

Armour, E. a., Carson, R.P., Ess, K.C., 2012. Cystogenesis and elongated primary cilia in Tsc1-deficient distal convoluted tubules. AJP: Renal Physiology 303, F584–F592. https://doi.org/10.1152/ajprenal.00141.2012

Astrinidis, A., Senapedis, W., Henske, E.P., 2006. Hamartin , the tuberous sclerosis complex 1 gene product , interacts with polo-like kinase 1 in a phosphorylation-dependent manner. Human molecular genetics 15, 287–297. https://doi.org/10.1093/hmg/ddi444

Bardet, P.-L., Guirao, B., Paoletti, C., Serman, F., Léopold, V., Bosveld, F., Goya, Y., Mirouse, V., Graner, F., Bellaïche, Y., 2013. PTEN Controls Junction Lengthening and Stability during Cell Rearrangement in Epithelial Tissue. Developmental Cell 25, 534–546. https://doi.org/10.1016/j.devcel.2013.04.020

Barilari, M., Bonfils, G., Treins, C., Koka, V., De Villeneuve, D., Fabrega, S., Pende, M., 2017. ZRF1 is a novel S6 kinase substrate that drives the senescence programme. The EMBO Journal 36, 736–750. https://doi.org/10.15252/embj.201694966

Bärlund, M., Monni, O., Kononen, J., Cornelison, R., Torhorst, J., Sauter, G., Kallioniemi OLLI-P, Kallioniemi, A., 2000. Multiple genes at 17q23 undergo amplification and overexpression in breast cancer. Cancer research 60, 5340–4.

Barth-Baus, D., 2002. S6 phosphorylation-independent pathways regulate translation of 5’-terminal oligopyrimidine tract-containing mRNAs in differentiating hematopoietic cells. Nucleic Acids Research 30, 1919–1928. https://doi.org/10.1093/nar/30.9.1919

Ben-Sahra, I., Howell, J.J., Asara, J.M., Manning, B.D., 2013. Stimulation of de Novo

Pyrimidine Synthesis by Growth Signaling Through mTOR and S6K1. Science 339, 1323–1328. https://doi.org/10.1126/science.1228792

Ben-Sahra, I., Manning, B.D., 2017. mTORC1 signaling and the metabolic control of cell growth. Current opinion in cell biology 45, 72–82. https://doi.org/10.1016/j.ceb.2017.02.012

Benvenuto, G., Li, S., Brown, S.J., Braverman, R., Vass, W.C., Cheadle, J.P., Halley, D.J., Sampson, J.R., Wienecke, R., DeClue, J.E., 2000. The tuberous sclerosis-1 (TSC1) gene product hamartin suppresses cell growth and augments the expression of the TSC2 product tuberin by inhibiting its ubiquitination. Oncogene 19, 6306–6316. https://doi.org/10.1038/sj.onc.1204009

Bergmann, C., Guay- Woodford, L.M., Harris, P.C., Horie, S., Dorien, J.M.P., Torres, V.E., 2018. Polycystic kidney disease. Nat Rev Dis Prim. https://doi.org/10.1007/978-3-319-19674-9_19

Blenis, J., Kuo, C.J., Erikson, R.L., 1987. Identification of a ribosomal protein S6 kinase regulated by transformation and growth-promoting stimuli. The Journal of biological chemistry 262, 14373–6.

Blouet, C., Ono, H., Schwartz, G.J., 2008. Mediobasal Hypothalamic p70 S6 Kinase 1 Modulates the Control of Energy Homeostasis. Cell Metabolism 8, 459–467. https://doi.org/10.1016/j.cmet.2008.10.004

Boehlke, C., Kotsis, F., Patel, V., Braeg, S., Voelker, H., Bredt, S., Beyer, T., Janusch, H., Hamann, C., Gödel, M., Müller, K., Herbst, M., Hornung, M., Doerken, M., Köttgen, M., Nitschke, R., Igarashi, P., Walz, G., Kuehn, E.W., 2010. Primary cilia regulate mTORC1 activity and cell size through Lkb1. Nature Cell Biology 12, 1115–1122. https://doi.org/10.1038/ncb2117

Boettner, B., Harjes, P., Ishimaru, S., Heke, M., Fan, H.Q., Qin, Y., Van Aelst, L., Gaul, U., 2003. The AF-6 homolog canoe acts as a Rap1 effector during dorsal closure of the Drosophila embryo. Genetics 165, 159–69.

Bonnet, C.S., Aldred, M., von Ruhland, C., Harris, R., Sandford, R., Cheadle, J.P., 2009. Defects in cell polarity underlie TSC and ADPKD-associated cystogenesis. Human molecular genetics 18, 2166–76. https://doi.org/10.1093/hmg/ddp149

Bosveld, F., Markova, O., Guirao, B., Martin, C., Wang, Z., Pierre, A., Balakireva, M., Gaugue, I., Ainslie, A., Christophorou, N., Lubensky, D.K., Minc, N., Bellaïche, Y., 2016. Epithelial tricellular junctions act as interphase cell shape sensors to orient mitosis. Nature 530, 495–498. https://doi.org/10.1038/nature16970

Bourneville, D.M., 1880. Contribution à l'étude de l'idiotie. Arch. Neurol. 1, 69–90.

Brown, E.J., Albers, M.W., Bum Shin, T., Ichikawa, K., Keith, C.T., Lane, W.S., Schreiber, S.L., 1994. A mammalian protein targeted by G1-arresting rapamycin–receptor complex. Nature 369, 756–758. https://doi.org/10.1038/369756a0

Buckley, C.D., Tan, J., Anderson, K.L., Hanein, D., Volkmann, N., Weis, W.I., Nelson, W.J., Dunn, A.R., 2014. Cell adhesion. The minimal cadherin-catenin complex binds to actin filaments under force. Science (New York, N.Y.) 346, 1254211. https://doi.org/10.1126/science.1254211

C., C., N., K., D.M., H., P.B., C., 2017. Genetics of tuberous sclerosis complex: Implications

for clinical practice. Application of Clinical Genetics 10, 1–8. https://doi.org/10.2147/TACG.S90262 LK - http://rd8hp6du2b.search.serialssolutions.com?sid=EMBASE&issn=1178704X&id=doi:10.2147%2FTACG.S90262&atitle=Genetics+of+tuberous+sclerosis+complex%3A+Implications+for+clinical+practice&stitle=Appl.+Clin.+Genet.&title=Application+of+Clinical+Genetics&volume=10&issue=&spage=&epage=&aulast=Caban&aufirst=Carolina&auinit=C.&aufull=Caban+C.&coden=&isbn=&pages=-&date=2017&auinit1=C&auinitm=

Carminati, M., Gallini, S., Pirovano, L., Alfieri, A., Bisi, S., Mapelli, M., 2016. Concomitant binding of Afadin to LGN and F-actin directs planar spindle orientation. Nature Structural and Molecular Biology 23, 155–163. https://doi.org/10.1038/nsmb.3152

Carnevalli, L.S., Masuda, K., Frigerio, F., Le Bacquer, O., Um, S.H., Gandin, V., Topisirovic, I., Sonenberg, N., Thomas, G., Kozma, S.C., 2010. S6K1 Plays a Critical Role in Early Adipocyte Differentiation. Developmental Cell 18, 763–774. https://doi.org/10.1016/j.devcel.2010.02.018

Castro, A.F., Rebhun, J.F., Clark, G.J., Quilliam, L.A., 2003. Rheb Binds Tuberous Sclerosis Complex 2 (TSC2) and Promotes S6 Kinase Activation in a Rapamycin- and Farnesylation-dependent Manner. Journal of Biological Chemistry 278, 32493–32496. https://doi.org/10.1074/jbc.C300226200

Cheadle, J.P., Dobbie, L., Idziaszczyk, S., Hodges, A.K., Smith, A.J.H., Sampson, J.R., Young, J., 2000. Genomic organization and comparative analysis of the mouse tuberous sclerosis 1 (Tsc1) locus. Mammalian Genome 11, 1135–1138. https://doi.org/10.1007/s003350010203

Chen, J.-K., Chen, J., Neilson, E.G., Harris, R.C., 2005. Role of Mammalian Target of Rapamycin Signaling in Compensatory Renal Hypertrophy. Journal of the American Society of Nephrology 16, 1384–1391. https://doi.org/10.1681/ASN.2004100894

Chen, J.-K., Chen, J., Thomas, G., Kozma, S.C., Harris, R.C., 2009. S6 kinase 1 knockout inhibits uninephrectomy- or diabetes-induced renal hypertrophy. American journal of physiology. Renal physiology 297, F585–F593. https://doi.org/10.1152/ajprenal.00186.2009

Choi, W., Acharya, B.R., Peyret, G., Fardin, M.A., Mège, R.M., Ladoux, B., Yap, A.S., Fanning, A.S., Peifer, M., 2016a. Remodeling the zonula adherens in response to tension and the role of afadin in this response. Journal of Cell Biology 213, 243–260. https://doi.org/10.1083/jcb.201506115

Choi, W., Acharya, B.R., Peyret, G., Fardin, M.-A., Mège, R.-M., Ladoux, B., Yap, A.S., Fanning, A.S., Peifer, M., 2016b. Remodeling the zonula adherens in response to tension and the role of afadin in this response. The Journal of Cell Biology 213, 243–260. https://doi.org/10.1083/jcb.201506115

Chugh, P., Clark, A.G., Smith, M.B., Cassani, D.A.D., Dierkes, K., Ragab, A., Roux, P.P., Charras, G., Salbreux, G., Paluch, E.K., 2017. Actin cortex architecture regulates cell surface tension. Nature Cell Biology 19, 689–697. https://doi.org/10.1038/ncb3525

Clark, A.G., Dierkes, K., Paluch, E.K., 2013. Monitoring actin cortex thickness in live cells. Biophysical Journal. https://doi.org/10.1016/j.bpj.2013.05.057

Costantini, F., Kopan, R., 2010. Patterning a complex organ: Branching morphogenesis and nephron segmentation in kidney development. https://doi.org/10.1016/j.devcel.2010.04.008

Cota, D., Proulx, K., Smith, K.A.B., Kozma, S.C., Thomas, G., Woods, S.C., Seeley, R.J., 2006. Regulates Food Intake. Science 927–930.

Cowley, M.A., Smart, J.L., Rubinstein, M., Cerdán, M.G., Diano, S., Horvath, T.L., Cone, R.D., Low, M.J., 2001. Leptin activates anorexigenic POMC neurons through a neural network in the arcuate nucleus. Nature 411, 480–484. https://doi.org/10.1038/35078085

Curatolo, P., Moavero, R., Roberto, D., Graziola, F., 2015. Genotype/Phenotype Correlations in Tuberous Sclerosis Complex. Seminars in Pediatric Neurology 22, 259–273. https://doi.org/10.1016/j.spen.2015.10.002

Dagon, Y., Hur, E., Zheng, B., Wellenstein, K., Cantley, L.C., Kahn, B.B., 2012. p70S6 Kinase Phosphorylates AMPK on Serine 491 to Mediate Leptin's Effect on Food Intake. Cell Metabolism 16, 104–112. https://doi.org/10.1016/j.cmet.2012.05.010

di Pietro, F., Echard, A., Morin, X., 2016. Regulation of mitotic spindle orientation: an integrated view. EMBO reports 17, 1106–1130. https://doi.org/10.15252/embr.201642292

Dibble, C.C., Asara, J.M., Manning, B.D., 2009. Characterization of Rictor Phosphorylation Sites Reveals Direct Regulation of mTOR Complex 2 by S6K1. Molecular and Cellular Biology 29, 5657–5670. https://doi.org/10.1128/MCB.00735-09

Dibble, C.C., Elis, W., Menon, S., Qin, W., Klekota, J., Asara, J.M., Finan, P.M., Kwiatkowski, D.J., Murphy, L.O., Manning, B.D., 2012. TBC1D7 Is a Third Subunit of the TSC1-TSC2 Complex Upstream of mTORC1. Molecular Cell 47, 535–546. https://doi.org/10.1016/j.molcel.2012.06.009

Dibella, L.M., Park, A., Sun, Z., 2009. Zebrafish Tsc1 reveals functional interactions between the cilium and the TOR pathway. Human Molecular Genetics 18, 595–606. https://doi.org/10.1093/hmg/ddn384

Djouder, N., Metzler, S.C., Schmidt, A., Wirbelauer, C., Gstaiger, M., Aebersold, R., Hess, D., Krek, W., 2007. S6K1-Mediated Disassembly of Mitochondrial URI/PP1γ Complexes Activates a Negative Feedback Program that Counters S6K1 Survival Signaling. Molecular Cell 28, 28–40. https://doi.org/10.1016/j.molcel.2007.08.010

Dorrello, N.V., Peschiaroli, A., Guardavaccaro, D., Colburn, N.H., Sherman, N.E., Pagano, M., 2006. S6K1- and bTRCP-Mediated Degradation of PDCD4 Promotes Protein Translation and Cell Growth. Science 314, 467–472.

Dos D. Sarbassov, Ali, S.M., Kim, D.-H., Guertin, D.A., Latek, R.R., Erdjument-Bromage, H., Tempst, P., Sabatini, D.M., 2004. Rictor, a Novel Binding Partner of mTOR, Defines a Rapamycin-Insensitive and Raptor-Independent Pathway that Regulates the Cytoskeleton. Current Biology 14, 1296–1302. https://doi.org/10.1016/j.cub.2004.06.054

Dowling, R.J.O., Topisirovic, I., Alain, T., Bidinosti, M., Fonseca, B.D., Petroulakis, E., Wang, X., Larsson, O., Selvaraj, A., Liu, Y., Kozma, S.C., Thomas, G., Sonenberg, N., 2010. mTORC1-Mediated Cell Proliferation, But Not Cell Growth, Controlled by the 4E-BPs. Science 328, 1172–1176. https://doi.org/10.1126/science.1187532

EKER, R., 1954. Familial renal adenomas in Wistar rats; a preliminary report. Acta pathologica et microbiologica Scandinavica 34, 554–62.

Elloul, S., Kedrin, D., Knoblauch, N.W., Beck, A.H., Toker, A., 2014. The Adherens Junction Protein Afadin Is an AKT Substrate that Regulates Breast Cancer Cell Migration. Molecular

Cancer Research 12, 464–476. https://doi.org/10.1158/1541-7786.MCR-13-0398

Eng, C.P., Sehgal, S.N., Vézina, C., 1984. Activity of rapamycin (AY-22,989) against transplanted tumors. The Journal of antibiotics 37, 1231–7.

European Chromosome 16 Tuberous Sclerosis Consortium, 1993. Identification and characterization of the tuberous sclerosis gene on chromosome 16. Cell 75, 1305–1315. https://doi.org/10.1016/0092-8674(93)90618-z

Filippakis, H., Belaid, A., Siroky, B., Wu, C., Alesi, N., Hougard, T., Nijmeh, J., Lam, H.C., Henske, E.P., 2018. Vps34-mediated macropinocytosis in Tuberous Sclerosis Complex 2-deficient cells supports tumorigenesis. Scientific Reports 8, 14161. https://doi.org/10.1038/s41598-018-32256-x

Finegan, T.M., Na, D., Cammarota, C., Skeeters, A.V., Nádasi, T.J., Dawney, N.S., Fletcher, A.G., Oakes, P.W., Bergstralh, D.T., 2019. Tissue tension and not interphase cell shape determines cell division orientation in the Drosophila follicular epithelium. The EMBO Journal 38, e100072. https://doi.org/10.15252/embj.2018100072

Fischer, E., Legue, E., Doyen, A., Nato, F., Torres, V., 2006. Defective planar cell polarity in polycystic kidney disease. Nature genetics 38, 2005–2007. https://doi.org/10.1038/ng1701

Fontana, L., Partridge, L., Longo, V.D., 2010. Extending Healthy Life Span–From Yeast to Humans. Science 328, 321–326. https://doi.org/10.1126/science.1172539

Gan, X., Wang, J., Wang, C., Sommer, E., Kozasa, T., Srinivasula, S., Alessi, D., Offermanns, S., Simon, M.I., Wu, D., 2012. PRR5L degradation promotes mTORC2-mediated PKC-δ phosphorylation and cell migration downstream of Gα12. Nature Cell Biology 14, 686–696. https://doi.org/10.1038/ncb2507

Gao, L., Yang, Z., Hiremath, C., Zimmerman, S.E., Long, B., Brakeman, P.R., Mostov, K.E., Bryant, D.M., Luby-Phelps, K., Marciano, D.K., 2017. Afadin orients cell division to position the tubule lumen in developing renal tubules. Development 144, 3511–3520. https://doi.org/10.1242/dev.148908

Gao, X., 2001. TSC1 and TSC2 tumor suppressors antagonize insulin signaling in cell growth. Genes & Development 15, 1383–1392. https://doi.org/10.1101/gad.901101

Gao, X., Zhang, Y., Arrazola, P., Hino, O., Kobayashi, T., Yeung, R.S., Ru, B., Pan, D., 2002. Tsc tumour suppressor proteins antagonize amino-acid-TOR signalling. Nature Cell Biology 4, 699–704. https://doi.org/10.1038/ncb847

Garami, A., Zwartkruis, F.J.T., Nobukuni, T., Joaquin, M., Roccio, M., Stocker, H., Kozma, S.C., Hafen, E., Bos, J.L., Thomas, G., 2003. Insulin activation of Rheb, a mediator of mTOR/S6K/4E-BP signaling, is inhibited by TSC1 and 2. Molecular cell 11, 1457–66.

García-Martínez, J.M., Alessi, D.R., 2008. mTOR complex 2 (mTORC2) controls hydrophobic motif phosphorylation and activation of serum- and glucocorticoid-induced protein kinase 1 (SGK1). Biochemical Journal 416, 375–385. https://doi.org/10.1042/BJ20081668

Ghata, J., Cowley, B.D., 2017. Polycystic Kidney Disease, in: Comprehensive Physiology. John Wiley & Sons, Inc., Hoboken, NJ, USA, pp. 945–975. https://doi.org/10.1002/cphy.c160018

Gloerich, M., Bianchini, J.M., Siemers, K.A., Cohen, D.J., Nelson, W.J., 2017. Cell division

orientation is coupled to cell-cell adhesion by the E-cadherin/LGN complex. Nature communications 8, 13996. https://doi.org/10.1038/ncomms13996

Gonçalves, A.F., Adlesic, M., Brandt, S., Hejhal, T., Harlander, S., Sommer, L., Shakhova, O., Wild, P.J., Frew, I.J., 2017. Evidence of renal angiomyolipoma neoplastic stem cells arising from renal epithelial cells. Nature Communications 8, 1466. https://doi.org/10.1038/s41467-017-01514-3

Gout, I., Minami, T., Hara, K., Tsujishita, Y., Filonenko, V., Waterfield, M.D., Yonezawa, K., 1998. Molecular Cloning and Characterization of a Novel p70 S6 Kinase, p70 S6 Kinase β Containing a Proline-rich Region. Journal of Biological Chemistry 273, 30061–30064. https://doi.org/10.1074/jbc.273.46.30061

Grahammer, F., Wanner, N., Huber, T.B., 2014. mTOR controls kidney epithelia in health and disease. Nephrology Dialysis Transplantation 29, i9–i18. https://doi.org/10.1093/ndt/gft491

Gressner, A.M., Wool, I.G., 1974. The stimulation of the phosphorylation of ribosomal protein S6 by cycloheximide and puromycin. Biochemical and biophysical research communications 60, 1482–90. https://doi.org/10.1016/0006-291x(74)90365-9

Grove, J.R., Banerjee, P., Balasubramanyam, A., Coffer, P.J., Price, D.J., Avruch, J., Woodgett, J.R., 1991. Cloning and expression of two human p70 S6 kinase polypeptides differing only at their amino termini. Molecular and Cellular Biology 11, 5541–5550. https://doi.org/10.1128/MCB.11.11.5541

Harada, H., Andersen, J.S., Mann, M., Terada, N., Korsmeyer, S.J., 2001. p70S6 kinase signals cell survival as well as growth, inactivating the pro-apoptotic molecule BAD. Proceedings of the National Academy of Sciences 98, 9666–9670. https://doi.org/10.1073/pnas.171301998

Harrington, L.S., Findlay, G.M., Gray, A., Tolkacheva, T., Wigfield, S., Rebholz, H., Barnett, J., Leslie, N.R., Cheng, S., Shepherd, P.R., Gout, I., Downes, C.P., Lamb, R.F., 2004. The TSC1-2 tumor suppressor controls insulin–PI3K signaling via regulation of IRS proteins. The Journal of Cell Biology 166, 213–223. https://doi.org/10.1083/jcb.200403069

Harrison, D.E., Strong, R., Sharp, Z.D., Nelson, J.F., Astle, C.M., Flurkey, K., Nadon, N.L., Wilkinson, J.E., Frenkel, K., Carter, C.S., Pahor, M., Javors, M.A., Fernandez, E., Miller, R.A., 2009. Rapamycin fed late in life extends lifespan in genetically heterogeneous mice. Nature 460, 392–395. https://doi.org/10.1038/nature08221

Hart, K.C., Tan, J., Siemers, K.A., Sim, J.Y., Pruitt, B.L., Nelson, W.J., Gloerich, M., 2017. E-cadherin and LGN align epithelial cell divisions with tissue tension independently of cell shape. Proceedings of the National Academy of Sciences of the United States of America 114, E5845–E5853. https://doi.org/10.1073/pnas.1701703114

Hartman, T.R., Liu, D., Zilfou, J.T., Robb, V., Morrison, T., Watnick, T., Henske, E.P., 2009. The tuberous sclerosis proteins regulate formation of the primary cilium via a rapamycin-insensitive and polycystin 1-independent pathway. Human Molecular Genetics 18, 151–163. https://doi.org/10.1093/hmg/ddn325

Heitman, J., Movva, N., Hall, M., 1991. Targets for cell cycle arrest by the immunosuppressant rapamycin in yeast. Science 253, 905–909. https://doi.org/10.1126/science.1715094

Henske, E.P., Jóźwiak, S., Kingswood, J.C., Sampson, J.R., Thiele, E.A., 2016. Tuberous sclerosis complex. Nature Reviews Disease Primers 2, 16035. https://doi.org/10.1038/nrdp.2016.35

Hildebrandt, F., Benzing, T., Katsanis, N., 2011. Ciliopathies. New England Journal of Medicine 364, 1533–1543. https://doi.org/10.1056/NEJMra1010172

Holz, M.K., Ballif, B.A., Gygi, S.P., Blenis, J., 2005. mTOR and S6K1 Mediate Assembly of the Translation Preinitiation Complex through Dynamic Protein Interchange and Ordered Phosphorylation Events. Cell 123, 569–580. https://doi.org/10.1016/j.cell.2005.10.024

Holz, M.K., Blenis, J., 2005. Identification of S6 Kinase 1 as a Novel Mammalian Target of Rapamycin (mTOR)-phosphorylating Kinase. Journal of Biological Chemistry 280, 26089–26093. https://doi.org/10.1074/jbc.M504045200

Hoshino, T., Sakisaka, T., Baba, T., Yamada, T., Kimura, T., Takai, Y., 2005. Regulation of E-cadherin Endocytosis by Nectin through Afadin, Rap1, and p120 ctn. Journal of Biological Chemistry 280, 24095–24103. https://doi.org/10.1074/jbc.M414447200

Hsu, P.P., Kang, S.A., Rameseder, J., Zhang, Y., Ottina, K.A., Lim, D., Peterson, T.R., Choi, Y., Gray, N.S., Yaffe, M.B., Marto, J.A., Sabatini, D.M., 2011. The mTOR-Regulated Phosphoproteome Reveals a Mechanism of mTORC1-Mediated Inhibition of Growth Factor Signaling. Science 332, 1317–1322. https://doi.org/10.1126/science.1199498

Huang, J., Manning, B.D., 2008. The TSC1–TSC2 complex: a molecular switchboard controlling cell growth. Biochemical Journal 412, 179–190. https://doi.org/10.1042/bj20080281

Huang, J., Wu, S., Wu, C.-L., Manning, B.D., 2009. Signaling Events Downstream of Mammalian Target of Rapamycin Complex 2 Are Attenuated in Cells and Tumors Deficient for the Tuberous Sclerosis Complex Tumor Suppressors. Cancer Research 69, 6107–6114. https://doi.org/10.1158/0008-5472.CAN-09-0975

Huang, Y., Hu, K., Zhang, S., Dong, X., Yin, Z., Meng, R., Zhao, Y., Dai, X., Zhang, T., Yang, K., Liu, L., Huang, K., Shi, S., Zhang, Y., Chen, J., Wu, G., Xu, S., 2018. S6K1 phosphorylation-dependent degradation of Mxi1 by β-Trcp ubiquitin ligase promotes Myc activation and radioresistance in lung cancer. Theranostics 8, 1286–1300. https://doi.org/10.7150/thno.22552

Inoki, K., 2003. Rheb GTPase is a direct target of TSC2 GAP activity and regulates mTOR signaling. Genes & Development 17, 1829–1834. https://doi.org/10.1101/gad.1110003

Inoki, K., Li, Y., Zhu, T., Wu, J., Guan, K.-L., 2002. TSC2 is phosphorylated and inhibited by Akt and suppresses mTOR signalling. Nature Cell Biology 4, 648–657. https://doi.org/10.1038/ncb839

Ito, N., Rubin, G.M., 1999. gigas, a Drosophila Homolog of Tuberous Sclerosis Gene Product-2, Regulates the Cell Cycle. Cell 96, 529–539. https://doi.org/10.1016/S0092-8674(00)80657-1

Jacinto, E., Loewith, R., Schmidt, A., Lin, S., Rüegg, M.A., Hall, A., Hall, M.N., 2004. Mammalian TOR complex 2 controls the actin cytoskeleton and is rapamycin insensitive. Nature Cell Biology 6, 1122–1128. https://doi.org/10.1038/ncb1183

Jefferies, H.B.J., 1997. Rapamycin suppresses 5'TOP mRNA translation through inhibition

of p70s6k. The EMBO Journal 16, 3693–3704. https://doi.org/10.1093/emboj/16.12.3693

Jenö, P., Jäggi, N., Luther, H., Siegmann, M., Thomas, G., 1989. Purification and characterization of a 40 S ribosomal protein S6 kinase from vanadate-stimulated Swiss 3T3 cells. The Journal of biological chemistry 264, 1293–7.

Jiang, M., Wei, Q., Dong, G., Komatsu, M., Su, Y., Dong, Z., 2012. Autophagy in proximal tubules protects against acute kidney injury. Kidney international 82, 1271–83. https://doi.org/10.1038/ki.2012.261

Kang, S.A., Pacold, M.E., Cervantes, C.L., Lim, D., Lou, H.J., Ottina, K., Gray, N.S., Turk, B.E., Yaffe, M.B., Sabatini, D.M., 2013. mTORC1 Phosphorylation Sites Encode Their Sensitivity to Starvation and Rapamycin. Science 341, 1236566–1236566. https://doi.org/10.1126/science.1236566

Karner, C.M., Chirumamilla, R., Aoki, S., Igarashi, P., Wallingford, J.B., Carroll, T.J., 2009. Wnt9b signaling regulates planar cell polarity and kidney tubule morphogenesis. Nature genetics 41, 793–9. https://doi.org/10.1038/ng.400

Karni, R., de Stanchina, E., Lowe, S.W., Sinha, R., Mu, D., Krainer, A.R., 2007. The gene encoding the splicing factor SF2/ASF is a proto-oncogene. Nature Structural & Molecular Biology 14, 185–193. https://doi.org/10.1038/nsmb1209

Kenyon, C., 2005. The Plasticity of Aging: Insights from Long-Lived Mutants. Cell 120, 449–460. https://doi.org/10.1016/j.cell.2005.02.002

Kim, J., Kundu, M., Viollet, B., Guan, K.-L., 2011. AMPK and mTOR regulate autophagy through direct phosphorylation of Ulk1. Nature Cell Biology 13, 132–141. https://doi.org/10.1038/ncb2152

Kim, Y.-M., Jung, C.H., Seo, M., Kim, E.K., Park, J.-M., Bae, S.S., Kim, D.-H., 2015. mTORC1 Phosphorylates UVRAG to Negatively Regulate Autophagosome and Endosome Maturation. Molecular Cell 57, 207–218. https://doi.org/10.1016/j.molcel.2014.11.013

Kingswood, J.C., Bissler, J.J., Budde, K., Hulbert, J., Guay-Woodford, L., Sampson, J.R., Sauter, M., Cox, J., Patel, U., Elmslie, F., Anderson, C., Zonnenberg, B.A., 2016. Review of the Tuberous Sclerosis Renal Guidelines from the 2012 Consensus Conference: Current Data and Future Study. Nephron 134, 51–58. https://doi.org/10.1159/000448293

Knudson, A.G.J., 2001. Mutation and Cancer: Statistical Study of Retinoblastoma. Proc. Nat. Acad. Sci. USA 68, 820–823.

Kobayashi, T., Hirayama, Y., Kobayashi, E., Kubo, Y., Hino, O., 1995. A germline insertion in the tuberous sclerosis (Tsc2) gene gives rise to the Eker rat model of dominantly inherited cancer. Nature Genetics 9, 70–74. https://doi.org/10.1038/ng0195-70

Kobayashi, T., Minowa, O., Kuno, J., Mitani, H., Hino, O., Noda, T., 1999. Renal carcinogenesis, hepatic hemangiomatosis, and embryonic lethality caused by a germ-line Tsc2 mutation in mice. Cancer research 59, 1206–11.

Kobayashi, T., Minowa, O., Sugitani, Y., Takai, S., Mitani, H., Kobayashi, E., Noda, T., Hino, O., 2001. A germ-line Tsc1 mutation causes tumor development and embryonic lethality that are similar, but not identical to, those caused by Tsc2 mutation in mice. Proceedings of the National Academy of Sciences 98, 8762–8767. https://doi.org/10.1073/pnas.151033798

Kobayashi, T., Mitani, H., Takahashi, R. -i., Hirabayashi, M., Ueda, M., Tamura, H., Hino,

O., 1997. Transgenic rescue from embryonic lethality and renal carcinogenesis in the Eker rat model by introduction of a wild-type Tsc2 gene. Proceedings of the National Academy of Sciences 94, 3990–3993. https://doi.org/10.1073/pnas.94.8.3990

Komatsu, M., Waguri, S., Ueno, T., Iwata, J., Murata, S., Tanida, I., Ezaki, J., Mizushima, N., Ohsumi, Y., Uchiyama, Y., Kominami, E., Tanaka, K., Chiba, T., 2005. Impairment of starvation-induced and constitutive autophagy in Atg7-deficient mice. The Journal of cell biology 169, 425–34. https://doi.org/10.1083/jcb.200412022

Kothare, S.V., Singh, K., Chalifoux, J.R., Staley, B.A., Weiner, H.L., Menzer, K., Devinsky, O., 2014. Severity of manifestations in tuberous sclerosis complex in relation to genotype. Epilepsia 55, 1025–1029. https://doi.org/10.1111/epi.12680

Kuma, A., Komatsu, M., Mizushima, N., 2017. Autophagy-monitoring and autophagy-deficient mice. Autophagy 13, 1619–1628. https://doi.org/10.1080/15548627.2017.1343770

Kunimoto, K., Bayly, R.D., Vladar, E.K., Vonderfecht, T., Gallagher, A.R., Axelrod, J.D., 2017. Disruption of Core Planar Cell Polarity Signaling Regulates Renal Tubule Morphogenesis but Is Not Cystogenic. Current Biology. https://doi.org/10.1016/j.cub.2017.09.011

Kunz, J., Henriquez, R., Schneider, U., Deuter-Reinhard, M., Movva, N.R., Hall, M.N., 1993. Target of rapamycin in yeast, TOR2, is an essential phosphatidylinositol kinase homolog required for G1 progression. Cell 73, 585–596. https://doi.org/10.1016/0092-8674(93)90144-F

Kwiatkowski, D.J., 2010. Rat and Mouse Models of Tuberous Sclerosis, in: Tuberous Sclerosis Complex. Wiley-VCH Verlag GmbH & Co. KGaA, Weinheim, Germany, pp. 117–143. https://doi.org/10.1002/9783527630073.ch7

Kwiatkowski, D.J., Zhang, H., Bandura, J.L., Heiberger, K.M., Glogauer, M., El-Hashemite, N., Onda, H., 2002. A mouse model of TSC1 reveals sex-dependent lethality from liver hemangiomas, and up-regulation of p70S6 kinase activity in Tsc1 null cells. Human molecular genetics 11, 525–534.

Lai, K.P., Leong, W.F., Chau, J.F.L., Jia, D., Zeng, L., Liu, H., He, L., Hao, A., Zhang, H., Meek, D., Velagapudi, C., Habib, S.L., Li, B., 2010. S6K1 is a multifaceted regulator of Mdm2 that connects nutrient status and DNA damage response. The EMBO Journal 29, 2994–3006. https://doi.org/10.1038/emboj.2010.166

Lam, H.C., Baglini, C.V., Lope, A.L., Parkhitko, A.A., Liu, H.-J., Alesi, N., Malinowska, I.A., Ebrahimi-Fakhari, D., Saffari, A., Yu, J.J., Pereira, A., Khabibullin, D., Ogorek, B., Nijmeh, J., Kavanagh, T., Handen, A., Chan, S.Y., Asara, J.M., Oldham, W.M., Diaz-Meco, M.T., Moscat, J., Sahin, M., Priolo, C., Henske, E.P., 2017. p62/SQSTM1 Cooperates with Hyperactive mTORC1 to Regulate Glutathione Production, Maintain Mitochondrial Integrity, and Promote Tumorigenesis. Cancer Research 77, 3255–3267. https://doi.org/10.1158/0008-5472.CAN-16-2458

Lam, H.C., Siroky, B.J., Henske, E.P., 2018. Renal disease in tuberous sclerosis complex: pathogenesis and therapy. Nature Reviews Nephrology 14, 704–716. https://doi.org/10.1038/s41581-018-0059-6

Le Bacquer, O., Petroulakis, E., Paglialunga, S., Poulin, F., Richard, D., Cianflone, K., Sonenberg, N., 2007. Elevated sensitivity to diet-induced obesity and insulin resistance in mice lacking 4E-BP1 and 4E-BP2. Journal of Clinical Investigation 117, 387–396.

https://doi.org/10.1172/JCI29528

Lee, G., Zheng, Y., Cho, S., Jang, C., England, C., Dempsey, J.M., Yu, Y., Liu, X., He, L., Cavaliere, P.M., Chavez, A., Zhang, E., Isik, M., Couvillon, A., Dephoure, N.E., Blackwell, T.K., Yu, J.J., Rabinowitz, J.D., Cantley, L.C., Blenis, J., 2017. Post-transcriptional Regulation of De Novo Lipogenesis by mTORC1-S6K1-SRPK2 Signaling. Cell 171, 1545–1558.e18. https://doi.org/10.1016/j.cell.2017.10.037

Lee-Fruman, K.K., Kuo, C.J., Lippincott, J., Terada, N., Blenis, J., 1999. Characterization of S6K2, a novel kinase homologous to S6K1. Oncogene 18, 5108–5114. https://doi.org/10.1038/sj.onc.1202894

Li, H., Peng, X., Wang, Yating, Cao, S., Xiong, L., Fan, J., Wang, Yihan, Zhuang, S., Yu, X., Mao, H., 2016. Atg5-mediated autophagy deficiency in proximal tubules promotes cell cycle G2/M arrest and renal fibrosis. Autophagy 12, 1472–86. https://doi.org/10.1080/15548627.2016.1190071

Li, X., Gao, T., 2013. mTORC2 phosphorylates protein kinase Cζ to regulate its stability and activity. EMBO reports n/a–n/a. https://doi.org/10.1002/embr.201338119

Li, Y., Corradetti, M.N., Inoki, K., Guan, K.-L., 2004. TSC2: filling the GAP in the mTOR signaling pathway. Trends in biochemical sciences 29, 32–8. https://doi.org/10.1016/j.tibs.2003.11.007

Liang, N., Zhang, C., Dill, P., Panasyuk, G., Pion, D., Koka, V., Gallazzini, M., Olson, E.N., Lam, H., Henske, E.P., Dong, Z., Apte, U., Pallet, N., Johnson, R.L., Terzi, F., Kwiatkowski, D.J., Scoazec, J.-Y., Martignoni, G., Pende, M., 2014. Regulation of YAP by mTOR and autophagy reveals a therapeutic target of tuberous sclerosis complex. The Journal of experimental medicine 211, 2249–63. https://doi.org/10.1084/jem.20140341

Lipton, J.O., Yuan, E.D., Boyle, L.M., Ebrahimi-Fakhari, D., Kwiatkowski, E., Nathan, A., Güttler, T., Davis, F., Asara, J.M., Sahin, M., 2015. The circadian protein BMAL1 regulates translation in response to S6K1-mediated phosphorylation. Cell 161, 1138–1151. https://doi.org/10.1016/j.cell.2015.04.002

Liu, P., Gan, W., Chin, Y.R., Ogura, K., Guo, J., Zhang, J., Wang, B., Blenis, J., Cantley, L.C., Toker, A., Su, B., Wei, W., 2015. PtdIns(3,4,5) P 3 -Dependent Activation of the mTORC2 Kinase Complex. Cancer Discovery 5, 1194–1209. https://doi.org/10.1158/2159-8290.CD-15-0460

Liu, P., Gan, W., Inuzuka, H., Lazorchak, A.S., Gao, D., Arojo, O., Liu, D., Wan, L., Zhai, B., Yu, Y., Yuan, M., Kim, B.M., Shaik, S., Menon, S., Gygi, S.P., Lee, T.H., Asara, J.M., Manning, B.D., Blenis, J., Su, B., Wei, W., 2013. Sin1 phosphorylation impairs mTORC2 complex integrity and inhibits downstream Akt signalling to suppress tumorigenesis. Nature Cell Biology 15, 1340–1350. https://doi.org/10.1038/ncb2860

Liu, Y.-C., Li, F., Handler, J., Huang, C.R.L., Xiang, Y., Neretti, N., Sedivy, J.M., Zeller, K.I., Dang, C.V., 2008. Global Regulation of Nucleotide Biosynthetic Genes by c-Myc. PLoS ONE 3, e2722. https://doi.org/10.1371/journal.pone.0002722

Long, X., Lin, Y., Ortiz-Vega, S., Yonezawa, K., Avruch, J., 2005a. Rheb Binds and Regulates the mTOR Kinase. Current Biology 15, 702–713. https://doi.org/10.1016/j.cub.2005.02.053

Long, X., Ortiz-Vega, S., Lin, Y., Avruch, J., 2005b. Rheb Binding to Mammalian Target of Rapamycin (mTOR) Is Regulated by Amino Acid Sufficiency. Journal of Biological Chemistry

280, 23433–23436. https://doi.org/10.1074/jbc.C500169200

Lundh, M., Petersen, P.S., Isidor, M.S., Kazoka-Sørensen, D.N., Plucińska, K., Shamsi, F., Ørskov, C., Tozzi, M., Brown, E.L., Andersen, E., Ma, T., Müller, U., Barrès, R., Kristiansen, V.B., Gerhart-Hines, Z., Tseng, Y.-H., Emanuelli, B., 2019. Afadin is a scaffold protein repressing insulin action via HDAC6 in adipose tissue. EMBO reports e48216. https://doi.org/10.15252/embr.201948216

Lustig, Y., Ruas, J.L., Estall, J.L., Lo, J.C., Devarakonda, S., Laznik, D., Choi, J.H., Ono, H., Olsen, J.V., Spiegelman, B.M., 2011. Separation of the gluconeogenic and mitochondrial functions of PGC-1 through S6 kinase. Genes & Development 25, 1232–1244. https://doi.org/10.1101/gad.2054711

Luxenburg, C., Amalia Pasolli, H., Williams, S.E., Fuchs, E., 2011. Developmental roles for Srf, cortical cytoskeleton and cell shape in epidermal spindle orientation. Nature Cell Biology 13, 203–214. https://doi.org/10.1038/ncb2163

Luyten, A., Su, X., Gondela, S., Chen, Y., Rompani, S., Takakura, A., Zhou, J., 2010. Aberrant Regulation of Planar Cell Polarity in Polycystic Kidney Disease. Journal of the American Society of Nephrology 21, 1521–1532. https://doi.org/10.1681/ASN.2010010127

Ma, X.M., Yoon, S.O., Richardson, C.J., Jülich, K., Blenis, J., 2008. SKAR Links Pre-mRNA Splicing to mTOR/S6K1-Mediated Enhanced Translation Efficiency of Spliced mRNAs. Cell 133, 303–313. https://doi.org/10.1016/j.cell.2008.02.031

Magnuson, B., Ekim, B., Fingar, D.C., 2012. Regulation and function of ribosomal protein S6 kinase (S6K) within mTOR signalling networks. Biochemical Journal 441, 1–21. https://doi.org/10.1042/bj20110892

Mandai, K., Rikitake, Y., Shimono, Y., Takai, Y., 2013. Afadin/AF-6 and canoe: roles in cell adhesion and beyond. Progress in molecular biology and translational science 116, 433–54. https://doi.org/10.1016/B978-0-12-394311-8.00019-4

Manning, B.D., Tee, A.R., Logsdon, M.N., Blenis, J., Cantley, L.C., 2002. Identification of the tuberous sclerosis complex-2 tumor suppressor gene product tuberin as a target of the phosphoinositide 3-kinase/akt pathway. Molecular cell 10, 151–62.

Martel, R.R., Klicius, J., Galet, S., 1977. Inhibition of the immune response by rapamycin, a new antifungal antibiotic. Canadian journal of physiology and pharmacology 55, 48–51.

McNeill, H., 2009. Planar Cell Polarity and the Kidney. Journal of the American Society of Nephrology 20, 2104–2111. https://doi.org/10.1681/ASN.2008111173

Menon, S., Dibble, C.C., Talbott, G., Hoxhaj, G., Valvezan, A.J., Takahashi, H., Cantley, L.C., Manning, B.D., 2014. Spatial control of the TSC complex integrates insulin and nutrient regulation of mTORC1 at the lysosome. Cell 156, 771–785. https://doi.org/10.1016/j.cell.2013.11.049

Meyuhas, O., Dreazen, A., 2009. Chapter 3 Ribosomal Protein S6 Kinase: From TOP mRNAs to Cell Size, 1st ed. Elsevier Inc. https://doi.org/10.1016/S1877-1173(09)90003-5

Mieulet, V., Roceri, M., Espeillac, C., Sotiropoulos, A., Ohanna, M., Oorschot, V., Klumperman, J., Sandri, M., Pende, M., 2007. S6 kinase inactivation impairs growth and translational target phosphorylation in muscle cells maintaining proper regulation of protein turnover. American Journal of Physiology-Cell Physiology 293, C712–C722.

https://doi.org/10.1152/ajpcell.00499.2006

Miloloza, A., Kubista, M., Rosner, M., Hengstschläger, M., 2002. Evidence for Separable Functions of Tuberous Sclerosis Gene Products in Mammalian Cell Cycle Regulation. Journal of Neuropathology & Experimental Neurology 61, 154–163. https://doi.org/10.1093/jnen/61.2.154

Montagne, J., Stewart, M.J., Stocker, H., Hafen, E., Kozma, S.C., Thomas, G., 1999. Drosophila S6 Kinase: A Regulator of Cell Size. Science 285, 2126 LP – 2129.

Nellist, M., Brouwer, R.W.W., Kockx, C.E.M., van Veghel-Plandsoen, M., Withagen-Hermans, C., Prins-Bakker, L., Hoogeveen-Westerveld, M., Mrsic, A., van den Berg, M.M.P., Koopmans, A.E., de Wit, M.C., Jansen, F.E., Maat-Kievit, A.J.A., van den Ouweland, A., Halley, D., de Klein, A., van IJcken, W.F.J., 2015. Targeted Next Generation Sequencing reveals previously unidentified and mutations. BMC Medical Genetics 16, 1–11. https://doi.org/10.1186/s12881-015-0155-4

Neuman, N.A., Henske, E.P., 2011. Non-canonical functions of the tuberous sclerosis complex-Rheb signalling axis. EMBO Molecular Medicine 3, 189–200. https://doi.org/10.1002/emmm.201100131

Nishio, S., Tian, X., Gallagher, A.R., Yu, Z., Patel, V., Igarashi, P., Somlo, S., 2010. Loss of Oriented Cell Division Does not Initiate Cyst Formation. Journal of the American Society of Nephrology 21, 295–302. https://doi.org/10.1681/ASN.2009060603

Nixon, R.A., 2013. The role of autophagy in neurodegenerative disease. Nature medicine 19, 983–97. https://doi.org/10.1038/nm.3232

Nyg\a ard, O., Nika, H., 1982. Identification by RNA-protein cross-linking of ribosomal proteins located at the interface between the small and the large subunits of mammalian ribosomes. The EMBO journal 1, 357–62.

Ohanna, M., Sobering, A.K., Lapointe, T., Lorenzo, L., Praud, C., Petroulakis, E., Sonenberg, N., Kelly, P.A., Sotiropoulos, A., Pende, M., 2005. Atrophy of S6K1−/− skeletal muscle cells reveals distinct mTOR effectors for cell cycle and size control. Nature Cell Biology 7, 286–294. https://doi.org/10.1038/ncb1231

O'Keefe, D.D., Gonzalez-Niño, E., Burnett, M., Dylla, L., Lambeth, S.M., Licon, E., Amesoli, C., Edgar, B.A., Curtiss, J., 2009. Rap1 maintains adhesion between cells to affect Egfr signaling and planar cell polarity in Drosophila. Developmental Biology 333, 143–160. https://doi.org/10.1016/j.ydbio.2009.06.032

Onda, H., Lueck, A., Marks, P.W., Warren, H.B., Kwiatkowski, D.J., 1999. Tsc2+/– mice develop tumors in multiple sites that express gelsolin and are influenced by genetic background. Journal of Clinical Investigation 104, 687–695. https://doi.org/10.1172/JCI7319

Patel, P.H., Thapar, N., Guo, L., Martinez, M., Maris, J., Gau, C.-L., Lengyel, J.A., Tamanoi, F., 2003. Drosophila Rheb GTPase is required for cell cycle progression and cell growth. Journal of Cell Science 116, 3601–3610. https://doi.org/10.1242/jcs.00661

Pavan, I.C.B., Silva, F.R., Morelli, A.P., Simabuco, F.M., 2016. S6K (S6 Kinase), in: Encyclopedia of Signaling Molecules. Springer New York, New York, NY, pp. 1–10. https://doi.org/10.1007/978-1-4614-6438-9_101816-1

Pema, M., Drusian, L., Chiaravalli, M., Castelli, M., Yao, Q., Ricciardi, S., Somlo, S., Qian, F.,

Biffo, S., Boletta, A., 2016. mTORC1-mediated inhibition of polycystin-1 expression drives renal cyst formation in tuberous sclerosis complex. Nature communications 7, 10786. https://doi.org/10.1038/ncomms10786

Pende, M., Kozma, S.C., Jaquet, M., Oorschot, V., Burcelin, R., Le Marchand-Brustel, Y., Klumperman, J., Thorens, B., Thomas, G., 2000. Hypoinsulinaemia, glucose intolerance and diminished beta-cell size in S6K1-deficient mice. Nature 408, 994–997. https://doi.org/10.1038/35050135

Pende, M., Um, S.H., Mieulet, V., Goss, V.L., Mestan, J., Mueller, M., Fumagalli, S., Kozma, S.C., Thomas, G., Sticker, M., 2004. S6K1-/-/S6K2-/- Mice Exibit Preinatal Lethality and Rapamycin-Sensitive 5 ′ -Terminal Oligopyrimidine mRNA Translation and Reveal a Mitogen-Activated Protein Kinase-Dependent S6 Kinase Pathway. Molecular and Cellular Biology 24, 3112–3124. https://doi.org/10.1128/MCB.24.8.3112

Peterson, T.R., Sengupta, S.S., Harris, T.E., Carmack, A.E., Kang, S.A., Balderas, E., Guertin, D.A., Madden, K.L., Carpenter, A.E., Finck, B.N., Sabatini, D.M., 2011. mTOR complex 1 regulates lipin 1 localization to control the SREBP pathway. Cell 146, 408–20. https://doi.org/10.1016/j.cell.2011.06.034

Peyre, E., Jaouen, F., Saadaoui, M., Haren, L., Merdes, A., Durbec, P., Morin, X., 2011. A lateral belt of cortical LGN and NuMA guides mitotic spindle movements and planar division in neuroepithelial cells. Journal of Cell Biology. https://doi.org/10.1083/jcb.201101039

Pinheiro, D., Bellaïche, Y., 2018. Mechanical Force-Driven Adherens Junction Remodeling and Epithelial Dynamics. https://doi.org/10.1016/j.devcel.2018.09.014

Plank, T.L., Yeung, R.S., Henske, E.P., 1998. Hamartin, the product of the tuberous sclerosis 1 (TSC1) gene, interacts with tuberin and appears to be localized to cytoplasmic vesicles. Cancer research 58, 4766–70.

Potter, C.J., Huang, H., Xu, T., 2001. Drosophila Tsc1 functions with Tsc2 to antagonize insulin signaling in Regulating Cell Growth, Cell Proliferation, and Organ Size. Cell 105, 357–368.

Potter, C.J., Pedraza, L.G., Xu, T., 2002. Akt regulates growth by directly phosphorylating Tsc2. Nature Cell Biology 4, 658–665. https://doi.org/10.1038/ncb840

Pradhan, S.A., Rather, M.I., Tiwari, A., Bhat, V.K., Kumar, A., 2014. Evidence that TSC2 acts as a transcription factor and binds to and represses the promoter of Epiregulin. Nucleic Acids Research 42, 6243–6255. https://doi.org/10.1093/nar/gku278

Rakowski, S.K., Winterkorn, E.B., Paul, E., Steele, D.J.R., Halpern, E.F., Thiele, E.A., 2006. Renal manifestations of tuberous sclerosis complex: Incidence, prognosis, and predictive factors. Kidney International 70, 1777–1782. https://doi.org/10.1038/sj.ki.5001853

Redemann, S., Pecreaux, J., Goehring, N.W., Khairy, K., Stelzer, E.H.K., Hyman, A.A., Howard, J., 2010. Membrane invaginations reveal cortical sites that pull on mitotic spindles in one-cell C. elegans embryos. PLoS ONE. https://doi.org/10.1371/journal.pone.0012301

Ren, S., Luo, Y., Chen, H., Warburton, D., Lam, H.C., Wang, L.L., Chen, P., Henske, E.P., Shi, W., 2016. Inactivation of Tsc2 in Mesoderm-Derived Cells Causes Polycystic Kidney Lesions and Impairs Lung Alveolarization. The American Journal of Pathology 186, 3261–3272. https://doi.org/10.1016/j.ajpath.2016.08.013

Richly, H., Rocha-Viegas, L., Ribeiro, J.D., Demajo, S., Gundem, G., Lopez-Bigas, N., Nakagawa, T., Rospert, S., Ito, T., Di Croce, L., 2010. Transcriptional activation of polycomb-repressed genes by ZRF1. Nature 468, 1124–1128. https://doi.org/10.1038/nature09574

Robitaille, A.M., Christen, S., Shimobayashi, M., Cornu, M., Fava, L.L., Moes, S., Prescianotto-Baschong, C., Sauer, U., Jenoe, P., Hall, M.N., 2013. Quantitative Phosphoproteomics Reveal mTORC1 Activates de Novo Pyrimidine Synthesis. Science 339, 1320–1323. https://doi.org/10.1126/science.1228771

Rodríguez-Fraticelli, A. E., Auzan, M., Alonso, M. A., Bornens, M. & Martín-Belmonte, F. Cell confinement controls centrosome positioning and lumen initiation during epithelial morphogenesis. J. Cell Biol. 198, 1011–23 (2012). https://doi.org/10.1083/jcb.201203075

Rousseau, A., Bertolotti, A., 2016. An evolutionarily conserved pathway controls proteasome homeostasis. Nature 536, 184–189. https://doi.org/10.1038/nature18943

Ruvinsky, I., 2005. Ribosomal protein S6 phosphorylation is a determinant of cell size and glucose homeostasis. Genes & Development 19, 2199–2211. https://doi.org/10.1101/gad.351605

Sabatini, D.M., Erdjument-Bromage, H., Lui, M., Tempst, P., Snyder, S.H., 1994. RAFT1: A mammalian protein that binds to FKBP12 in a rapamycin-dependent fashion and is homologous to yeast TORs. Cell 78, 35–43. https://doi.org/10.1016/0092-8674(94)90570-3

Sabers, C.J., Martin, M.M., Brunn, G.J., Williams, J.M., Dumont, F.J., Wiederrecht, G., Abraham, R.T., 1995. Isolation of a Protein Target of the FKBP12-Rapamycin Complex in Mammalian Cells. Journal of Biological Chemistry 270, 815–822. https://doi.org/10.1074/jbc.270.2.815

Saburi, S., Hester, I., Fischer, E., Pontoglio, M., Eremina, V., Gessler, M., Quaggin, S.E., Harrison, R., Mount, R., McNeill, H., 2008. Loss of Fat4 disrupts PCP signaling and oriented cell division and leads to cystic kidney disease. Nature Genetics 40, 1010–1015. https://doi.org/10.1038/ng.179

Sato, T., Fujita, N., Yamada, A., Ooshio, T., Okamoto, R., Irie, K., Takai, Y., 2006. Regulation of the assembly and adhesion activity of E-cadherin by nectin and afadin for the formation of adherens junctions in Madin-Darby canine kidney cells. Journal of Biological Chemistry 281, 5288–5299. https://doi.org/10.1074/jbc.M510070200

Saucedo, L.J., Gao, X., Chiarelli, D.A., Li, L., Pan, D., Edgar, B.A., 2003. Rheb promotes cell growth as a component of the insulin/TOR signalling network. Nature Cell Biology 5, 566–571. https://doi.org/10.1038/ncb996

Sawyer, J.K., Choi, W., Jung, K.-C., He, L., Harris, N.J., Peifer, M., 2011. A contractile actomyosin network linked to adherens junctions by Canoe/afadin helps drive convergent extension. Molecular Biology of the Cell 22, 2491–2508. https://doi.org/10.1091/mbc.e11-05-0411

Saxton, R.A., Sabatini, D.M., 2017. mTOR Signaling in Growth, Metabolism, and Disease. Cell 168, 960–976. https://doi.org/10.1016/j.cell.2017.02.004

Schmelzle, T., Hall, M.N., 2000. TOR, a Central Controller of Cell Growth. Cell 103, 253–262.

Schreiber, S., 1991. Chemistry and biology of the immunophilins and their immunosuppressive ligands. Science 251, 283–287. https://doi.org/10.1126/science.1702904

Selman, C., Tullet, J.M.A., Wieser, D., Irvine, E., Lingard, S.J., Choudhury, A.I., Claret, M., Al-Qassab, H., Carmignac, D., Ramadani, F., Woods, A., Robinson, I.C. a, Schuster, E., Batterham, R.L., Kozma, S.C., Thomas, G., Carling, D., Okkenhaug, K., Thornton, J.M., Partridge, L., Gems, D., Withers, D.J., 2009. Ribosomal Protein S6 Kinase 1 Signaling Regulates Mammalian Life Span. Science 326, 140–144. https://doi.org/10.1126/science.1177221

Settembre, C., Zoncu, R., Medina, D.L., Vetrini, F., Erdin, Serkan, Erdin, SerpilUckac, Huynh, T., Ferron, M., Karsenty, G., Vellard, M.C., Facchinetti, V., Sabatini, D.M., Ballabio, A., 2012. A lysosome-to-nucleus signalling mechanism senses and regulates the lysosome via mTOR and TFEB. The EMBO Journal 31, 1095–1108. https://doi.org/10.1038/emboj.2012.32

Shah, O.J., Wang, Z., Hunter, T., 2004. Inappropriate Activation of the TSC/Rheb/mTOR/S6K Cassette Induces IRS1/2 Depletion, Insulin Resistance, and Cell Survival Deficiencies. Current Biology 14, 1650–1656. https://doi.org/10.1016/j.cub.2004.08.026

Shima, H., 1998. Disruption of the p70s6k/p85s6k gene reveals a small mouse phenotype and a new functional S6 kinase. The EMBO Journal 17, 6649–6659. https://doi.org/10.1093/emboj/17.22.6649

Simons, M., Gloy, J., Ganner, A., Bullerkotte, A., Bashkurov, M., Krönig, C., Schermer, B., Benzing, T., Cabello, O.A., Jenny, A., Mlodzik, M., Polok, B., Driever, W., Obara, T., Walz, G., 2005. Inversin, the gene product mutated in nephronophthisis type II, functions as a molecular switch between Wnt signaling pathways. NATURE GENETICS 37. https://doi.org/10.1038/ng1552

Siroky, B.J., Towbin, A.J., Trout, A.T., Schäfer, H., Thamann, A.R., Agricola, K.D., Tudor, C., Capal, J., Dixon, B.P., Krueger, D.A., Franz, D.N., 2017. Improvement in Renal Cystic Disease of Tuberous Sclerosis Complex After Treatment with Mammalian Target of Rapamycin Inhibitor. The Journal of pediatrics 187, 318–322.e2. https://doi.org/10.1016/j.jpeds.2017.05.015

Stocker, H., Hafen, E., 2000. Genetic control of cell size. Current Opinion in Genetics and Development 10, 529–535. https://doi.org/10.1016/S0959-437X(00)00123-4

Stocker, H., Radimerski, T., Schindelholz, B., Wittwer, F., Belawat, P., Daram, P., Breuer, S., Thomas, G., Hafen, E., 2003. Rheb is an essential regulator of S6K in controlling cell growth in Drosophila. Nature Cell Biology 5, 559–566. https://doi.org/10.1038/ncb995

Su, B., Jacinto, E., 2011. Mammalian TOR signaling to the AGC kinases. Critical Reviews in Biochemistry and Molecular Biology 46, 527–547. https://doi.org/10.3109/10409238.2011.618113

Tapon, N., Ito, N., Dickson, B.J., Treisman, J.E., Hariharan, I.K., 2001. The Drosophila Tuberous Sclerosis Complex Gene Homologs Restrict Cell Growth and Cell Proliferation. Cell 105, 345–355. https://doi.org/10.1016/s0092-8674(01)00332-4

Tee, A.R., Manning, B.D., Roux, P.P., Cantley, L.C., Blenis, J., 2003. Tuberous sclerosis complex gene products, Tuberin and Hamartin, control mTOR signaling by acting as a GTPase-activating protein complex toward Rheb. Current biology : CB 13, 1259–68.

Théry, M., Racine, V., Pépin, A., Piel, M., Chen, Y., Sibarita, J.B., Bornens, M., 2005. The extracellular matrix guides the orientation of the cell division axis. Nature Cell Biology.

https://doi.org/10.1038/ncb1307

Thomas, G., Hall, M.N., 1997. TOR signalling and control of cell growth George Thomas* and Michael N Hall. Current opinion in cell biology 9, 782–787. https://doi.org/10.1016/S0955-0674(97)80078-6

Thomas, G., Siegmann, M., Kubler, A.-M., Gordon, J., Jimenez de Asua, L., 1980. Regulation of 40S ribosomal protein S6 phosphorylation in Swiss mouse 3T3 cells. Cell 19, 1015–1023. https://doi.org/10.1016/0092-8674(80)90092-6

Thoreen, C.C., Kang, S.A., Chang, J.W., Liu, Q., Zhang, J., Gao, Y., Reichling, L.J., Sim, T., Sabatini, D.M., Gray, N.S., 2009. An ATP-competitive Mammalian Target of Rapamycin Inhibitor Reveals Rapamycin-resistant Functions of mTORC1. Journal of Biological Chemistry 284, 8023–8032. https://doi.org/10.1074/jbc.M900301200

Tinevez, J.-Y., Schulze, U., Salbreux, G., Roensch, J., Joanny, J.-F., Paluch, E., 2009. Role of cortical tension in bleb growth. Proceedings of the National Academy of Sciences of the United States of America 106, 18581–6. https://doi.org/10.1073/pnas.0903353106

Torres, V.E., Boletta, A., Chapman, A., Gattone, V., Pei, Y., Qian, Q., Wallace, D.P., Weimbs, T., Wüthrich, R.P., 2010. Prospects for mTOR inhibitor use in patients with polycystic kidney disease and hamartomatous diseases. Clinical Journal of the American Society of Nephrology 5, 1312–1329. https://doi.org/10.2215/CJN.01360210

Treins, C., Warne, P.H., Magnuson, M.A., Pende, M., Downward, J., 2010. Rictor is a novel target of p70 S6 kinase-1. Oncogene 29, 1003–1016. https://doi.org/10.1038/onc.2009.401

Tremblay, F., Brule, S., Hee Um, S., Li, Y., Masuda, K., Roden, M., Sun, X.J., Krebs, M., Polakiewicz, R.D., Thomas, G., Marette, A., 2007. Identification of IRS-1 Ser-1101 as a target of S6K1 in nutrient- and obesity-induced insulin resistance. Proceedings of the National Academy of Sciences 104, 14056–14061. https://doi.org/10.1073/pnas.0706517104

Tyburczy, M.E., Jozwiak, S., Malinowska, I.A., Chekaluk, Y., Pugh, T.J., Wu, C.L., Nussbaum, R.L., Seepo, S., Dzik, T., Kotulska, K., Kwiatkowski, D.J., 2014. A shower of second hit events as the cause of multifocal renal cell carcinoma in tuberous sclerosis complex. Human Molecular Genetics 24, 1836–1842. https://doi.org/10.1093/hmg/ddu597

Um, S.H., Frigerio, F., Watanabe, M., Picard, F., Joaquin, M., Sticker, M., Fumagalli, S., Allegrini, P.R., Kozma, S.C., Auwerx, J., Thomas, G., 2004. Absence of S6K1 protects against age- and diet-induced obesity while enhancing insulin sensitivity. Nature 431, 200–205. https://doi.org/10.1038/nature02866

van Roy, F., Berx, G., 2008. The cell-cell adhesion molecule E-cadherin. Cellular and Molecular Life Sciences 65, 3756–3788. https://doi.org/10.1007/s00018-008-8281-1

van Slegtenhorst, M., 1998. Interaction between hamartin and tuberin, the TSC1 and TSC2 gene products. Human Molecular Genetics 7, 1053–1057. https://doi.org/10.1093/hmg/7.6.1053

van Slegtenhorst, M., de Hoogt, R., Hermans, C., Nellist, M., Janssen, B., Verhoef, S., Lindhout, D., van den Ouweland, A., Halley, D., Young, J., Burley, M., Jeremiah, S., Woodward, K., Nahmias, J., Fox, M., Ekong, R., Osborne, J., Wolfe, J., Povey, S., Snell, R.G., Cheadle, J.P., Jones, A.C., Tachataki, M., Ravine, D., Sampson, J.R., Reeve, M.P., Richardson, P., Wilmer, F., Munro, C., Hawkins, T.L., Sepp, T., Ali, J.B., Ward, S., Green, A.J., Yates, J.R., Kwiatkowska, J.,

Henske, E.P., Short, M.P., Haines, J.H., Jozwiak, S., Kwiatkowski, D.J., 1997. Identification of the tuberous sclerosis gene TSC1 on chromosome 9q34. Science 277, 805–808. https://doi.org/10.1126/science.277.5327.805

Vézina, C., Kudelski, A., Sehgal, S.N., 1975. Rapamycin (AY-22,989), a new antifungal antibiotic. I. Taxonomy of the producing streptomycete and isolation of the active principle. The Journal of antibiotics 28, 721–6.

Vogt, H., 1908. Zur Pathologie und pathologischen Anatomie der verschiedenen Idiotieformen. Monatsschr Psychiatr Neurol 116–117.

Wang, X., Li, W., Williams, M., Terada, N., Alessi, D.R., Proud, C.G., 2001. Regulation of elongation factor 2 kinase by p90RSK1 and p70 S6 kinase. EMBO Journal 20, 4370–4379. https://doi.org/10.1093/emboj/20.16.4370

Wang, Y., Ding, Q., Yen, C.-J., Xia, W., Izzo, J.G., Lang, J.-Y., Li, C.-W., Hsu, J.L., Miller, S.A., Wang, X., Lee, D.-F., Hsu, J.-M., Huo, L., LaBaff, A.M., Liu, D., Huang, T.-H., Lai, C.-C., Tsai, F.-J., Chang, W.-C., Chen, C.-H., Wu, T.-T., Buttar, N.S., Wang, K.K., Wu, Y., Wang, H., Ajani, J., Hung, M.-C., 2012. The Crosstalk of mTOR/S6K1 and Hedgehog Pathways. Cancer Cell 21, 374–387. https://doi.org/10.1016/j.ccr.2011.12.028

Wienecke, R., König, A., DeClue, J.E., 1995. Identification of Tuberin, the Tuberous Sclerosis-2 Product. TUBERIN POSSESSES SPECIFIC Rap1GAP ACTIVITY. Journal of Biological Chemistry 270, 16409–16414. https://doi.org/10.1074/jbc.270.27.16409

Wilson, K.F., Wu, W.J., Cerione, R.A., 2000. Cdc42 stimulates RNA splicing via the S6 kinase and a novel S6 kinase target, the nuclear cap-binding complex. Journal of Biological Chemistry 275, 37307–37310. https://doi.org/10.1074/jbc.C000482200

Wolf, B., Busso, C., Gönczy, P., n.d. Live imaging screen reveals that TYRO3 and GAK ensure accurate spindle positioning in human cells. https://doi.org/10.1038/s41467-019-10446-z

Xiao, G.-H., Shoarinejad, F., Jin, F., Golemis, E.A., Yeung, R.S., 1997. The Tuberous Sclerosis 2 Gene Product, Tuberin, Functions as a Rab5 GTPase Activating Protein (GAP) in Modulating Endocytosis. Journal of Biological Chemistry 272, 6097–6100. https://doi.org/10.1074/jbc.272.10.6097

Xu, J., Chen, J., Dong, Z., Meyuhas, O., Chen, J.-K., 2015a. Phosphorylation of ribosomal protein S6 mediates compensatory renal hypertrophy. Kidney International 87, 543–556. https://doi.org/10.1038/ki.2014.302

Xu, J., Chen, J., Dong, Z., Meyuhas, O., Chen, J.-K., 2015b. Phosphorylation of ribosomal protein S6 mediates compensatory renal hypertrophy HHS Public Access. Kidney Int 87, 543–556. https://doi.org/10.1038/ki.2014.302

Yang, G., Murashige, D.S., Humphrey, S.J., James, D.E., 2015. A Positive Feedback Loop between Akt and mTORC2 via SIN1 Phosphorylation. Cell Reports 12, 937–943. https://doi.org/10.1016/j.celrep.2015.07.016

Yeung, R.S., Xiao, G.H., Jin, F., Lee, W.C., Testa, J.R., Knudson, A.G., 1994. Predisposition to renal carcinoma in the Eker rat is determined by germ-line mutation of the tuberous sclerosis 2 (TSC2) gene. Proceedings of the National Academy of Sciences 91, 11413–11416. https://doi.org/10.1073/pnas.91.24.11413

Yi, S.A., Um, S.H., Lee, J., Yoo, J.H., Bang, S.Y., Park, E.K., Lee, M.G., Nam, K.H., Jeon, Y.J.,

Park, J.W., You, J.S., Lee, S.J., Bae, G.U., Rhie, J.W., Kozma, S.C., Thomas, G., Han, J.W., 2016. S6K1 Phosphorylation of H2B Mediates EZH2 Trimethylation of H3: A Determinant of Early Adipogenesis. Molecular Cell 62, 443–452. https://doi.org/10.1016/j.molcel.2016.03.011

Yu, Y., Yoon, S.-O., Poulogiannis, G., Yang, Q., Ma, X.M., Villen, J., Kubica, N., Hoffman, G.R., Cantley, L.C., Gygi, S.P., Blenis, J., 2011. Phosphoproteomic Analysis Identifies Grb10 as an mTORC1 Substrate That Negatively Regulates Insulin Signaling. Science 332, 1322–1326. https://doi.org/10.1126/science.1199484

Yuan, S., Li, J., Diener, D.R., Choma, M.A., Rosenbaum, J.L., Sun, Z., 2012. Target-of-rapamycin complex 1 (Torc1) signaling modulates cilia size and function through protein synthesis regulation. Proceedings of the National Academy of Sciences of the United States of America 109, 2021–6. https://doi.org/10.1073/pnas.1112834109

Zhang, H.H., Lipovsky, A.I., Dibble, C.C., Sahin, M., Manning, B.D., 2006. S6K1 Regulates GSK3 under Conditions of mTOR-Dependent Feedback Inhibition of Akt. Molecular Cell 24, 185–197. https://doi.org/10.1016/j.molcel.2006.09.019

Zhang, Y., Gao, X., Saucedo, L.J., Ru, B., Edgar, B.A., Pan, D., 2003. Rheb is a direct target of the tuberous sclerosis tumour suppressor proteins. Nature Cell Biology 5, 578–581. https://doi.org/10.1038/ncb999

Zhang, Y., Nicholatos, J., Dreier, J.R., Ricoult, S.J.H., Widenmaier, S.B., Hotamisligil, G.S., Kwiatkowski, D.J., Manning, B.D., 2014. Coordinated regulation of protein synthesis and degradation by mTORC1. Nature 513, 440–443. https://doi.org/10.1038/nature13492

Zheng, Z., Wan, Q., Liu, J., Zhu, H., Chu, X., Du, Q., 2013. Evidence for dynein and astral microtubule-mediated cortical release and transport of G i/LGN/NuMA complex in mitotic cells. Molecular Biology of the Cell. https://doi.org/10.1091/mbc.e12-06-0458

Zhu, J., Blenis, J., Yuan, J., 2008. Activation of PI3K/Akt and MAPK pathways regulates Myc-mediated transcription by phosphorylating and promoting the degradation of Mad1. Proceedings of the National Academy of Sciences 105, 6584–6589. https://doi.org/10.1073/pnas.0802785105

Zinzalla, V., Stracka, D., Oppliger, W., Hall, M.N., 2011. Activation of mTORC2 by Association with the Ribosome. Cell 144, 757–768. https://doi.org/10.1016/j.cell.2011.02.014

Table of figures

Figure A. Most common affected systems in TSC patients and associated lesions..... 3
Figure B. “Two-hit” model in inherited and somatic TSC..... 6
Figure C. The kidney. 7
Figure D. The renal lesions in TSC patients 9
Figure E. Epithelium in TSC-associated cyst 10
Figure F. Human RCC..... 11
Figure G. Eker rat kidney tumors 15
Figure H. Immunohistological analysis of renal tumors of *CAGGGCre–ER; Tsc1$^{fl/fl}$* animals.... 16
Figure I. Tsc1 and Tsc2 function in *Drosophila*..... 22
Figure J. Regulation of GTPases..... 23
Figure K. Rapamycin and FK506 structure 26
Figure L. mTORC1 27
Figure M. mTORC2 subunits and respective binding sites on mTOR..... 28
Figure N. Scheme of the complex of regulation of mTORC1 at the lysosome..... 30
Figure O. mTORC1: input and output signals..... 32
Figure P. Translation initiation complex..... 33
Figure Q. mTORC1-dependent regulation of translation initiation 33
Figure R. mTORC2 activation..... 37
Figure S. Evolutionary conservation of TSC1 and TSC2 structure..... 40
Figure T. Model of regulation of S6K1 activity by multi-site phosphorylation. 43
Figure U. Reduced body size in S6K1-mutant 45
Figure V. Substrates of S6K1 49
Figure W. Hyperactive S6K1 affects cortical tension in 3D culture..... 113
Figure X. LGN and NuMA localize at the membrane in *Tsc1* KO cells..... 114
Figure Y. Convergent extension 120
Figure Z. Formation of adherens junctions..... 122